

Solar twins in Gaia DR3 GSP-Spec

I. Building a large catalog of Solar twins with ages

Daisuke Taniguchi^{1,2,*}, Patrick de Laverny³, Alejandra Recio-Blanco³, Takuji Tsujimoto², and Pedro A. Palicio³

¹ Department of Physics, Tokyo Metropolitan University, 1-1 Minami-Osawa, Hachioji, Tokyo 192-0397, Japan
 e-mail: d.taniguchi.astro@gmail.com

² National Astronomical Observatory of Japan, 2-21-1 Osawa, Mitaka, Tokyo 181-8588, Japan

³ Université Côte d’Azur, Observatoire de la Côte d’Azur, CNRS, Laboratoire Lagrange, Bd de l’Observatoire, CS 34229, 06304 Nice cedex 4, France

Received ?? ; accepted ??

ABSTRACT

Context. Solar twins, stars whose stellar parameters (effective temperature T_{eff} , surface gravity $\log g$, and metallicity [M/H]) are very close to the Solar ones, offer a unique opportunity to investigate Galactic archaeology with very high accuracy and precision. However, most previous catalogs of Solar twins contain only a small number of objects (typically a few tens), and their selection functions are poorly characterized.

Aims. We aim at building a large catalog of Solar twins from *Gaia* DR3 GSP-Spec, providing stellar parameters including ages determined using a model-driven, rather than data-driven, method, together with a well-characterized selection function.

Methods. Using stellar parameters from the *Gaia* DR3 GSP-Spec catalog, we selected Solar-twin candidates whose parameters lie within ± 200 K in T_{eff} , ± 0.2 in $\log g$, and ± 0.1 dex in [M/H] of the Solar values. Candidates unlikely to be genuine Solar twins were removed using *Gaia* flags and photometric constraints. We determined accurate ages for individual twins with a Bayesian isochrone-projection method, considering three combinations of parameters: T_{eff} , [M/H], and either $\log g$, M_G , or M_{K_s} . We also constructed a mock catalog to characterize the properties and selection function of our observed sample.

Results. Our final GSP-Spec Solar-twin catalog contains 6,594 stars. The mock catalog consisting of 75,588 artificial twins well reproduces the main characteristics of the observed catalog, especially for ages determined with M_G or M_{K_s} . To demonstrate the usefulness of our catalog, we compared chemical abundances [X/Fe] with age. We statistically confirmed the age-[X/Fe] relations for several species (e.g., Al, Si, Ca, and Y), demonstrating that trends previously identified in small but very high-precision samples persist in a much larger, independent sample.

Conclusions. Our study bridges small high-precision Solar-twin samples and large data-driven ones by providing a large sample with model-driven stellar parameters and a quantified selection function, enabling demographic studies of Solar twins.

Key words. Stars: solar-type – Stars: fundamental parameters – Hertzsprung–Russell and C-M diagrams – Stars: abundances – Stars: statistics – Galaxy: evolution

1. Introduction

Solar twins are defined as stars with stellar parameters (i.e., effective temperature T_{eff} , surface gravity $\log g$, and metallicity [M/H]) very close to those of the Sun (Hardorp 1978; Cayrel de Strobel et al. 1981)¹. By performing differential analyses between stars with very similar stellar parameters—Solar twins in our case—one can achieve extremely high accuracy in the measurements of stellar parameters and chemical abundances because systematic biases associated with T_{eff} and $\log g$ are reduced (Bedell et al. 2014; Nissen & Gustafsson 2018). Such very precise and accurate stellar parameters, sometimes combined with precise parallaxes, can also yield accurate stellar ages through isochrone modeling (e.g., Nissen 2015; Spina et al. 2016a), even though Solar twins are main-sequence stars, for

which isochrones of different ages are closely spaced in the Hertzsprung–Russell (HR) diagram.

By exploiting these advantages, Solar twins have been used, for example, to determine the Solar properties such as its color (Holmberg et al. 2006; Casagrande & VandenBerg 2018), to study planet–host interactions through photospheric chemical abundances (Israelian et al. 2004, 2009; Meléndez et al. 2009), to construct chemical clocks (Tucci Maia et al. 2016; Casali et al. 2020), and to investigate the chemodynamical evolution of the Milky Way (Jofré et al. 2017; Bedell et al. 2018; Tsujimoto 2021). Among these applications, the ability to determine accurate stellar ages is particularly valuable for Galactic archaeology, where ages are crucial for tracing the history of the Milky Way but are often difficult to obtain (e.g., Ness et al. 2019; Magrini et al. 2023).

There have been great efforts to identify Solar twins. In early studies, Solar twins in a narrow sense, i.e., stars whose stellar parameters are identical to the Solar values within the errors, were explored. In that era, only a few very similar Solar twins were spectroscopic

* The Tokyo Center For Excellence Project, Tokyo Metropolitan University.

¹ The level of similarity required, and whether other parameters (e.g., age, rotational velocity, or Li abundance) are included, depends on the specific purpose of a given Solar-twin study.

cally confirmed: 18 Sco (Porto de Mello & da Silva 1997; Soubiran & TrPrsa2016d 2004), HD 143436 (King et al. 2005), HD 98618 (Meléndez et al. 2006), HIP 100963 (Takeda et al. 2007), and HIP 56948 (Meléndez & Ramírez 2007; Takeda & Tajitsu 2009); see also the review by Cayrel de Strobel (1996). Later, motivated by these identifications and also by the growing interest in understanding planet–host interactions, several dedicated surveys of Solar twins were conducted, yielding samples of several tens of Solar twins (e.g., Takeda et al. 2007; Meléndez et al. 2009). In particular, archival spectral data obtained with the HARPS spectrograph (Mayor et al. 2003), originally collected for exoplanet detection via radial-velocity monitoring, have been extensively used to derive high-precision chemical abundances and ages of Solar twins through differential analysis of high signal-to-noise-ratio (S/N) stacked spectra (e.g., Nissen 2015; Martos et al. 2025). Furthermore, recent massive spectroscopic surveys are capable of identifying thousands of Solar twins. Nevertheless, only a few such large samples of Solar twins have so far been published: using GALAH DR3 by Walsen et al. (2024) and Lehmann et al. (2025) and *Gaia* DR3 Radial Velocity Spectrometer (RVS) data by Rampalli et al. (2024). In the present contribution, we aim at building a large catalog of Solar twins based on non-data-driven stellar parameters, with strict filtering and a well-characterized selection function.

To obtain the largest possible catalog of high-quality Solar-twin candidates, the most effective approach is to mine the catalogs published by large spectroscopic surveys, at the expense of some loss in precision compared to dedicated surveys targeting individual objects. The largest such catalog in terms of sample size (by more than one order of magnitude compared to ground-based surveys) is the homogeneous General Stellar Parametrizer from Spectroscopy (GSP-Spec) catalog collected from space by the ESA/*Gaia* mission and published as part of the third *Gaia* data release (DR3, Gaia Collaboration et al. 2016, 2023c; Recio-Blanco et al. 2023). GSP-Spec is based on the analysis of ~ 5.6 million *Gaia*/RVS stellar spectra for which the main atmospheric parameters are provided, together with the mean enrichment in α -elements with respect to iron ($[\alpha/\text{Fe}]$, in dex) and individual chemical abundances of up to 13 elements (including two ions for iron). With the magnitude limit of $G \lesssim 12$ for Solar-type stars with best GSP-Spec parameterization, GSP-Spec Solar twins extend out to distances of ~ 300 pc. This reachable distance is about three times larger than that of high-precision dedicated spectroscopic surveys, which typically reach ~ 100 pc. Hence, the volume covered, and therefore the expected number of objects, is increased by a factor of ~ 30 .

This paper is organized as follows. We first select thousands of Solar twins found in the GSP-Spec catalog (Sect. 2). Then, by comparing their stellar parameters and *Gaia* parallaxes with theoretical isochrones, we determine their ages and initial masses in a homogeneous and consistent way (Sect. 3), we validate the resulting ages (Sect. 4), and we place our work in the context of previous Solar-twin studies (Sect. 5). Finally, we take a brief look at several applications of our catalog to assess its scientific potential (Sect. 6).

2. Solar-twin selection

2.1. GSP-Spec sample of Solar-twin candidates

To look for robustly parametrized Solar twins within the GSP-Spec catalog, we first considered the ~ 2 million stars whose first 13 GSP-Spec quality flags (flags_gspspec) are all equal to

zero, refer to the quality of the T_{eff} , $\log g$, $[\text{M}/\text{H}]^2$, and $[\alpha/\text{Fe}]$ derivations. They mostly depend on the quality of the input RVS spectra, and “0” means “Best Quality” (see, Sect. 8 of Recio-Blanco et al. 2023, for more details). The seventh digit of the quality flag indicates the uncertainty of the parameterization; “0” means that the statistical uncertainties on T_{eff} , $\log g$, $[\text{M}/\text{H}]$, and $[\alpha/\text{Fe}]$ are less than 100 K, 0.2, 0.1 dex, and 0.05 dex, respectively. We moreover selected stars with a very high-quality GSP-Spec goodness-of-fit (`logchisq_gspspec`), $\log \chi^2 < -3.2$, ensuring the high quality of the parameterization.

We also imposed the following criteria to analyze only stars with good astrometric solutions and to remove possible binary stars: renormalized unit weight error (RUWE) is smaller than 1.4, `astrometric_params_solved` is 0, `duplicated_source` is False, and `non_single_star` is 0. We confirmed that the `fidelity_v2` index introduced by Rybizki et al. (2022) is larger than 0.5 for all the selected Solar-twin candidates, indicating that the quality of the astrometric solution is good.

We then calibrated $\log g$ and $[\text{M}/\text{H}]$ for these stars, by following the relations as a function of T_{eff} provided in Recio-Blanco et al. (2024). The applied corrections imply changes of ~ 0.1 –0.2 for $\log g$ and < 0.01 dex for $[\text{M}/\text{H}]$. We further calibrated the stellar parameters so that they are well differential against the Sun (see Appendix A)³. In short, for T_{eff} and $[\text{M}/\text{H}]$, we added offsets of 1 K and 0.062 dex, respectively. For $\log g$, we applied Equation A.3. Hereafter, we call the stellar parameters after the calibration described in Appendix A the “calibrated” parameters and use them unless otherwise specified, while we refer to the parameters before this second calibration as the “original” ones, though they have already been subjected to the first-stage calibration following Recio-Blanco et al. (2024).

With the zero-point biases reduced, the 7,918 Solar-twin candidates were defined as having their T_{eff} , $\log g$, and $[\text{M}/\text{H}]$ within ± 200 K, ± 0.2 , and ± 0.1 dex around the Solar values, respectively. In the following, we adopted the standard Solar values: $T_{\text{eff},\odot} = 5777$ K, $\log g_{\odot} = 4.44$, and $[\text{M}/\text{H}]_{\odot} = 0.0$ dex. The typical parameter uncertainties are much smaller than the above-mentioned filtering: for these 7,918 candidates, their median uncertainties are actually equal to 50 K, 0.05⁴, and 0.03 dex for T_{eff} , $\log g$, and $[\text{M}/\text{H}]$, respectively.

2.2. Interstellar extinctions

Since the absolute magnitudes of all these Solar twins are necessary for their accurate age determination, we computed their interstellar extinctions in the *Gaia* *G*-band by comparing their *Gaia* observed colors ($G_{\text{BP}} - G_{\text{RP}}$) to theoretical ones estimated from the Casagrande et al. (2021) relation between atmospheric parameters and color. For that relation, we adopted the “original” spectroscopic atmospheric parameters. These computations were performed for 1,000 Monte-Carlo realizations, propagating the uncertainties on each atmospheric parameter and *Gaia* magnitudes in the different bands. The adopted extinctions (A_G)

² Within GSP-Spec, $[\text{M}/\text{H}]$ is a proxy for $[\text{Fe}/\text{H}]$ abundance (Recio-Blanco et al. 2023, 2024).

³ We note that, throughout this paper, we shifted the zero-points in literature T_{eff} and $\log g$ values to our adopted scale, $T_{\text{eff},\odot} = 5777$ K and $\log g_{\odot} = 4.44$, if the reference Solar values are explicitly mentioned.

⁴ During the calibration process described in Appendix A, the errors in $\log g$ shrank. The adopted broken-line relation implies that the largest shrinkage occurs in stars with higher $\log g$ (original $\log g \gtrsim 4.5$, or equivalently, calibrated $\log g \gtrsim 4.48$), where they were reduced to $a_2 = 0.133$ times their original error values.

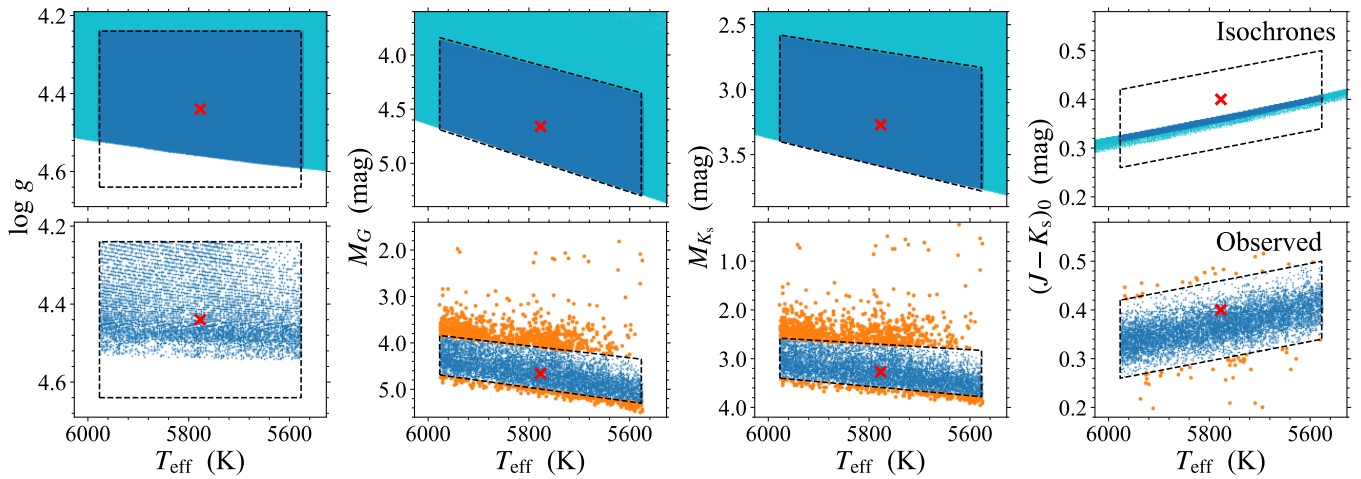


Fig. 1: Some parameters of theoretical isochrones (top) and observed Solar-twin candidates (bottom). The horizontal axes in all the panels represent T_{eff} , while the vertical axes represent some other parameters ($\log g$, M_G , M_{K_s} , and $(J - K_s)_0$). Cyan dots in the upper panels show the isochrone grid points satisfying $-0.1 < [\text{M}/\text{H}]_{\text{curr}} < +0.1$ dex. Blue dots in the upper panels show a subset of them having T_{eff} and $\log g$ between ± 200 K and ± 0.2 around the Solar values, which is the selection criterion of our Solar-twin candidates in Sect. 2.1 and is represented as a black dashed rectangle in the left panels. Black dashed trapezoids in the rest of the panels show the selection criteria for good Solar twins in Sect. 2.4. Dots in the lower panels show the parameters of the 7,775 observed Solar-twin candidates with good distances and 2MASS data. Orange dots in the lower panels show a subset of them that do not satisfy the selection criteria (i.e., outside the black trapezoids). Red crosses show the reference Solar values provided in Sect. 4.1 and $(J - K_s)_0 = 0.40$ (Willmer 2018). We note that several outliers of observed Solar-twin candidates fall outside the plotted range and are not shown in the figures.

are the medians of the Monte-Carlo distributions, and their associated uncertainties are half of the difference between the 84th and 16th percentiles, as it corresponds to a 1σ uncertainty for a normal distribution. The extinctions to our Solar twins are small, with the median and 95th percentile of 0.02 and 0.15 mag, respectively, in the G band. We refer to de Laverny et al. (in preparation) for more details on these extinction calculations and to Barbillon et al. (2025) for their validation in a Galactic and interstellar-medium context.

2.3. Absolute magnitudes and de-reddened colors

We retrieved the *Gaia* DR3 photometry (`phot_g_mean_mag`, `phot_bp_mean_mag`, and `phot_rp_mean_mag`) of the Solar-twin candidates from the *Gaia* Archive. Their 2MASS JHK_s photometry (Cutri et al. 2003; Skrutskie et al. 2006) was extracted using the cross-matched result in the `gaiadr3.tmass_psc_xsc_best_neighbour` catalog. We then converted the G -band extinction A_G determined in Sect. 2.2 to the extinctions in the *Gaia* EDR3 and 2MASS passbands using the `DUSTAPPROX` code (Fouesneau et al. 2022). Then, combining these extinctions with the distances from Bailer-Jones et al. (2021), we calculated the absolute magnitudes and de-reddened colors of the Solar-twin candidates.

2.4. Flagging with absolute magnitudes

In order to further clean our sample, we made use of the absolute magnitudes and de-reddened colors computed in Sect. 2.3 together with PARSEC isochrones retrieved in Sect. 3.1 and interpolated in Appendix B. From the 7,918 Solar-twin candidates, we removed stars falling under any of the following conditions from the subsequent analysis:

- Without a 2MASS entry in the JK_s bands (41 stars)

- Whose 2MASS counterpart is not uniquely matched, i.e., it also matched to another Solar-twin candidate (2 stars)
- With the Qflg in the 2MASS JK_s bands of E, F, U, X, or Z (i.e., poor photometry; 100 stars).

These conditions left 7,775 stars with good distances and 2MASS data.

We found that some of the Solar-twin candidates have absolute magnitudes and/or de-reddened colors that are far from those of the Sun. For example, some stars have absolute G - and K_s -band magnitudes that are systematically higher (or lower) than the Solar values (orange dots in lower middle panels of Fig. 1). Such systematic deviations, regardless of wavelength, indicate either poor parallax, poor $\log g$ determination, and/or binarity. As another example, some other stars have their de-reddened $J - K_s$ colors far from the Solar value (orange dots in lower right panel of Fig. 1). Regardless of the reason for such deviation, e.g., poorer image FWHM in 2MASS than in *Gaia*, such stars should be treated with caution, given that we will use the 2MASS K_s magnitude in one of our age-determination methods.

To exclude stars having unexpected absolute magnitudes and/or de-reddened colors, we plotted $\log g$, M_G , M_{K_s} , and $(J - K_s)_0$ against T_{eff} in the lower panels of Fig. 1. In order to select Solar-twin candidates having good absolute magnitudes, we first gathered isochrone points having current metallicity $[\text{M}/\text{H}]_{\text{curr}}$, T_{eff} , and $\log g$ within ± 0.1 dex, ± 200 K, and ± 0.2 around the Solar values (blue dots in the upper panels), which is equivalent to our selection criterion for Solar-twin candidates in Sect. 2.1. Then, in the T_{eff} vs M_G and T_{eff} vs M_{K_s} diagrams, we drew trapezoids that provide a near-minimal enclosure of the selected sample (black-dashed trapezoids). Finally, the two trapezoids were used to remove 1,129 suspicious candidates.

In contrast to the absolute magnitudes of theoretical Solar twins, which show a spread of ~ 1 mag, their $(J - K_s)_0$ col-

ors follow a very tight T_{eff} –color relation with a spread of ~ 0.01 mag (upper right panel of Fig. 1). Hence, the observed color spread of Solar-twin candidates is dominated by the photometric error of ~ 0.03 mag, which is larger than the intrinsic absolute-magnitude spreads. We also found that the Solar color of 0.40 (Willmer 2018) deviates from the isochrones by 0.04 mag. As such, it is practically impossible to select good Solar-twin candidates using the theoretical $(J - K_s)_0$ colors. Instead, we removed 52 candidates by excluding stars that clearly lie outside the main locus in the diagram, using a rectangular selection box of 0.16 mag width chosen based on visual inspection.

With all the conditions listed in this section considered, there remain 6,594 good Solar twins suitable for the subsequent analysis.

2.5. Orbital parameters

Since orbital parameters of Solar twins are useful for discussing their origins, we computed their dynamical properties as in Gaia Collaboration et al. (2023b) and Palicio et al. (2023). In particular, we will consider the guiding radius, by numerically solving $|L_z| = R_g V_{\text{circ}}(R_g)$, where L_z is the angular momentum and $V_{\text{circ}}(R)$ is the circular velocity at radii R . For these orbit determinations, we adopted the *Gaia* coordinates, geometric distances from Bailer-Jones et al. (2021), *Gaia* DR3 radial velocities (V_{rad} ; Katz et al. 2023), and *Gaia* EDR3 proper motions, together with a local standard of rest (LSR) velocity at the Sun’s position equal to $V_{\text{LSR}} = 238.5 \text{ km s}^{-1}$ (Schönrich et al. 2010), and a Galactic center distance of $R_0 = 8.249 \text{ kpc}$ (GRAVITY Collaboration et al. 2020). The determined orbital parameters are used in our companion papers (Papers II and III; Tsujimoto et al. 2026; Taniguchi et al. 2026).

3. Age determination of the Solar twins

We computed the ages of Solar twins having precise *Gaia* stellar parameters by adopting the so-called isochrone method, which has been widely used for dating stars including Solar twins (e.g., Jørgensen & Lindegren 2005; Ramírez et al. 2014; Spina et al. 2018). Basically, our methodology consists of an adaptation of those of Zwitter et al. (2010) and Kordopatis et al. (2023), with optimization for Solar-twin ages. As we detail in this section, we determined the ages using three combinations of parameters: T_{eff} , $[\text{M}/\text{H}]$, and either $\log g$, G -band absolute magnitude, or K_s -band absolute magnitude.

3.1. PARSEC isochrone library

As the isochrone library used in the subsequent analysis and in Sect. 2.4, we retrieved PARSEC isochrones version 1.2S (Bressan et al. 2012; Chen et al. 2015) using the CMD 3.8 web interface⁵. We used the “YBC+new Vega” bolometric corrections (Chen et al. 2019; Bohlin et al. 2020) to obtain photometric magnitudes in the 2MASS (Cohen et al. 2003) and *Gaia* (Riello et al. 2021) wavelength passbands.

For the ages of the isochrones, we considered two grids of ages: a logarithmically evenly spaced age grid between $10^{8.0} - 10^{8.95} \text{ yr}$ with 0.05 dex increments and a linearly evenly spaced age grid between 1–20 Gyr with 0.1 Gyr increments. The former was considered to densely populate the HR diagram with

isochrone grids, given that isochrones of young massive stars move quickly on the HR diagram. The latter was considered to determine the ages and accompanying errors as precisely as ~ 0.1 Gyr. The two grids are almost continuously connected at 1 Gyr; in other words, the step size of the former grid at 1 Gyr of $0.05 \ln 10 \sim 0.1$ Gyr is very similar to the interval in the latter grid.

For the initial metallicity, we considered the range from -0.5 to $+0.5$ dex with increments of 0.005 dex⁶. The interval of the initial-metallicity grid is equal to the minimum error in $[\text{M}/\text{H}]$ of our GSP-Spec Solar-twin sample.

In total, we retrieved $(20 + 191) \times 201 = 42411$ isochrone tracks. We only considered isochrone grid points with labels “0” (pre main sequence), “1” (main sequence), or “2” (subgiant branch) to reduce the data size of the isochrone library.

In the subsequent analysis, we used the following quantities tabulated in the isochrones: age τ , initial mass M_{ini} , current surface metallicity $[\text{M}/\text{H}]_{\text{curr}}$ ⁷, T_{eff} , $\log g$, and absolute magnitudes in the *Gaia* EDR3 G -band and 2MASS JHK_s -bands.

3.2. Bayesian age determination

As in several previous studies, we determined the age τ , initial mass M_{ini} , and initial metallicity $[\text{M}/\text{H}]_{\text{ini}}$ using a Bayesian isochrone projection method, weighting individual isochrone points. We used three sets of three observed quantities for the projection: T_{eff} , $[\text{M}/\text{H}]_{\text{curr}}$ ⁸, and one of the following three quantities: $\log g$, G -band absolute magnitude, or K_s -band absolute magnitude. The use of $[\text{M}/\text{H}]_{\text{curr}}$, rather than $[\text{M}/\text{H}]_{\text{ini}}$, is necessary because atomic diffusion changes the surface metallicity of a star from its initial metallicity, and hence changes the determined ages with the amount depending on the evolutionary phase (Christensen-Dalsgaard et al. 1996; Nissen 2016; Dotter et al. 2017). Atomic diffusion is indeed implemented in the PARSEC model used here, and the surface metallicity (i.e., common logarithm of the surface Z/X plus an offset) decreased by ~ 0.1 dex almost steadily during the main-sequence lifetime of a $1M_{\odot}$ model.

We calculated the weight w_i of each isochrone grid point i as

$$w_i \equiv p_i^{\tau} p_i^{M_{\text{ini}}} p_i^{[\text{M}/\text{H}]_{\text{ini}}} \exp\left(-\sum_k \frac{(\theta_{i,k} - \theta_k^{\text{obs}})^2}{2\sigma_{\theta_k^{\text{obs}}}^2}\right), \quad (1)$$

where k labels the three observed quantities, p_i^{τ} , $p_i^{M_{\text{ini}}}$, and $p_i^{[\text{M}/\text{H}]_{\text{ini}}}$ represent factors corresponding to priors, $\theta_{i,k}$ represents the value for the quantity k in the isochrone library, and θ_k^{obs} and $\sigma_{\theta_k^{\text{obs}}}$ represent the point estimate and accompanying error in the observed quantity k . Since Solar twins are located in a narrow region of stellar parameter space, we assumed flat priors in τ , M_{ini} , and $[\text{M}/\text{H}]_{\text{ini}}$. Thus, the factors p_i^{τ} , $p_i^{M_{\text{ini}}}$, and $p_i^{[\text{M}/\text{H}]_{\text{ini}}}$ were set

⁶ The zero-point in the initial-metallicity scale is assumed to be $(Z/X)_{\odot} = 0.0207$ as suggested by Bressan et al. (2012), who compiled literature Solar abundances from Grevesse & Sauval (1998), Caffau et al. (2011), and references therein.

⁷ We used $Y_S = 0.24787$ and $Z_S = 0.01597$ (Bressan et al. 2012), and hence $(Z/X)_S = 0.02169$ to set the zero-point in the current metallicity $[\text{M}/\text{H}]_{\text{curr}}$, which is different from the zero-point in the initial metallicity $[\text{M}/\text{H}]_{\text{ini}}$, $(Z/X)_{\odot} = 0.0207$. The use of $(Z/X)_S$ as the zero-point is intended to ensure that the Solar T_{eff} and $\log g$ can be reproduced with the Solar-age, Solar- $[\text{M}/\text{H}]_{\text{curr}}$ model.

⁸ For the observed $[\text{M}/\text{H}]_{\text{curr}}$ and its error, we corrected for the effect of $[\alpha/\text{Fe}]$ on isochrones using the equation in Salaris et al. (1993).

⁵ <https://stev.oapd.inaf.it/cgi-bin/cmd>

to the increments of the corresponding values in the isochrones. For example, since we retrieved an isochrone library sampled on a linear grid in $[M/H]_{\text{ini}}$, the value of $p_i^{[M/H]_{\text{ini}}}$ is constant across all isochrone points. The calculated weights assigned to individual isochrone points represent the discrete posterior distribution of the output quantities (τ , M_{ini} , and $[M/H]_{\text{ini}}$).

We note that in cases where the “calibrated” $\log g$ precision is smaller than 0.005 (46 stars), we assigned an uncertainty of 0.005 in calculating the weights, which corresponds to the minimum allowed error value in the “original” GSP-Spec catalog (i.e., those before the calibration in Appendix A), given that the $\log g_{\text{gspspec}}$ values are rounded to two decimal places. The maximum $\log g$ step in our isochrone grid is ~ 0.003 (Appendix B), which is smaller than the minimum assigned $\log g$ uncertainty of 0.005, and is therefore sufficiently fine to accurately project $\log g$ onto τ and M_{ini} . Similarly, we assigned an uncertainty of 0.005 dex to $[M/H]$ values with reported uncertainties smaller than 0.005 dex (4 stars)⁹. Since the maximum step sizes of our isochrone grid are ~ 4 K, 0.01 mag, and 0.01 mag for T_{eff} , M_G , and M_{K_s} , respectively (see, Appendix B), we adopted these values as uncertainties when the quoted observational errors were smaller (0, 2,745, and 0 stars, respectively).

To obtain the point estimates of the output quantities, we generated 10^6 Monte Carlo samples with replacement, where each sample i was selected with a probability proportional to its weight w_i . Since the isochrone library is discrete, the Monte Carlo samples drawn from them are also discrete. To recover continuity, we added Gaussian noise to each sample with standard deviations of 0.1 Gyr, $0.001 M_{\odot}$, and 0.005 dex for τ , M_{ini} , and $[M/H]_{\text{ini}}$, respectively, reflecting typical isochrone increments. We then adopted the 50.0, 15.8, and 84.2 percentiles as the median and 1σ uncertainties.

4. Validation of the age determination

We publish the full catalog of Solar twins (Table E.1) at CDS. Column descriptions are provided in Table E.2. In this section, we validate the determined ages in two ways: by testing whether we recover the age of the Sun (Sect. 4.1) and by comparing our observed catalog to a mock Solar-twin sample (Sect. 4.3). We also take a look at the determined age and M_{ini} (Sect. 4.2). We then discuss which of the three age estimates, i.e., those determined from $\log g$, M_G , and M_{K_s} , should be preferred in practice (Sect. 4.4).

4.1. Age of the Sun

The age of the Sun has been measured precisely using both helioseismology (Dziembowski et al. 1999; Bonanno et al. 2002; Houdek & Gough 2011) and radiometric dating of meteorites (Patterson 1956; Amelin et al. 2002; Bouvier & Wadhwa 2010). These studies concluded that the age of the Sun (or the Solar system) is ~ 4.5 –4.6 Gyr. Here, we apply our age-determination procedure to the Sun and check whether we can recover this age. We note that PARSEC isochrones version 1.2S were calibrated to reproduce Solar stellar parameters at an age

⁹ In our catalog of Solar twins, similar to the $\log g$ error, the errors in $[M/H]$ and $[\alpha/\text{Fe}]$ are quantized in 0.005 increments. Thus, there are 4 and 12 stars with the $[M/H]$ and $[\alpha/\text{Fe}]$ errors of 0.000 dex, respectively. Since we used the $[M/H]$ value with the effect of $[\alpha/\text{Fe}]$ on isochrones corrected, the error in the adopted (or corrected) “[M/H]” values are not in increments of 0.005.

Table 1: Recovered age, M_{ini} , and $[M/H]_{\text{ini}}$ of the Sun.

Input	Age τ [Gyr]	Initial mass M_{ini} [M_{\odot}]	Initial metallicity $[M/H]_{\text{ini}}$ [dex] ^a
$([M/H]_{\text{curr}}, T_{\text{eff}}, \log g)$	$4.53_{-0.24}^{+0.23}$	$0.9984_{-0.0026}^{+0.0026}$	$0.0828_{-0.0070}^{+0.0070}$
$([M/H]_{\text{curr}}, T_{\text{eff}}, M_G)$	$4.47_{-0.25}^{+0.25}$	$0.9985_{-0.0028}^{+0.0027}$	$0.0821_{-0.0067}^{+0.0067}$
$([M/H]_{\text{curr}}, T_{\text{eff}}, M_{K_s})$	$4.34_{-0.23}^{+0.23}$	$0.9989_{-0.0027}^{+0.0027}$	$0.0805_{-0.0067}^{+0.0067}$

Notes. ^(a) Zero-point of $[M/H]_{\text{ini}}$ is $(Z/X)_{\odot} = 0.0207$, which is different from the zero-point of $[M/H]_{\text{curr}}$, $(Z/X)_S = 0.02169$.

of 4.593 Gyr (Table 3 of Bressan et al. 2012), and thus our procedure should accurately recover the Solar age if our implementation is correct.

As inputs for the Solar parameters, we adopted $M_{G,\odot} = 4.66$ (see, Creevey et al. 2023, which adopt the Solar bolometric absolute magnitude $M_{\text{bol},\odot} = 4.74$ from Prša et al. 2016) and $M_{K_s,\odot} = 3.27$ (Willmer 2018). We also used reference Solar values given in Sect. 2.1, namely, $T_{\text{eff},\odot} = 5777$ K, $\log g_{\odot} = 4.44$, $[M/H]_{\text{curr},\odot} = 0.0$ dex, and $[\alpha/\text{M}]_{\text{curr},\odot} = 0.0$ dex. The uncertainties in the input values were assumed to be 0.01 mag for $M_{G,\odot}$ and $M_{K_s,\odot}$, 4 K for $T_{\text{eff},\odot}$, 0.005 for $\log g_{\odot}$, 0.005 dex for $[M/H]_{\text{curr},\odot}$, as in Sect. 3.2 for cases with very small errors.

The recovered Solar age is summarized in Table 1. We found that the recovered Solar age is consistent with the literature value in all cases where $\log g$, M_G , or M_{K_s} is used as input. We also found that the recovered Solar M_{ini} is consistent with $1M_{\odot}$.

As expected, the recovered Solar $[M/H]_{\text{ini}}$ is 0.08 dex (or 0.06 dex when adopting the zero-point used for $[M/H]_{\text{curr}}$), which is higher than the Solar surface value by $\sim 10\sigma$. This offset reflects the decrease in surface metallicity with age in the $1M_{\odot}$ PARSEC model at a rate of ~ 0.015 dex Gyr $^{-1}$. This level of atomic diffusion has been supported by homogeneous spectroscopy of cluster stars; e.g., in the Solar-metallicity, Solar-age open cluster M67 (Bertelli Motta et al. 2018; Souto et al. 2019; Liu et al. 2019).

For comparison, we also determined the age of the Sun under the assumption that the observed $[M/H]$ is equal to $[M/H]_{\text{ini}}$. In that case, the recovered age is $5.49_{-0.27}^{+0.27}$, $6.28_{-0.30}^{+0.29}$, or $6.09_{-0.28}^{+0.28}$ Gyr when using $\log g$, M_G , or M_{K_s} , respectively. As expected, these values deviate significantly from the true Solar age, demonstrating the importance of treating $[M/H]$ and atomic diffusion consistently when determining ages.

4.2. Overview of the determined Solar-twin parameters

Figure 2 shows the scatter plots between the age and initial mass M_{ini} for our Solar-twin catalog. If the isochrone library retrieved from the CMD 3.8 web interface were used without further interpolation, stars would concentrate at discrete M_{ini} values, producing strip-like density patterns corresponding to the coarse initial-mass grid ($0.05M_{\odot}$ spacing). In contrast, thanks to the fine interpolation of the PARSEC isochrones described in Appendix B, no such artificial striping is visible in our results.

Our Solar twins occupy a limited region in the age– M_{ini} plane in two respects. First, the M_{ini} values lie within ~ 0.9 – $1.1 M_{\odot}$, reflecting the fact that we only analyzed Solar twins, i.e., main-sequence stars around the Solar T_{eff} . Second, there are no stars in the upper-right region (older and more massive stars). Stars in that region would have already evolved off the main sequence; for example, the main-sequence lifetime of a $1M_{\odot}$ star is ~ 10 Gyr.

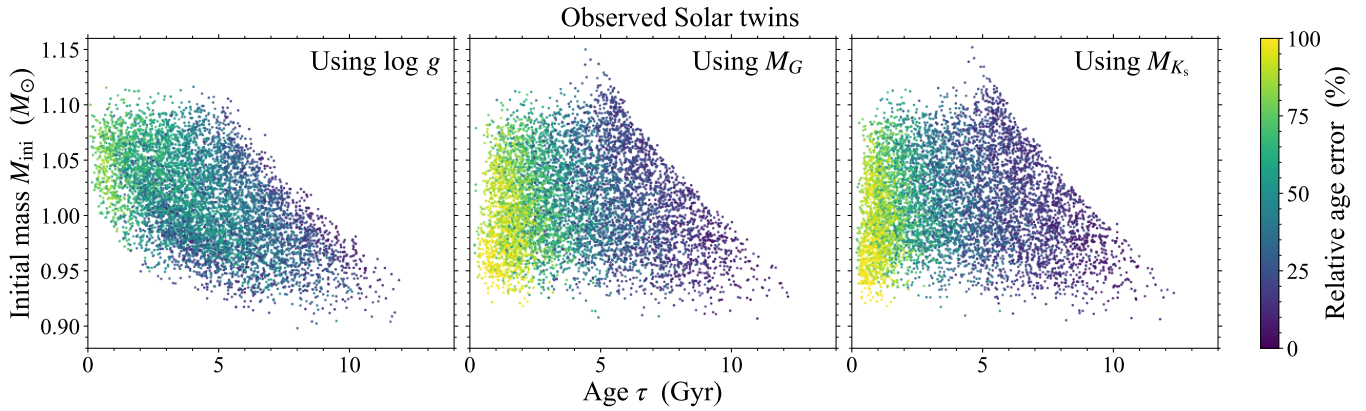


Fig. 2: Recovered parameters in the resulting observed Solar-twin catalog. Each panel shows a scatter plot between the determined age τ and initial mass M_{ini} , color-coded by the relative age error. Left, middle, and right panels show the results obtained when using $\log g$, M_G , and M_{K_s} , respectively, as the third input parameter in addition to $[\text{M}/\text{H}]_{\text{curr}}$ and T_{eff} .

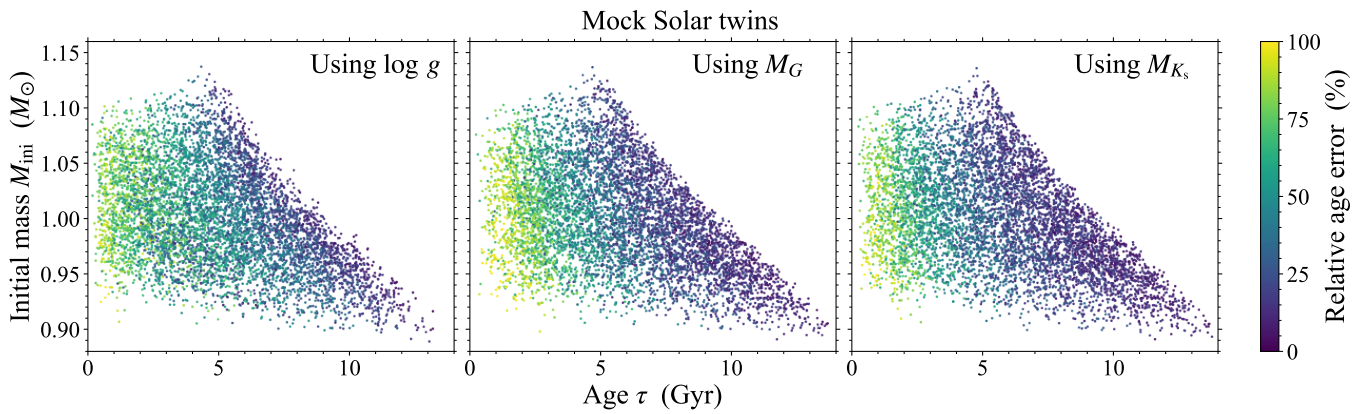


Fig. 3: Recovered parameters in the mock catalog of Solar twins. We show only random 6,594 mock stars, i.e., the same number of stars as in the observed Solar-twin catalog. All the panels are defined in the same way as in Fig. 2.

There is also a strong dependence of the relative age error on age and M_{ini} . Older stars and stars with higher M_{ini} have smaller relative age errors. These stars lie more closely to the main-sequence turn-off, where isochrones move rapidly on the HR diagram, and hence ages can be more tightly constrained. Within this general trend, the decrease in relative age error toward older ages is clearly seen for the M_G -based and M_{K_s} -based ages, but is less apparent for the $\log g$ -based ages, especially at young ages, where the behavior appears more scattered. This difference may be related to the calibration of $\log g$ (Appendix A), in which the original-calibrated relation becomes nearly flat at high $\log g$ (i.e., for young stars). This flattening can reduce the propagated calibrated $\log g$ uncertainties for young stars and may affect the relative age errors derived from $\log g$.

4.3. Comparison with mock Solar twins

As we saw in Sect. 4.2, there are selection effects in our Solar-twin catalog. Any analysis based on the catalog needs to account for selection effects and the distribution of age errors. To facilitate this, we here constructed a mock Solar-twin catalog that mimics our observed selection function (Sect. 4.3.1), and then compared the observed and mock samples (Sect. 4.3.2).

4.3.1. Creation of a mock Solar-twin sample

We constructed a mock sample of Solar twins as follows. First, we sampled stars across the age– M_{ini} grid points of the PARSEC isochrone library used in Sect. 3 for age determination. At each grid point, stars were sampled from a uniform distribution in age and $[\text{M}/\text{H}]_{\text{ini}}$, with a density of 4×10^8 stars $\text{Gyr}^{-1} \text{dex}^{-1}$. This corresponds to, for example, for ages > 1 Gyr, where the grid spacing is 0.1 Gyr in age and 0.005 dex in $[\text{M}/\text{H}]_{\text{ini}}$ (Sect. 3.1), 4×10^5 stars per grid point.

The initial mass M_{ini} of each star was sampled from the Kroupa (2001) initial mass function (IMF). The distance D to each star was sampled between 20–350 pc assuming an uniform underlying spatial density, corresponding to a probability distribution proportional to D^2 . Other stellar parameters (i.e., T_{eff} , $\log g$, $[\text{M}/\text{H}]_{\text{curr}}$, and absolute magnitudes in the G and K_s bands) of each star were assigned by interpolating the PARSEC isochrones.

The α abundance $[\alpha/\text{Fe}]$ was assigned using the linear age– $[\text{Ca}/\text{Fe}]$ relation from Bedell et al. (2018), because GSP-Spec $[\alpha/\text{Fe}]$ closely tracks $[\text{Ca}/\text{Fe}]$ (Recio-Blanco et al. 2023, 2024). We then computed an “observed” $[\text{M}/\text{H}]$ value, i.e., without correcting for the effect of $[\alpha/\text{Fe}]$ on the isochrones using the equation from Salaris et al. (1993).

Sky coordinates were assigned assuming an uniform distribution over the celestial sphere. G -band extinction A_G was es-

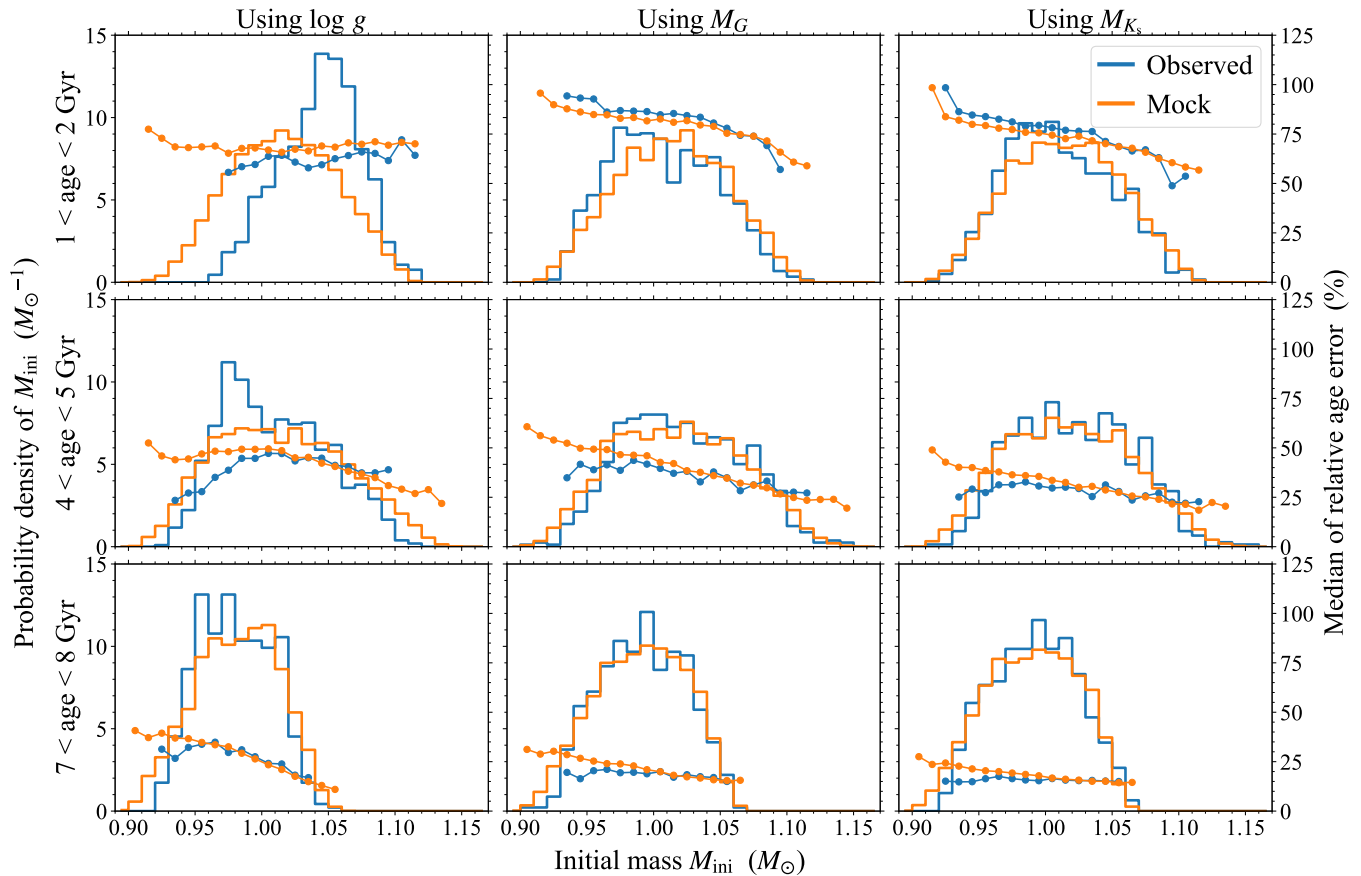


Fig. 4: Comparison between the observed (blue) and mock (orange) Solar-twin catalogs in different age bins. Top, middle, and bottom panels show results for twins with the determined ages between 1–2, 4–5, and 7–8 Gyr, respectively. Left, middle, and right panels correspond to ages determined using $\log g$, M_G , and M_{K_s} , respectively, as the third input parameter, together with $[\text{M}/\text{H}]_{\text{curr}}$ and T_{eff} . In each panel, the histograms show the probability density of the initial mass M_{ini} (i.e., the normalized number of twins per M_{ini} bin), while line plots show the median relative age errors in each M_{ini} bins.

timated using the 3D dust map of Leike et al. (2020) as implemented in the `dustmaps` code (Green 2018; Green et al. 2019), and the apparent G -band magnitude was then computed. Because the 3D dust map of Leike et al. (2020) has a finite spatial coverage of $740 \text{ pc} \times 740 \text{ pc} \times 540 \text{ pc}$, some mock stars between 270–350 pc fall outside the map and therefore have undefined A_G . For such stars, new sky coordinates were repeatedly assigned until A_G could be estimated.

Given the apparent G -band magnitude, we then assigned S/N and observational uncertainties according to Equations C.1 and C.2, respectively, adding Gaussian scatter to reproduce the observed dispersion around these relations (see, Appendix C for more details).

Finally, we applied to the noise-added mock catalog the same selection criteria used for the real Solar twins. That is, we required T_{eff} , $\log g$, and $[\text{M}/\text{H}]$ to be close to the Solar values (Sect. 2.1), small errors in these parameters and in $[\alpha/\text{Fe}]$ (Sect. 2.1), and consistency of M_G and M_{K_s} as being Solar twins (Sect. 2.4). In this way, selection effects such as the Malmquist bias are embedded in the mock sample.

This procedure yielded a mock Solar-twin catalog consisting of 75,588 artificial stars, more than ten times the size of the observed Solar-twin sample (6,594 stars). We note that the number of stars passing the selection depends on age. For example, the number of selected stars with ages between 10–11 Gyr is ~ 2.5

times smaller than that with ages between 5–6 Gyr, because the range of M_{ini} values satisfying the Solar-twin selection criteria becomes narrower at older ages. We then determined the ages of these mock stars using exactly the same procedure as for the observed stars in Sect. 3.2.

4.3.2. Comparison of observed and mock Solar twins

Figure 3 shows the scatter plots between age and M_{ini} of for the mock Solar-twin catalog. In this figure, we display only 6,594 stars randomly drawn from the full set of 75,588 mock twins, so that the number of plotted stars matches that of the observed sample in Fig. 2. We found that the overall shape of the distribution and the dependence of relative age error on age and M_{ini} are very similar between the observed and mock samples, confirming the overall good accuracy in our Solar-twin catalog.

The observed catalog contains fewer old stars ($\gtrsim 10$ Gyr) than the mock catalog. This difference likely reflects the underlying age distribution: we assumed a flat age distribution in the mock sample, whereas the observed sample may have a non-flat age distribution due to the star-formation history and radial migration. This topic is investigated in detail in our companion paper (Paper II; Tsujimoto et al. 2026).

To assess our Solar-twin catalog more closely, we divided both the observed and mock samples into 1 Gyr age bins and

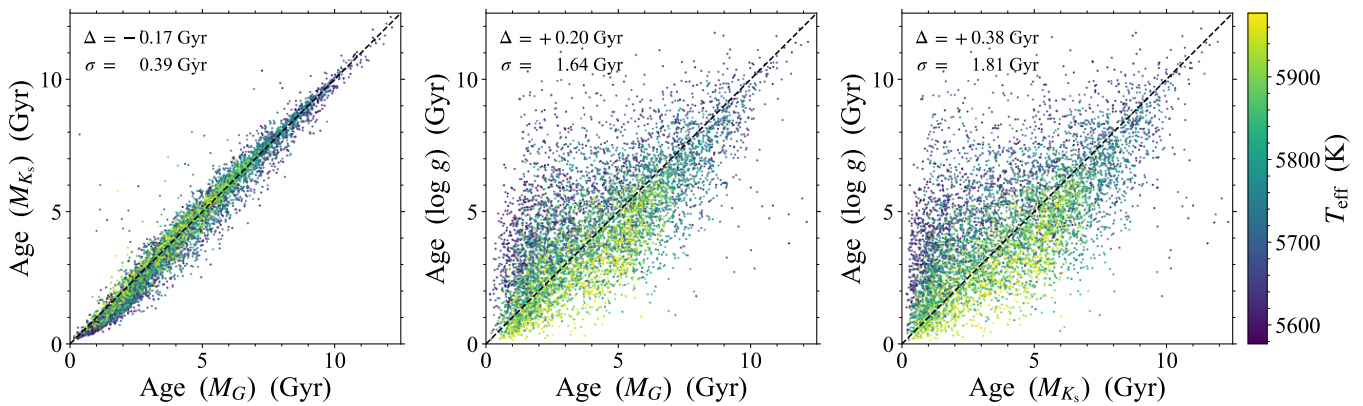


Fig. 5: Comparison between the Solar-twin ages determined with $\log g$, M_G , and M_{K_s} , color-coded with T_{eff} .

examined the Solar-twin mass function, i.e., the number of Solar twins at each M_{ini} within a given age bin. Given the relatively narrow age bins, the mass function should be similar between the observed and mock samples as long as the assumed IMF and stellar-evolution model are accurate and the efficiency of radial migration does not depend strongly on stellar mass.

Histograms in Fig. 4 show the Solar-twin mass function for the observed (blue) and mock (orange) samples. For the ages determined using M_G or M_{K_s} (middle and right panels, respectively), the observed and mock histograms are nearly identical in shape. This agreement suggests that our determinations of age and M_{ini} based on M_G or M_{K_s} are accurate. In contrast, the histograms for ages based on $\log g$ (left panels) show significant differences, especially at younger ages (top and middle panels). This discrepancy could be due to a residual systematic bias in $\log g$, which we will discuss in Sect. 4.4.

We also examined the median relative age error in each M_{ini} bin for each age bin as a function of M_{ini} (line plots in Fig. 4; again, blue for the observed sample and orange for the mock sample). At high mass ($M_{\text{ini}} \gtrsim 0.95M_{\odot}$), the observed and mock age errors behave similarly, confirming that the error prescriptions in the mock sample well reproduce those in the observed sample. At lower masses, however, we found differences in the median relative age error of up to $\sim 20\%$. Detailed comparisons between the observed and mock samples revealed that this difference arises from the dependence of metallicity on the distance present in the observed sample. In the observed catalog, there is a weak tendency for metal-rich stars (within our narrow metallicity range of ± 0.1 dex around the Solar value) to lie at larger distances (and hence to have lower S/N and larger errors), regardless the direction, though the origin of this trend is unclear. No such trend appears in the mock sample. Because, for $M_{\text{ini}} \lesssim 0.95M_{\odot}$, stars with higher metallicity do not satisfy the Solar-twin selection criteria due to the metallicity dependence of T_{eff} , the lower-mass bins are dominated by lower-metallicity stars in the observed sample. These stars tend to lie at closer distances and therefore have smaller errors, resulting in smaller median relative age error for the observed sample than the mock sample at lower masses. This tendency should be kept in mind when analyzing our catalog.

4.4. Comparison of the three age determinations

Figure 5 compares the ages of Solar twins determined using $\log g$, M_G , and M_{K_s} . As shown in the left panel, the ages derived from M_G and M_{K_s} agree very well. The mean bias and

standard deviation are -0.17 and 0.39 Gyr, respectively, both of which are much smaller than the typical age uncertainties of 2.8 and 2.2 Gyr for the M_G - and M_{K_s} -based ages. This is expected because both M_G and M_{K_s} are tied to the bolometric luminosity L_{bol} through the bolometric corrections implemented in the isochrone library (Chen et al. 2019; Bohlin et al. 2020), and hence both sets of ages are essentially determined by T_{eff} , [M/H], and L_{bol} . In other words, the close agreement between M_G - and M_{K_s} -based ages supports the accuracy of the adopted bolometric corrections.

A small number of outliers deviate from this one-to-one relation between M_G and M_{K_s} -based ages, most of them having M_{K_s} -based ages larger than those from M_G . Though the exact cause is unclear, unresolved multiplicity in 2MASS likely plays a role. *Gaia* photometry resolves these multiple systems that are unresolved in 2MASS due to its poorer spatial resolution. In such cases, the K_s magnitude could be biased by unresolved companions, making stars appearing brighter and, hence, older in the M_{K_s} -based age estimates.

Middle and right panels of Fig. 5 show the ages based on $\log g$ against those based on M_G and M_{K_s} , respectively. In both panels, there is a large scatter around the one-to-one line (1.64 and 1.81 Gyr, respectively), and the relation between the two age estimates depends on T_{eff} . Since $\log g$ is related to L_{bol} via the Stefan-Boltzmann law, and we have already demonstrated the reliability of the bolometric corrections linking L_{bol} to M_G and M_{K_s} , any model-related uncertainties would affect all three age estimates in a similar way. Hence, the scatter could be due to a T_{eff} -dependent systematic bias in $\log g$, which we could not fully correct in Sect. 2.1 and Appendix A.

As discussed in this section and in Sect. 4.3.2, a residual systematic bias in $\log g$ appears to remain despite our calibration efforts. This likely reflects the difficulty of determining spectroscopically $\log g$ accurately. Unlike absolute magnitudes, which can be determined accurately from photometry and astrometry when extinction is not severe, determinations of $\log g$ requires specific spectral features such as combinations of neutral and ionized lines from a specific element and/or the wings of very strong lines (Gray 2005). In our case, GSP-Spec $\log g$ is primarily constrained by the wings of the Ca II IR triplet, weak metallic lines, and molecular lines (Recio-Blanco et al. 2016), and the limited wavelength coverage associated to a medium spectral resolution of RVS makes the problem challenging. Indeed, we found a systematic trend between the original GSP-Spec $\log g$ estimates and literature $\log g$ values based on higher-resolution, wider-wavelength-coverage spectra (Appendix A). If

a sufficiently large calibration sample densely covering the T_{eff} – $\log g$ plane would have been available, this bias could be removed more accurately, but with only a few dozen stars in common, the calibration remains not enough accurate when examining tiny effects.

Given these difficulties in determining $\log g$, we do not recommend using our $\log g$ -based ages for statistical analysis of the sample. In contrast, both the M_G - and M_{K_s} -based ages appear sufficiently reliable for such applications. Either can be used, but M_G -based ages have the advantage that *Gaia* offers higher spatial resolution, thereby reducing the risk of age overestimation due to unresolved companions. On the other hand, M_{K_s} -based ages are less sensitive to extinction. Since in our companion paper, [Tsujimoto et al. \(2026, Paper II\)](#) adopted the M_{K_s} -based age for their analysis, for which selection effects are weaker, we will also use the M_{K_s} -based ages in the subsequent discussion of this paper.

5. Comparison with previous Solar-twin catalogs

In this section, we first compare our Solar-twin catalog with literature, in particular focusing on the number of twins in each sample (Sect. 5.1). Then, we compare different sets of stellar parameters, ages, and M_{ini} , to further validate our catalog and to place this work in the context of previous Solar-twins studies (Sect. 5.2).

5.1. Properties of the literature and this Solar-twin catalogs

Table 2 summarizes information on our catalog of Solar twins along with that of a (comprehensive but not complete) compilation of literature studies based on high-resolution spectroscopy. We mostly included studies that determined stellar parameters by themselves and that mainly focused on Solar twins (or at least Solar analogs).

As shown in the table, most catalogs contain only a limited number of Solar twins (typically several tens), but in some of these catalogs the stellar parameters are measured with very high precision, if we consider the reported uncertainties. Many recent catalogs are based on archival spectra from the HARPS spectrograph ([Mayor et al. 2003](#)), originally obtained for exoplanet searches. By stacking time-series spectra, HARPS data provide extremely high spectral resolution ($R = 115,000$) and S/N of $\sim 1,000$ over most of its wide 378–691 nm wavelength range, and hence extremely high precision in the derived stellar parameters and chemical abundances (e.g., 10 K in T_{eff} , 0.02 in $\log g$, and 0.01 dex in [Fe/H] and other abundances, in the work by [Martos et al. 2025](#), see Table 2 for precisions in other studies). Such small but highly precise and accurate samples are particularly valuable for identifying stars whose parameters must be determined with high accuracy relative to the Solar values. For example, “true” Solar twins, defined as stars whose parameters are not only close to those of the Sun, as in ordinary Solar twins, but effectively indistinguishable within very small uncertainties (e.g., ~ 10 K in T_{eff}), have been sought for many years (e.g., [Porto de Mello & da Silva 1997](#); [Meléndez & Ramírez 2007](#)). Another example is the search for Solar siblings, i.e., stars whose ages and chemical abundances are identical to those of the Sun, and which therefore could have formed in the same star cluster as the Sun (e.g., [Adibekyan et al. 2018](#)). Since cluster-to-cluster dispersions (or azimuthal scatter) in chemical abundances are suggested to be of the order of a few hundredths of a dex (e.g., [Freeman & Bland-Hawthorn 2002](#); [Bellardini et al. 2021](#); [Bhattarai et al. 2024](#), and references therein), searching

for Solar siblings (or, in other words, carrying out strong chemical tagging) requires this level of precision and accuracy in abundance determinations. In general-purpose spectroscopic surveys with moderate S/N, in contrast to high-precision Solar-twin studies, the achievable precision and accuracy for individual stars are still insufficient for this purpose (e.g., [Casamiquela et al. 2021](#); [Ness et al. 2022](#)).

In contrast, our work and a few recent studies have constructed large samples by homogeneously exploiting recent huge datasets from general-purpose spectroscopic surveys: *Gaia* DR3 GSP-Spec in this study, *Gaia* DR3 RVS in [Rampalli et al. \(2024\)](#), and GALAH DR3 in [Walsen et al. \(2024\)](#) and [Lehmann et al. \(2025\)](#). Stellar parameters and chemical abundances of $\sim 1,700$ Solar twins from APOGEE DR16 were also used by [Nibauer et al. \(2021\)](#). Such samples are generally limited in wavelength coverage, spectral resolution, and/or S/N, and thus the achievable precisions and accuracies in stellar parameters are lower. For example, in our case with *Gaia* DR3 GSP-Spec, RVS spectra cover only 846–870 nm with $R = 11,500$, and the median S/N per pixel (`rv_expected_sig_to_noise`) is 83¹⁰. As a result, the precision of the derived stellar parameters degrades to 51 K in T_{eff} , 0.05 in $\log g$, 0.03 dex in [M/H], and ~ 0.1 dex in other abundances.

Nevertheless, the ~ 100 times larger sample size (6,594 stars in our case), even with a lower precision, enables us to investigate the statistical properties of Solar twins, such as the age–abundance relation, with comparable significance, as demonstrated in Sect. 6. Moreover, only such large samples allow us to study the density distributions of stellar parameters for Solar twins, including the probability density of M_{ini} at a given age (as shown in Fig. 4) and the probability density of ages (presented in our companion paper, Paper II; [Tsujimoto et al. 2026](#)).

To date, all previous large Solar-twin samples ([Rampalli et al. 2024](#); [Walsen et al. 2024](#); [Lehmann et al. 2025](#)) relied on data-driven approaches to determine stellar parameters and chemical abundances (see, Appendix D, for an in-depth review of their methods and results). As a result, they achieved internal precisions that are comparable to or higher than those in our GSP-Spec study, in which a traditional spectral-fitting technique was used. However, as a trade-off, some of their reported results may reflect correlations learned from the training data, since data-driven approaches infer, rather than directly measure, chemical abundances. Indeed, [Rampalli et al. \(2024\)](#) pointed out that their model inferred the abundances of C, O, Na, V, Al, and Y, even though no atomic lines of these elements with sufficient strengths are present in the *Gaia* RVS spectra of Solar twins, and abundances of these elements are not included in the GSP-Spec catalog¹¹. Further indications that data-driven inferences may be influenced by training-set correlations are discussed in Sects. 5.2 and 6.2. Catalogs with model-driven abundances therefore offer a complementary way to validate data-driven results.

In light of these previous large-sample studies of Solar twins, all of which rely on data-driven methods, our catalog based on

¹⁰ Given the oversampling of *Gaia* RVS, this translates into the median S/N per spectral resolution element of ~ 140 .

¹¹ Because CN molecular lines are present in the RVS wavelength range ([Recio-Blanco et al. 2024](#)), and their strengths depend on the C, N, and O abundances through temperature-dependent molecular equilibrium (see, e.g., [Yong et al. 2015](#); [Taniguchi et al. 2025](#)), the RVS spectra in principle contain information on the C and O abundances. Nevertheless, judging from Fig. A1 in [Rampalli et al. \(2024\)](#), their derived [C/H] and [O/H] abundances do not appear to rely strongly on CN lines.

Table 2: Solar twin catalogs adopted for comparison (incomplete manual compilation).

Paper	Spectrograph	Typical error			# samples		Available?	
		T_{eff} [K]	$\log g$	[M/H]	N_{total}^a	N_{twin}^b	Age	Abundances ^c
This work	<i>Gaia</i> DR3 GSP-Spec	51	0.05	0.03	6594	6594	Yes	Yes
Lehmann et al. (2025) ^d	GALAH DR3	38	0.03	0.02	72288	14571	Yes	
Walsen et al. (2024) ^d	GALAH DR3	4	0.01	0.00	38320	13132	^e	Yes
Rampalli et al. (2024) ^d	<i>Gaia</i> DR3 RVS	61	0.09	0.04	17412	5347	Yes	Yes
Sun et al. (2025a)	MIKE	22	0.05	0.01	25	13	Yes	Yes
Carlos et al. (2025)	HARPS		0.02	0.01	50	10	Yes	Yes
Martos et al. (2025)	HARPS	10	0.02	0.01	99	61		Yes
Carvalho-Silva et al. (2025)	HARPS	7	0.02	0.01	126	7	Yes	
Sun et al. (2025b)	MIKE	20	0.05	0.01	17	7	Yes	Yes
Plotnikova et al. (2024)	HARPS	9	0.03	0.01	130	48	Yes	Yes
Shejelammal et al. (2024)	HARPS	5	0.02	0.01	233	83	Yes	Yes
Rathsam et al. (2023)	HARPS	6	0.02	0.01	74	17	Yes	
Martos et al. (2023)	HARPS	4	0.01	0.00	118	62	Yes	
Lehmann et al. (2023) ^d	HERMES	77	0.06	0.04	877	99	Yes	
Spina et al. (2021)	HARPS	10	0.03	0.01	60	10	Yes	Yes
Yana Galarza et al. (2021)	Goodman/ARCES/2dcoude	11	0.03	0.01	129	58	Yes	
Nissen et al. (2020)	HARPS	9	0.02	0.01	72	27	Yes	Yes
Liu et al. (2020)	HIERES	14	0.03	0.01	83	7	Yes	Yes
Casali et al. (2020)	HARPS	8	0.02	0.01	560	223	Yes	Yes
Delgado Mena et al. (2019)	HARPS				1059	93	Yes	
Lorenzo-Oliveira et al. (2018)	HARPS	4	0.01	0.00	82	64	Yes	
Adibekyan et al. (2018)	HARPS/UVES/FEROS	26	0.04	0.02	54	17	Yes	Yes
Bedell et al. (2018)	HARPS				79	64	^f	Yes
Spina et al. (2018)	HARPS	4	0.01	0.00	79	64	Yes	Yes
Delgado Mena et al. (2017)	HARPS	28	0.04	0.02	1059	93	Yes	
Reddy & Lambert (2017)	HARPS				24	22	Yes	Yes
Beck et al. (2017)	HERMES	70	0.15	0.04	18	3	Yes	
López-Valdivia et al. (2017)	CanHIS	59	0.27	0.08	38	5		Yes
Spina et al. (2016a)	UVES	3	0.01	0.00	9	9	Yes	Yes
Nissen (2016)	HARPS	6	0.01	0.01	21	18	Yes	Yes
Adibekyan et al. (2016)	HARPS/UVES	22	0.03	0.02	39	9	Yes	Yes
Tucci Maia et al. (2016)	MIKE	6	0.02	0.01	88	75	Yes	Yes
Mahdi et al. (2016)	ELODIE	10	0.02	0.01	56	40	Yes	Yes
Spina et al. (2016b)	HIERES	10	0.03	0.01	14	14	Yes	Yes
Nissen (2015)	HARPS	6	0.01	0.01	21	18	Yes	Yes
Datson et al. (2015)	FEROS	40	0.07	0.03	148	77		
Gonzalez (2015)	Sandiford	50	0.07	0.04	31	6	Yes	
Ramírez et al. (2014)	MIKE	6	0.02	0.01	88	75	Yes	
López-Valdivia et al. (2014)	B&C	50	0.25	0.06	233	34		
Gonzalez (2014)	Sandiford/2dcoude	40	0.06	0.03	37	13	Yes	Yes
Porto de Mello et al. (2014)	OPD/FEROS				55	29	Yes	
Tsantaki et al. (2013)	HARPS	23	0.06	0.02	451	38	Yes	
Adibekyan et al. (2012)	HARPS				1111	93	Yes	
da Silva et al. (2012)	CTIO				25	7	Yes	Yes
Sousa et al. (2011)	HARPS	35	0.05	0.02	582	49		
González Hernández et al. (2010)	HARPS/UVES/UES	31	0.04	0.02	11	1		Yes
Ghezzi et al. (2010)	FEROS	38	0.13	0.03	262	22	Yes	
Baumann et al. (2010)	2dcoude/HARPS	39	0.06	0.03	117	65	Yes	
Gonzalez et al. (2010)	2dcoude	33	0.05	0.02	159	18	Yes	Yes
Ramírez et al. (2009)	2dcoude			0.02	64	37	Yes	
Neves et al. (2009)	HARPS				451	44	Yes	
Pasquini et al. (2008)	FLAMES	60			59	36 ^g		
Sousa et al. (2008)	HARPS	24	0.04	0.02	451	44		
Meléndez & Ramírez (2007)	2dcoude	36	0.04	0.02	4	4	Yes	
Takeda et al. (2007)	HIDES				118	55	Yes	
Meléndez et al. (2006)	HIERES	30	0.03	0.03	2	2	Yes	Yes
Laws et al. (2003)	2dcoude/CTIO	44	0.07	0.03	31	3	Yes	
Gonzalez et al. (2001)	2dcoude/CTIO	39	0.07	0.03	22	1	Yes	Yes

Notes. ^(a) Total number of targets analyzed. ^(b) Number of targets satisfying our Solar-twin criteria (T_{eff} , $\log g$, and [M/H] within ± 200 K, ± 0.2 , and ± 0.1 dex around the Solar values, respectively). ^(c) We did not mark studies that provide abundances for only a very limited set of elements (e.g., Li only) as having abundances available. ^(d) Using a data-driven method for determining stellar parameters. ^(e) Walsen et al. (2024) adopted ages from GALAH DR3 (Sharma et al. 2018; Buder et al. 2021). ^(f) Bedell et al. (2018) adopted ages determined by Spina et al. (2018). ^(g) We only considered T_{eff} in calculating N_{twin} for Pasquini et al. (2008) because they did not determine [Fe/H] and $\log g$ of their M67 stars.

Gaia DR3 GSP-Spec aims to provide a large, homogeneous catalog in which all stellar parameters, age, and elemental abundances are determined from forward modeling based on stellar atmosphere and evolutionary models, rather than inferred solely through data-driven methods, thereby avoiding the propagation of trends learned from small training samples. In this way, we

aim to provide a basis for confirming results previously obtained from small, high-precision samples (e.g., age-[X/Fe] relations) in a scaled, statistical manner, as demonstrated in Sect. 6. Moreover, our characterization of the selection function (Sect. 4.3) facilitates analyses that are sensitive to selection effects (e.g., the interpretation of histograms). Taken together, our catalog

offers model-driven parameters with a characterized selection function, serving as a complementary reference to both small high-precision samples and large data-driven samples.

Beyond differences in the sample size and analysis methods, some of the previous studies adopted rather loose criteria on [M/H] when defining Solar twins. For example, Lehmann et al. (2025) allowed stars with any [Fe/H] to be included in their sample. Such a loose criterion on [M/H] helps to investigate trends with metallicity and to enlarge the sample size without introducing large systematic uncertainties in chemical abundances. However, our strict criterion on [M/H], namely ± 0.1 dex around the Solar value, is essential for associating age with birth radius (Minchev et al. 2013; Plotnikova et al. 2024). With such a criterion, the age–[X/Fe] relation for Solar twins can effectively provide information on the relation between birth radius and [X/Fe] at a given metallicity. Our moderately strict threshold on $\log g$ of ± 0.2 dex around the Solar value is also important for selecting only main-sequence stars, in contrast to some recent studies (e.g., ± 0.3 dex around the Solar value adopted by Walsen et al. 2024; Rampalli et al. 2024).

5.2. Comparison of stellar parameters, ages, and initial mass

Figures 6 and 7 show comparisons of stellar parameters (T_{eff} , $\log g$, and [M/H] or [Fe/H]), age, and M_{ini} between this work and selected literature; Fig. 6 for the studies used for the calibration of zero-points in Appendix A (Tucci Maia et al. 2016; Nissen et al. 2020; Shejelammal et al. 2024) and Fig. 7 for the studies building large catalogs using spectra from general-purpose spectroscopic surveys (Rampalli et al. 2024; Walsen et al. 2024; Lehmann et al. 2025)¹². We plotted only stars whose three parameters from both this work and the literature satisfy the Solar-twin criteria, regardless of their errors. We note that we plot the calibrated stellar parameters in these figures, rather than the original parameters shown in Fig. A.1.

In Fig. 6, we found good agreement in all five parameters with those reported by Tucci Maia et al. (2016), Nissen et al. (2020), and Shejelammal et al. (2024). The mean and standard deviation of the differences between our parameters and those from the literature are annotated in each panel. The agreement for the stellar parameters (T_{eff} , $\log g$, and [M/H]) is expected, given that we calibrated our stellar parameters against these three studies. The agreement for age and M_{ini} supports the reliability of our isochrone projection. We found similar agreements with many other studies.

In contrast, we found discrepancies with several other studies, most notably those based on large Solar-twin samples, namely Walsen et al. (2024), Lehmann et al. (2025), and Rampalli et al. (2024), as shown in Fig. 6. In the studies by Walsen et al. (2024) and Lehmann et al. (2025), [Fe/H] values are systematically 0.08 and 0.04 dex, respectively, lower than our [M/H], and hence the ages in Lehmann et al. (2025) are systematically 1.5 Gyr larger than ours. These systematic differences may be due to the fact that the two studies employed stellar parameters from GALAH DR3 and DR2, respectively, as training references for their data-driven analyses, which possibly have systematic zero-point biases, or at least zero points that differ from those in many high-precision Solar-twin studies¹³.

¹² Comparisons to all the literature listed in Table 2 are available in Fig. E.2 and at Zenodo (<https://doi.org/10.5281/zenodo.XXXXXXX>).

¹³ Ideally, the stellar parameters reported by Walsen et al. (2024) and Lehmann et al. (2025) would be directly compared with those

In our comparison with Rampalli et al. (2024), we found weak correlations between the two studies for $\log g$, [M/H], and age¹⁴, even though both studies are based on *Gaia* DR3 RVS spectra. In particular, whereas our ages remain consistent with those from high-precision studies down to very young ages ($\lesssim 1$ Gyr; see Fig. 6), the ages reported by Rampalli et al. (2024) show an apparent lower limit of ~ 2 –3 Gyr. As a result, stars that we identify as very young Solar twins are generally assigned significantly older ages in their study, contributing to the weak overall correlation. Because most of the stars analyzed by Rampalli et al. (2024) do not overlap with high-precision Solar-twin samples, it remains unclear whether the observed scatter in stellar parameters and age between our results and those by Rampalli et al. (2024) can be fully explained by the combined statistical uncertainties, or whether additional systematic uncertainties are present.

6. Age–chemical abundance trends

The precise and accurate chemical abundances of Solar twins have been used to address various astronomical questions, from planet–host interactions to the chemodynamical evolution of the Milky Way (see, references in Sect. 1). [X/Fe] abundances, rather than [X/H], are particularly useful for these purposes, because the surface [X/Fe] ratios for most elements change by only <0.004 dex during main-sequence stellar evolution (Turcotte & Wimmer-Schweingruber 2002), which is markedly smaller than the change in surface [X/H] of $\sim 10\%$ (Christensen-Dalsgaard et al. 1996). To briefly assess the usefulness of our catalog, we here show results obtained using our ages and chemical abundances.

In our *Gaia* DR3 GSP-Spec catalog, abundance measurements are available for only a fraction of Solar twins for most elements, with Ca being the exception, for which abundances are available for all twins. Restricting the analysis to stars with reliable abundance measurements, defined by the 14th–39th digits of the GSP-Spec Quality Flag corresponding to $\text{XUpLim} \leq 2$ and $\text{XUncer} \leq 1$, the resulting fractions are 0.70% for [N/Fe], 3.4% for [Mg/Fe], 49% for [Si/Fe], 17% for [S/Fe], 100% for [Ca/Fe], 3.8% for [Ti/Fe], 0.11% for [Cr/Fe], 90% for [Fe/M], and 1.5% for [Ni/Fe], in order of atomic number. The GSP-Spec [X/Fe] abundances used throughout this work were calibrated following Recio-Blanco et al. (2023, 2024). To complement the chemical information of our catalog, we cross-matched the *Gaia* DR3 source_id of our Solar twins with those in APOGEE DR17 (Majewski et al. 2017; Abdurro'uf et al. 2022) and GALAH DR4 (De Silva et al. 2015; Buder et al. 2025) to obtain their abundance measurements, applying their recommended filtering. We also cross-matched these identifiers with the exoplanet data from NASA Exoplanet

from high-precision Solar-twin studies (e.g., Tucci Maia et al. 2016; Nissen et al. 2020; Shejelammal et al. 2024). In practice, however, such a comparison is not feasible because the distance ranges of the Solar-twin samples differ substantially between these studies: the samples in Walsen et al. (2024) and Lehmann et al. (2025) are dominated by more distant stars, whereas high-precision Solar-twin studies focus on nearby targets to achieve very high S/N (see, Fig. XX). As a result, there are very few (if any) Solar twins in common between the two sets of studies, preventing a meaningful star-by-star comparison.

¹⁴ Because the ages of Rampalli et al. (2024) were determined using T_{eff} , [M/H], and $\log g$, they correlate more strongly with our $\log g$ -based ages ($r = 0.52$) than with our adopted M_{K_s} -based ages ($r = 0.36$), although the correlation remains modest in both cases.

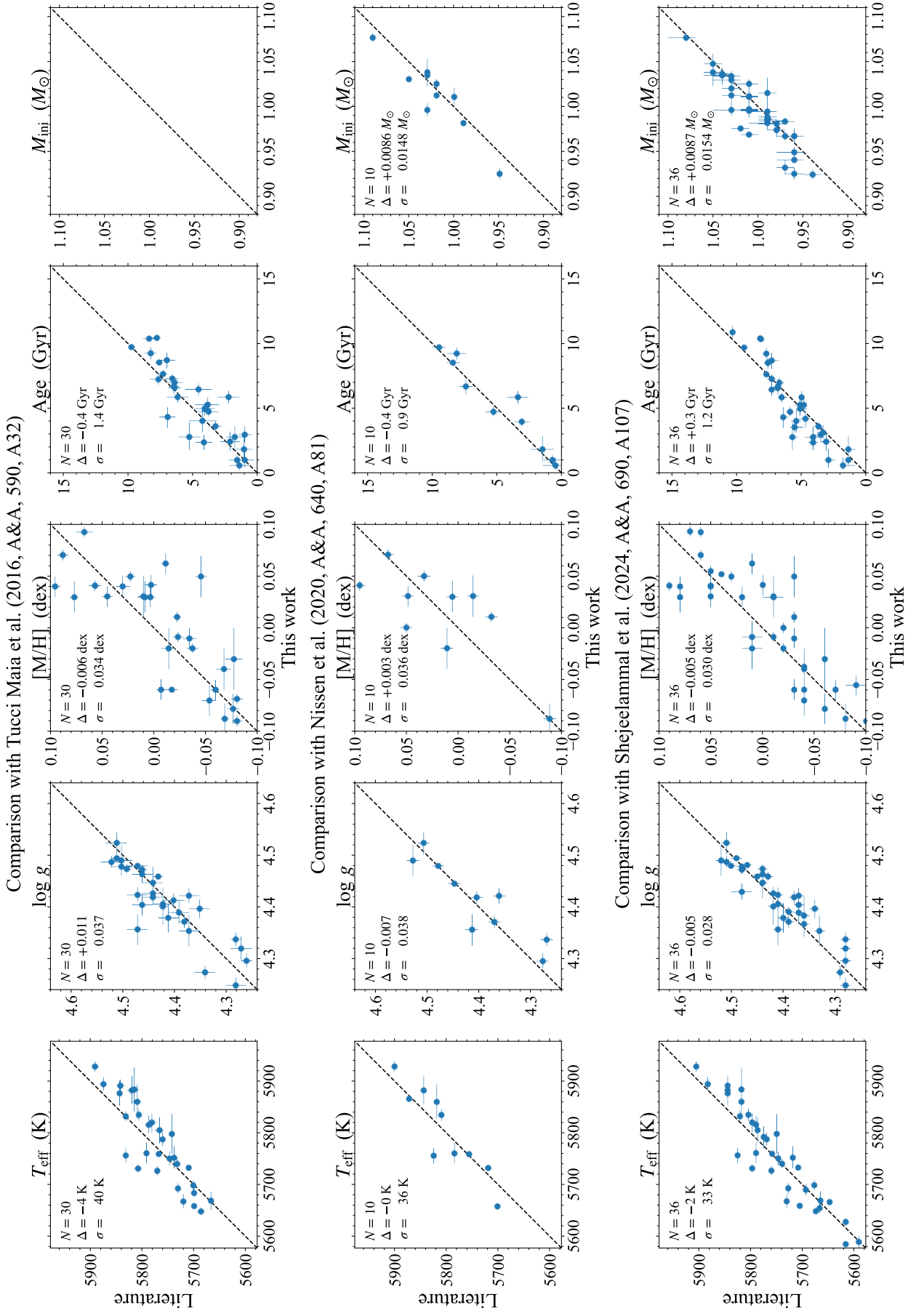


Fig. 6: Comparison of stellar parameters with literature (Tucci Maia et al. 2016; Nissen et al. 2020; Shejelammal et al. 2024). Each panel shows a comparison for T_{eff} , $\log g$, $[\text{M}/\text{H}]$ (or $[\text{Fe}/\text{H}]$), age, and M_{ini} , from left to right. Three values are annotated: the number N of stars in common between this work and literature, the mean difference Δ and the standard deviation σ of the difference between this work and literature. Also available at Zenodo (<https://doi.org/10.5281/zenodo.5555555>).

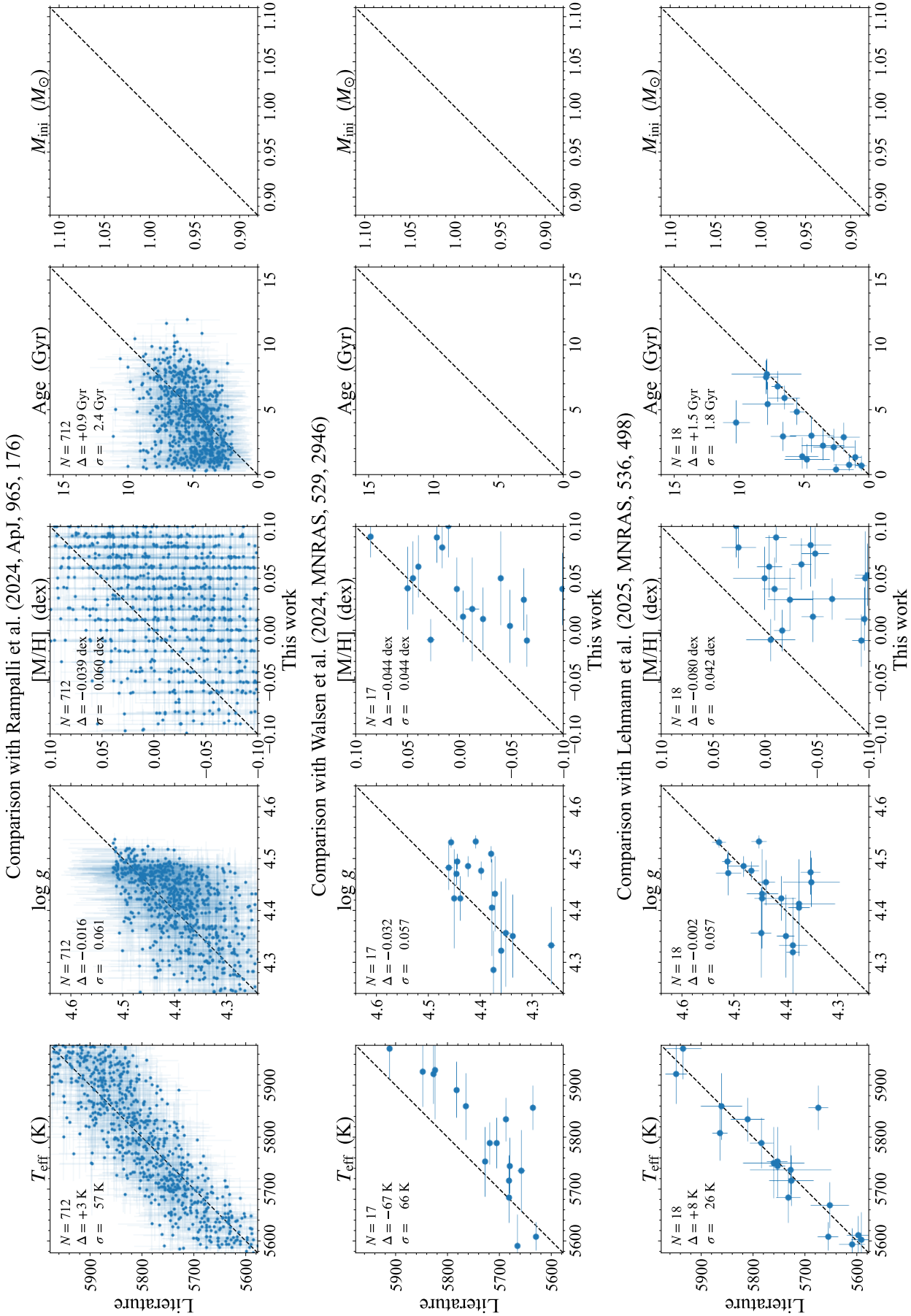


Fig. 7: Same as Fig. 6 but for three other studies (Walsen et al. 2024; Lehmann et al. 2025; Rampalli et al. 2024).

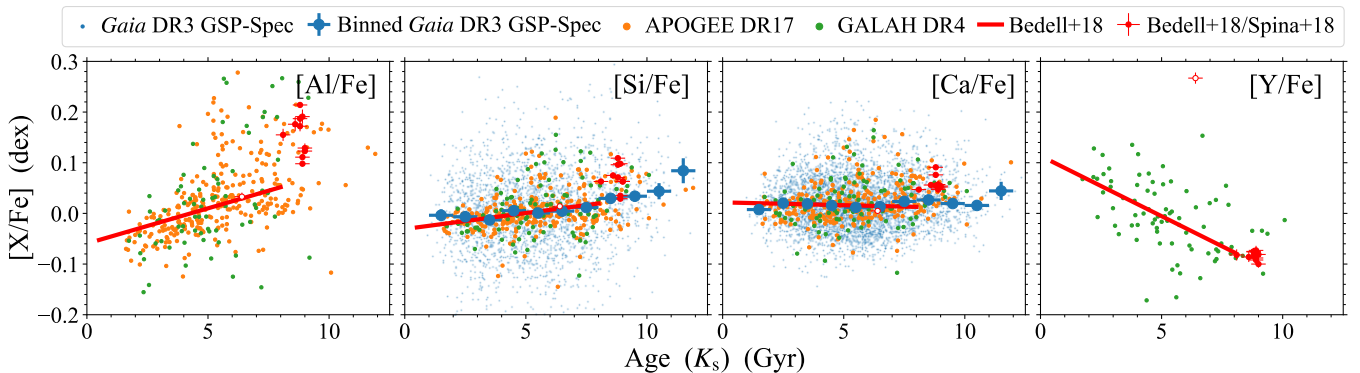


Fig. 8: Age–abundance relations for selected elements ([Al/Fe], [Si/Fe], [Ca/Fe], and [Y/Fe], from left to right). Blue dots show the GSP-Spec abundances of individual Solar twins, while blue filled circles with error bars indicate the medians of [X/Fe] within each 1 Gyr age bin. Orange and green dots represent abundances from APOGEE DR17 (Majewski et al. 2017; Abdurro’uf et al. 2022) and GALAH DR4 (De Silva et al. 2015; Buder et al. 2025), respectively. Red thick line shows the linear age–abundance relation by Bedell et al. (2018) for comparison. Red filled circles and an open circle with error bars represent old α -enhanced stars and an s-enhanced star, respectively, from Spina et al. (2018) and Bedell et al. (2018). For each element from each survey, we applied a zero-point correction in [X/Fe] to make the abundance scale consistent with that of the age–[X/Fe] relation by Bedell et al. (2018). The ages are determined using the K_s -band magnitude, and only stars with relative age errors smaller than 50% are included. For APOGEE DR17 and GALAH DR4, we include only stars with abundance errors below 0.05 dex. We note that a small fraction of blue dots, as well as one [Al/Fe] measurement from APOGEE DR17 and one [Al/Fe] measurement from GALAH DR4, fall outside the plotted range and are therefore not shown. Plots for all the elements are presented in Fig. E.1.

Archive (Christiansen et al. 2025)¹⁵ retrieved on August 13, 2025 (see, also de Laverny et al. 2025, for a catalog of exoplanet host stars with *Gaia* DR3 GSP-Spec). The retrieved APOGEE and GALAH abundances, as well as a flag indicating the presence or absence of confirmed exoplanets, are provided as part of our published Solar-twin catalog for reference (Table E.2).

Figure 8 shows the relations between the derived stellar ages and elemental abundances¹⁶. Here we show results only for four elements (Al, Si, Ca, and Y). These four elements are selected on the grounds that (i) [Al/Fe] and [Y/Fe] are known to show tight and steep correlations with stellar age (e.g., Sharma et al. 2022), and (ii) [Si/Fe] and [Ca/Fe] are measured for a relatively large number of stars with good precisions in our catalog. Results for the other elements available in our catalog are shown in Fig. E.1 for reference. To ensure reliable age estimates, we include only stars with relative age uncertainties better than 50%. This cut, which naturally excludes most of the young Solar twins ($\lesssim 2$ Gyr) due to our selection effects (Sect. 4.3), is also beneficial because the stellar parameters of the youngest Solar twins could be less accurate owing to activity effects (Yana Galarza et al. 2019).

Age–abundance trends can serve as a diagnostic of the robustness and reliability of our age estimates, given that clear trends for Solar twins have already been reported by Bedell et al. (2018, among others) using a small but high-precision sample. In addition, theoretical basis of these correlations can be understood within a framework that combines Galactic chemical evolution with radial migration of stars, in which the inner regions formed faster and became more metal-rich than the outer regions (Tsujimoto 2021). This view suggests that older Solar twins were born at smaller Galactocentric distances, i.e., closer

to the Galactic center, because all Solar twins considered here have a common metallicity, nearly Solar. On the basis of this picture, we emphasize that age and birth radius are tightly coupled. Hence, our age–[X/Fe] relations are not relations defined at a fixed Galactocentric distance, nor, of course, at a fixed age.

In the following, we discuss two topics regarding the age–[X/Fe] trends: slopes (Sect. 6.1) and s-enhanced Solar twins (Sect. 6.2).

6.1. Slopes of age–[X/Fe] trends

From Fig. 8, we found that the age–[X/Fe] relations in our catalog, regardless of which abundance source is adopted (*Gaia* DR3 GSP-Spec, APOGEE DR17, or GALAH DR4), show good agreement with the relations reported by Bedell et al. (2018) based on a small but very precise sample. In particular, for [Al/Fe] and [Y/Fe], whose age–abundance relations exhibit steep positive and negative slopes, respectively, our measurements reproduce the slopes obtained by Bedell et al. (2018) very well. These agreements support the reliability of our age determinations. Comparable agreement is also seen for most of the other elements shown in Fig. E.1. Although the uncertainties for individual stars in our catalog are relatively large, the consistency emerging from our much larger sample enables us to verify the age–[X/Fe] trends measured by Bedell et al. (2018) across a much larger Solar-twin sample.

The exceptions to this behavior are the age–[X/Fe] relations for [S/Fe] and [Ni/Fe] from *Gaia* DR3 GSP-Spec. Even though Bedell et al. (2018) presented positive age–[S/Fe] and [Ni/Fe] slopes, the age–[X/Fe] relations from GSP-Spec are rather flat for S and Ni. These flat trends from GSP-Spec are most likely due to selection effects (i.e., stars with small [X/Fe], and hence weak lines of element X, tend to lack [X/Fe] measurements), given that the lines from S and Ni are very weak in Solar-type stars in the RVS domain, although although the presence of unknown systematic errors in the GSP-Spec abundances cannot be

¹⁵ <https://exoplanetarchive.ipac.caltech.edu/index.html>

¹⁶ For all the *Gaia* DR3 GSP-Spec, APOGEE DR17, and GALAH DR4 abundances, we added zero-point offsets in [X/Fe] so that, for elements analyzed by Bedell et al. (2018), our Solar twins in the 0.5–8 Gyr range show no systematic offset from the linear age–[X/Fe] relations in that study, which were calibrated over a similar age interval. The added offsets are listed in Table E.3.

entirely ruled out. Below, we examine this possibility for S and Ni in more detail.

For [S/Fe], abundances from APOGEE DR17 indicate a positive relation with a slope of $+0.0082 \pm 0.0023$ dex Gyr $^{-1}$ (fitted using only Solar twins with ages younger than 8 Gyr, to be consistent with the sample of [Bedell et al. \(2018\)](#)), which is in good agreement with the slope of $+0.0098 \pm 0.0015$ dex Gyr $^{-1}$ by [Bedell et al. \(2018\)](#). GALAH DR4 does not provide [S/Fe]. Since S is an α element (e.g., [Duffau et al. 2017](#); [Perdigon et al. 2021](#), and references therein), the positive slope for [S/Fe] is expected, given that other α elements such as O and Mg also exhibit positive age-[X/Fe] trends. Nevertheless, because S sometimes exhibits behavior that differs from typical α elements (e.g., the negative radial [S/Fe] gradient seen in Cepheids; [Luck 2018](#); [da Silva et al. 2023](#)), caution is warranted when treating S as a standard α element. Taken together, we conclude that the age-[S/Fe] relation likely has positive relation, expected from its α -element nature, and that the flat relation from *Gaia* DR3 GSP-Spec is probably due to selection effects.

For [Ni/Fe], when restricting ourselves to the stars plotted in Fig. 8 (i.e., stars with relative age errors smaller than 50%), APOGEE DR17 indicates a flat age-[X/Fe] relation within 1σ , and GALAH DR4 indicates a possibly positive but nearly flat relation within 2σ , seemingly contradicting the positive slope presented by [Bedell et al. \(2018\)](#). However, when we remove the constraint on the relative age error, and hence include stars with very young ages ($\lesssim 2$ Gyr), we more or less recovered the age-[Ni/Fe] slope presented by [Bedell et al. \(2018\)](#) of $+0.0071 \pm 0.0009$ dex Gyr $^{-1}$, obtaining $+0.0043 \pm 0.0006$ dex Gyr $^{-1}$ from APOGEE DR17 and $+0.0061 \pm 0.0009$ dex Gyr $^{-1}$ from GALAH DR4 (again, including only stars with ages < 8 Gyr). This is because, in APOGEE DR17 and GALAH DR4, stars with ages $\lesssim 3$ Gyr have systematically ~ 0.02 – 0.03 dex lower [Ni/Fe] than older stars. We also see a similar age-[Ni/Fe] trend in Fig. 3 of [Bedell et al. \(2018\)](#), i.e., a nearly flat age-[Ni/Fe] relation for stars with ages ~ 2 – 8 Gyr and lower [Ni/Fe] for stars with $\lesssim 2$ Gyr. In contrast, the *Gaia* DR3 GSP-Spec age-[Ni/Fe] relation is continuously flat (or even possibly negative) over the entire 0– 10 Gyr age range. Therefore, we conclude that the age-[Ni/Fe] relation likely has a flat trend, as in other Fe-peak elements, at $\gtrsim 2$ Gyr, lower [Ni/Fe] at young ages, and that the flat *Gaia* DR3 GSP-Spec relation is again probably due to selection effects.

For several elements other than Ni (e.g., Mg, Co, and Sr), inspection of Fig. 3 of [Bedell et al. \(2018\)](#) suggests that the youngest Solar twins ($\lesssim 2$ Gyr) may exhibit slightly lower (or, for a few elements, slightly higher) [X/Fe] than would be expected from a linear extrapolation of the age-[X/Fe] relation of the older stars, as well as a larger dispersion than seen for the older stars, although this trend is not entirely clear. The apparent transition at an age of ~ 2 Gyr, if real, coincides with the epoch of the recent star-formation peak ([Mor et al. 2019](#); [Ruiz-Lara et al. 2020](#); [Tsujimoto et al. 2026](#)). Such bursty star formation could have modified the relative contributions of type Ia and core-collapse supernovae and other nucleosynthetic sources, thereby altering the [X/Fe] ratios of Solar twins younger than ~ 2 Gyr (e.g., [Tsujimoto et al. 1995](#); [Johnson et al. 2021](#); [Sun et al. 2025c](#)), since the X-to-Fe yield ratios are expected to differ among sources. Whether such bursts drive [X/Fe] upward or downward is rather complicated, it depends on several ingredients such as the differences in nucleosynthetic [X/Fe] yields among sources, the star-formation history, and the subsequent mixing of metals, and it is therefore not straightforward to predict the exact trend. The physical trigger of the recent

star-formation peak also remains under debate. Nonetheless, it is intriguing that the epoch of ~ 2 Gyr ago coincides with the timing of possible external perturbations. For example, several studies have proposed that pericentric passages of the Sagittarius dwarf galaxy (Sgr) may have enhanced disk star formation (e.g., [Ruiz-Lara et al. 2020](#); [Annem & Khoperskov 2024](#)). As another example, a recent sudden drop in [Fe/H] has been observed and interpreted as evidence for a low-metallicity gas infall event ([Spitoni et al. 2023](#); [Palla et al. 2024](#)). Whatever the trigger of the bursty star formation, the resulting change in the relative contributions of nucleosynthetic sources might account for the departure of the young Solar twins from a simple linear age-[X/Fe] extrapolation. Aside from such physical scenarios for the departure, systematic [X/Fe] errors associated with stellar activity in the youngest stars ([Yana Galarza et al. 2019](#)) could provide another contribution.

In light of the above discussion of [S/Fe] and [Ni/Fe], care should be taken when analyzing mean *Gaia* DR3 GSP-Spec abundances at the very high precision level of a few-hundredths of a dex, even though with *Gaia* DR3 GSP-Spec we succeeded in confirming the age-[X/Fe] trends by [Bedell et al. \(2018\)](#) for most elements. Larger, higher-precision samples are required to reach firm conclusions regarding the age-[X/Fe] trends. GSP-Spec abundances in *Gaia* DR4 will be valuable in this context, given the expected increase in S/N thanks to an observing duration roughly twice as long as that of DR3. At the same time, characterizing activity-related systematics will also be important for interpreting abundances at young ages.

6.2. *s*-process-enhanced stars

Other key findings by [Spina et al. \(2018\)](#) and [Bedell et al. \(2018\)](#) from the age-[X/Fe] plots are (1) higher $[\alpha/\text{Fe}]$ ratios for most stars with ages $\gtrsim 8$ Gyr than expected from a linear trend defined by stars with ages $\lesssim 8$ Gyr, and (2) one star (HIP 64150) showing an anomalously high [s/Fe] ratio. Here we investigate the latter, *s*-enhanced stars in this section, while the former, α -enhanced stars are investigated in our companion paper (Paper III; [Taniguchi et al. 2026](#)).

[Spina et al. \(2018\)](#) found that one star (HIP 64150) among their 79 Solar twins shows an enhanced [s/Fe] ratio but not an enhanced [r/Fe]. As representative elements for the *s*- and *r*-processes, they measured $[\text{Y}/\text{Fe}] = +0.267$ and $[\text{Eu}/\text{Fe}] = +0.041$ dex, respectively. This $[\text{Y}/\text{Fe}]$ value is $+0.31$ dex higher than the linear age-[Y/Fe] relation by [Bedell et al. \(2018\)](#), whereas $[\text{Eu}/\text{Fe}]$ is only 0.01 dex smaller than the relation. Such enhancements in [s/Fe] with normal [r/Fe] have also been observed in two other Solar analogs, with $[\text{Y}/\text{Fe}] = +0.533$ dex for HIP 10725¹⁷ ([Schirbel et al. 2015](#)) and $[\text{Y}/\text{Fe}] = +0.92$ dex for HD 138004¹⁸ ([Liu et al. 2020](#)). For HIP 64150 and HIP 10725, time variations in their radial velocities, most likely due to unseen white-dwarf companions, have been found ([Schirbel et al. 2015](#); [dos Santos et al. 2017](#), respectively), and pollution from a former AGB companion was suggested. For the last star, HD 138004, a radial-velocity variation of ~ 10 km s $^{-1}$ has been reported ([Butler et al. 2017](#); [Tal-Or et al. 2019](#)). Combined with the astrometric acceleration measurements by [Brandt \(2018\)](#),

¹⁷ [Fe/H] of HIP 10725 is -0.173 , which is much lower than our Solar-twin criterion (± 0.1 dex around the Solar value).

¹⁸ [Fe/H] of HD 138004 is -0.109 ± 0.011 dex, slightly outside our Solar-twin criterion (± 0.1 dex around the Solar value), but consistent with it within the uncertainty. Thus, we include this star in our discussion.

2021), this variation implies a companion with a mass of $0.658M_{\odot}$ (An et al. 2025). The same technique was also applied to HIP 64150, yielding a companion mass of $0.603M_{\odot}$ (An et al. 2025). We searched for other s-enhanced stars in the literature listed in Table 2, but no clear additional cases were found. If we relax the conditions on the stellar parameters for being Solar twins, several probable s-enhanced Solar analogs (2, 4, and 1 stars) appear in the samples from da Silva et al. (2012), Liu et al. (2020), and Shejelammal et al. (2024), respectively, though these objects have large ages ($\gtrsim 10$ Gyr). Interestingly, Rampalli et al. (2024) published the [Y/Fe] abundances for 17,412 Solar twins (in their definition), but none of these stars has [Y/Fe] larger than 3σ (≈ 0.2 dex) from their age–[Y/Fe] relation. This lack of s-enhanced stars might be related to the data-driven nature of their analysis and the lack of detectable s-process lines in *Gaia* RVS spectra of Solar twins with low or moderate s-process enhancements (see Fig. 1 of Contursi et al. 2023 and Fig. 2 of Contursi et al. 2024 for Ce and Nd, respectively).

Using our catalog of Solar twins, we searched for s-enhanced twins using GALAH DR4 [Y/Fe] abundances. We found that none of the 80 Solar twins plotted in Fig. E.1 has a zero-point corrected [Y/Fe] value that is 0.2 dex or more above the age–[Y/Fe] relation by Bedell et al. (2018). There is one star (Gaia DR3 5365738724921515776) with a zero-point-corrected [Y/Fe] of 0.153 ± 0.022 dex, which is 0.199 dex higher than the relation by Bedell et al. (2018), but even in this case the enhancement in [Y/Fe] is modest. The absence (or presence of only one) s-enhanced star among our 80 stars could simply be due to small-number statistics, given that there is only one such star among the 79 Solar twins of Bedell et al. (2018). However, it could also reflect our removal of possible binary stars as much as possible using *Gaia* flags and photometric constraints. To assess this possibility, we examined the absolute [Y/Fe] values for all Solar-twin candidates with GALAH DR4 [Y/Fe] abundances, without applying the astrometric and photometric criteria used to remove binaries in our final sample. We found that 3 out of 286 such stars ($\sim 1\%$) have [Y/Fe] values exceeding 0.2 dex, a fraction comparable to that found by Bedell et al. (2018), although this comparison is based on absolute [Y/Fe] values rather than offsets from the age–[Y/Fe] relation. This interpretation is also partly supported by the fact that the s-enhanced star HD 138004 is included in our parent *Gaia* sample but removed by its RUWE value and non_single_star flag, whereas another s-enhanced star, HIP 64150, passes our selection.

7. Summary

This study constructed a large catalog of Solar twins with isochrone ages using model-driven, rather than data-driven, *Gaia* DR3 GSP-Spec stellar parameters (T_{eff} , $\log g$, [M/H], and $[\alpha/\text{Fe}]$).

We selected candidate Solar twins with high-quality GSP-Spec parameterization (Sect. 2.1). We required two quality criteria for GSP-Spec: all the 13 first GSP-Spec Quality Flags equal to zero, and the goodness-of-fit satisfies $\log \chi^2 < -3.2$. With these constraints, the uncertainties in the stellar parameters are smaller than 100 K in T_{eff} , 0.2 in $\log g$, 0.1 dex in [M/H], and 0.05 dex in $[\alpha/\text{Fe}]$. We calibrated the stellar parameters in two steps (first using the relations provided by Recio-Blanco et al. (2024), and then applying the corrections described in Appendix A) to place them on a scale consistent with high-resolution, high-precision spectroscopic results (Tucci Maia et al. 2016; Nissen et al. 2020;

Shejelammal et al. 2024). We then selected 7,918 Solar-twin candidates whose T_{eff} , $\log g$, and [M/H] fall within ± 200 K, ± 0.2 , and ± 0.1 dex of the Solar values, respectively. We filtered out stars with inaccurate parameterization and possible non-single stars as much as possible using RUWE, a few *Gaia* flags (astrometric_params_solved, duplicated_source, and non_single_star) and photometric constraints (Sects. 2.1 and 2.4 and Fig. 1). Applying these constraints yielded our final Solar-twin sample consisting of 6,594 stars.

We determined ages, initial masses M_{ini} , and initial metallicities [M/H]_{ini} for individual Solar twins with a Bayesian isochrone-projection (Sects. 3.1 and 3.2). In this step, we employed the PARSEC isochrones version 1.2S (Bressan et al. 2012; Chen et al. 2015) obtained with the CMD 3.8 web interface. Because the native isochrone grid is too sparse to determine ages accurately for Solar twins, we interpolated it to construct a sufficiently dense grid (Appendix B). Assuming flat priors on age, M_{ini} , and [M/H]_{ini}, we derived posterior estimates using three observable triplets: (T_{eff} , $\log g$, [M/H]_{curr}), (T_{eff} , M_G , [M/H]_{curr}), and (T_{eff} , M_{K_s} , [M/H]_{curr}).

We validated the resulting ages in two ways (Sect. 4). First, we applied our age-determination procedure to the Sun (Sect. 4.1 and Table 1). We confirmed that the recovered age and M_{ini} agree with literature values of 4.5–4.6 Gyr and $1M_{\odot}$ for all three age-determination scheme. Second, we constructed a mock Solar-twin sample consisting of 75,588 artificial stars (Sect. 4.3.1 and Appendix C) and compared its statistical properties with those of the observed sample (Sect. 4.3.2). Comparisons of the age– M_{ini} distributions (Figs. 2 and 3) and the distribution of M_{ini} at a fixed age (Fig. 4) show good consistency between the observed and mock catalogs for ages based on M_G or M_{K_s} . This fact supports the reliability of the GSP-Spec parameterization, our age determination, and the mock construction. In contrast, we found inconsistencies for ages derived from $\log g$, likely reflecting the difficulty of determining enough accurate $\log g$ from the limited wavelength range of the *Gaia* RVS. Taken together with direct comparisons among the three age estimates (Fig. 5) we concluded that both M_G - and M_{K_s} -based ages are reliable and hence suitable for statistical analyses. We adopted the M_{K_s} -based ages in the subsequent analysis (Sect. 4.4).

To place our catalog in the context of a decade of Solar-twin studies, we compared our Solar-twin catalog with earlier catalogs (Sect. 5). A comparison of basic metrics (Sect. 5.1 and Table 2) shows that some previous high-resolution Solar-twin samples contain only several tens of stars but achieve extremely high precision in T_{eff} , $\log g$, [Fe/H], and abundances. In contrast, our catalog and a few other recent works based on large spectroscopic surveys provide samples that are about two orders of magnitude larger but have worse precision in individual stellar parameters. While previous large Solar-twin catalogs (Rampalli et al. 2024; Walsen et al. 2024; Lehmann et al. 2025) rely on data-driven methods, our catalog is built from model-driven stellar parameters, ages, M_{ini} , and chemical abundances. The reasoning behind this choice is to avoid propagating trends learned from training samples (i.e., previous small-scale datasets) and to verify the results obtained from past high-precision studies using our lower-precision but substantially larger sample. We adopted a strict criterion of ± 0.1 dex around Solar [M/H] to ensure that our Solar twins are near-Solar-metallicity main-sequence stars and that their ages can be tightly linked to their birth radii. Moreover, our construction of the mock sample is valuable for characterizing the selection function of our sample and, consequently, for investigating the probability distributions of stellar parameters (e.g., for investi-

gating the underlying age distribution in our companion paper, Paper II; [Tsujimoto et al. 2026](#)). By comparing our stellar parameters, ages, and M_{ini} with values from high-precision literature samples (Sect. 5.2), we found good agreement with many previous differential Solar-twin studies (Fig. 6), but discrepancies relative to some large, data-driven catalogs (Fig. 7).

To showcase the scientific potential of our catalog, we investigated age-[X/Fe] relations (Sect. 6). For this purpose, we combined GSP-Spec, APOGEE DR17, and GALAH DR4 abundances to compare the resulting age-[X/Fe] trends with those from high-precision studies by [Bedell et al. \(2018\)](#) and [Spina et al. \(2018\)](#) (Figs. 8 and E.1). We discussed the age-[X/Fe] relations in two regards: slopes and s-enhanced stars. Focusing first on the slopes of the age-[X/Fe] relations (Sect. 6.1), we recovered the classical positive age-[Al/Fe] and negative age-[Y/Fe] trends, supporting the reliability of our age determinations. For most elements, the age-[X/Fe] slopes agree well with those derived from a small high-precision sample by [Bedell et al. \(2018\)](#), supporting these relations in a more statistical regime. Nevertheless, we found discrepancies for S and Ni measured by *Gaia* DR3 GSP-Spec, for which selection effects or systematic errors may have altered the GSP-Spec abundances. We also pointed out that age-[X/Fe] relations are not necessarily linear and that the age distribution of the Solar-twin sample can modify the measured slopes, potentially even changing their signs. In addition, we identified a possible sudden drop in [Ni/Fe] (and in some other elements) around 2 Gyr ago. Second, we searched for s-process-enhanced Solar twins using GALAH DR4 [Y/Fe] measurements (Sect. 6.2). We found no clear examples (at most one candidate) among the 80 Solar twins with available [Y/Fe]. We will also investigate the α -enhanced Solar twins in our companion paper (Paper III; [Taniguchi et al. 2026](#)).

Beyond the analyses presented in this study, our large, homogeneous, and well-characterized catalog provides a complementary resource to both high-precision small samples and large data-driven catalogs. It enables further investigations that benefit from model-driven stellar parameters with a quantified selection function. In our companion paper (Paper II; [Tsujimoto et al. 2026](#)), we will use our catalog to examine the age distribution of Solar twins, and the implied efficiency of radial migration of the Sun. Our final catalog of 6,594 Solar twins is published online at CDS (see Table E.2 for a description of the catalog columns).

Acknowledgements. This work has been supported by the Tokyo Center For Excellence Project, Tokyo Metropolitan University. DT acknowledges financial support from JSPS Research Fellowship for Young Scientists and accompanying Grants-in-Aid for JSPS Fellows (23KJ2149). PDL and ARB acknowledge partial funding from the European Union’s Horizon 2020 research and innovation program under SPACE-H2020 grant agreement number 101004214 (EXPLORE project). TT acknowledges the support by JSPS KAKENHI Grant No. 23H00132.

This work presents results from the European Space Agency (ESA) space mission *Gaia*. *Gaia* data are being processed by the *Gaia* Data Processing and Analysis Consortium (DPAC). Funding for the DPAC is provided by national institutions, in particular the institutions participating in the *Gaia* MultiLateral Agreement (MLA). The *Gaia* mission website is <https://www.cosmos.esa.int/gaia>. The *Gaia* archive website is <https://archives.esac.esa.int/gaia>. This publication makes use of data products from the Two Micron All Sky Survey, which is a joint project of the University of Massachusetts and the Infrared Processing and Analysis Center/California Institute of Technology, funded by the National Aeronautics and Space Administration and the National Science Foundation.

Adibekyan, V. Z., Sousa, S. G., Santos, N. C., et al. 2012, *A&A*, 545, A32
 Amelin, Y., Krot, A. N., Hutcheon, I. D., & Ulyanov, A. A. 2002, *Science*, 297, 1678
 An, Q., Brandt, T. D., Brandt, G. M., & Venner, A. 2025, *ApJS*, 280, 61
 Annem, B. & Khoperskov, S. 2024, *MNRAS*, 527, 2426
 Bailer-Jones, C. A. L., Rybizki, J., Fouesneau, M., Demleitner, M., & Andrae, R. 2021, *AJ*, 161, 147
 Barbillon, M., Recio-Blanco, A., de Laverny, P., & Palicio, P. A. 2025, arXiv e-prints, arXiv:2511.12156
 Baumann, P., Ramírez, I., Meléndez, J., Asplund, M., & Lind, K. 2010, *A&A*, 519, A87
 Beck, P. G., do Nascimento, Jr., J. D., Duarte, T., et al. 2017, *A&A*, 602, A63
 Bedell, M., Bean, J. L., Meléndez, J., et al. 2018, *ApJ*, 865, 68
 Bedell, M., Meléndez, J., Bean, J. L., et al. 2014, *ApJ*, 795, 23
 Bellardini, M. A., Wetzel, A., Loebman, S. R., et al. 2021, *MNRAS*, 505, 4586
 Berger, T. A., Huber, D., van Saders, J. L., et al. 2020, *AJ*, 159, 280
 Bernstein, R., Shectman, S. A., Gunnels, S. M., Mochnacki, S., & Athey, A. E. 2003, in Society of Photo-Optical Instrumentation Engineers (SPIE) Conference Series, Vol. 4841, Instrument Design and Performance for Optical/Infrared Ground-based Telescopes, ed. M. Iye & A. F. M. Moorwood, 1694–1704
 Bertelli Motta, C., Pasquali, A., Richer, J., et al. 2018, *MNRAS*, 478, 425
 Bhattarai, B., Loebman, S. R., Ness, M. K., et al. 2024, *ApJ*, 977, 70
 Bohlin, R. C., Hubeny, I., & Rauch, T. 2020, *AJ*, 160, 21
 Bonanno, A., Schlattl, H., & Paternò, L. 2002, *A&A*, 390, 1115
 Bouvier, A. & Wadhwa, M. 2010, *Nature Geoscience*, 3, 637
 Brandt, T. D. 2018, *ApJS*, 239, 31
 Brandt, T. D. 2021, *ApJS*, 254, 42
 Bressan, A., Marigo, P., Girardi, L., et al. 2012, *MNRAS*, 427, 127
 Brewer, J. M. & Fischer, D. A. 2018, *ApJS*, 237, 38
 Brewer, J. M., Fischer, D. A., Valenti, J. A., & Piskunov, N. 2016, *ApJS*, 225, 32
 Buder, S., Asplund, M., Duong, L., et al. 2018, *MNRAS*, 478, 4513
 Buder, S., Kos, J., Wang, X. E., et al. 2025, *PASA*, 42, e051
 Buder, S., Sharma, S., Kos, J., et al. 2021, *MNRAS*, 506, 150
 Butler, R. P., Vogt, S. S., Laughlin, G., et al. 2017, *AJ*, 153, 208
 Caffau, E., Ludwig, H. G., Steffen, M., Freytag, B., & Bonifacio, P. 2011, *Sol. Phys.*, 268, 255
 Carlos, M., Amarsi, A. M., Nissen, P. E., & Canoccchi, G. 2025, *A&A*, 700, A127
 Carvalho-Silva, G., Meléndez, J., Rathsam, A., et al. 2025, *ApJ*, 983, L31
 Casagrande, L., Lin, J., Rains, A. D., et al. 2021, *MNRAS*, 507, 2684
 Casagrande, L. & Vandenberg, D. A. 2018, *MNRAS*, 479, L102
 Casali, G., Spina, L., Magrini, L., et al. 2020, *A&A*, 639, A127
 Casamiquela, L., Castro-Ginard, A., Anders, F., & Soubiran, C. 2021, *A&A*, 654, A151
 Cayrel de Strobel, G. 1996, *A&A Rev.*, 7, 243
 Cayrel de Strobel, G., Knowles, N., Hernandez, G., & Bentolila, C. 1981, *A&A*, 94, 1
 Chen, Y., Bressan, A., Girardi, L., et al. 2015, *MNRAS*, 452, 1068
 Chen, Y., Girardi, L., Fu, X., et al. 2019, *A&A*, 632, A105
 Christensen-Dalsgaard, J., Dappen, W., Ajukov, S. V., et al. 1996, *Science*, 272, 1286
 Christiansen, J. L., McElroy, D. L., Harbut, M., et al. 2025, *PSJ*, 6, 186
 Cohen, M., Wheaton, W. A., & Megeath, S. T. 2003, *AJ*, 126, 1090
 Contursi, G., de Laverny, P., Recio-Blanco, A., Palicio, P. A., & Abia, C. 2024, *A&A*, 683, A138
 Contursi, G., de Laverny, P., Recio-Blanco, A., et al. 2023, *A&A*, 670, A106
 Creevey, O. L., Sordo, R., Pailler, F., et al. 2023, *A&A*, 674, A26
 Cropper, M., Katz, D., Sartoretti, P., et al. 2018, *A&A*, 616, A5
 Cutri, R. M., Skrutskie, M. F., van Dyk, S., et al. 2003, 2MASS All Sky Catalog of point sources.
 da Silva, R., D’Orazi, V., Palla, M., et al. 2023, *A&A*, 678, A195
 da Silva, R., Porto de Mello, G. F., Milone, A. C., et al. 2012, *A&A*, 542, A84
 Datson, J., Flynn, C., & Portinari, L. 2015, *A&A*, 574, A124
 de Laverny, P., Ligi, R., Crida, A., Recio-Blanco, A., & Palicio, P. A. 2025, *A&A*, 699, A100
 De Silva, G. M., Freeman, K. C., Bland-Hawthorn, J., et al. 2015, *MNRAS*, 449, 2604
 Delgado Mena, E., Moya, A., Adibekyan, V., et al. 2019, *A&A*, 624, A78
 Delgado Mena, E., Tsantaki, M., Adibekyan, V. Z., et al. 2017, *A&A*, 606, A94
 dos Santos, L. A., Meléndez, J., Bedell, M., et al. 2017, *MNRAS*, 472, 3425
 Dotter, A., Conroy, C., Cargile, P., & Asplund, M. 2017, *ApJ*, 840, 99
 Duffau, S., Caffau, E., Sbordone, L., et al. 2017, *A&A*, 604, A128
 Dziembowski, W. A., Fiorentini, G., Ricci, B., & Sienkiewicz, R. 1999, *A&A*, 343, 990
 Fouesneau, M., Andrae, R., Sordo, R., & Dharmawardena, T. 2022, *dustapprox*, <https://github.com/mfouesneau/dustapprox>, version 0.1
 Fouesneau, M., Frémat, Y., Andrae, R., et al. 2023, *A&A*, 674, A28
 Freeman, K. & Bland-Hawthorn, J. 2002, *ARA&A*, 40, 487
 Gaia Collaboration, Creevey, O. L., Sarro, L. M., et al. 2023a, *A&A*, 674, A39
 Gaia Collaboration, Prusti, T., de Bruijne, J. H. J., et al. 2016, *A&A*, 595, A1

References

Abdurro’uf, Accetta, K., Aerts, C., et al. 2022, *ApJS*, 259, 35
 Adibekyan, V., de Laverny, P., Recio-Blanco, A., et al. 2018, *A&A*, 619, A130
 Adibekyan, V., Delgado-Mena, E., Figueira, P., et al. 2016, *A&A*, 592, A87

Gaia Collaboration, Recio-Blanco, A., Kordopatis, G., et al. 2023b, *A&A*, 674, A38

Gaia Collaboration, Vallenari, A., Brown, A. G. A., et al. 2023c, *A&A*, 674, A1

Ghezzi, L., Cunha, K., Smith, V. V., et al. 2010, *ApJ*, 720, 1290

Gonzalez, G. 2014, *MNRAS*, 441, 1201

Gonzalez, G. 2015, *MNRAS*, 446, 1020

Gonzalez, G., Carlson, M. K., & Tobin, R. W. 2010, *MNRAS*, 403, 1368

Gonzalez, G., Laws, C., Tyagi, S., & Reddy, B. E. 2001, *AJ*, 121, 432

González Hernández, J. I., Israelian, G., Santos, N. C., et al. 2010, *ApJ*, 720, 1592

GRAVITY Collaboration, Abuter, R., Amorim, A., et al. 2020, *A&A*, 636, L5

Gray, D. F. 2005, *The Observation and Analysis of Stellar Photospheres* (Cambridge: Cambridge Univ. Press)

Green, G. M. 2018, *The Journal of Open Source Software*, 3, 695

Green, G. M., Schlaflay, E., Zucker, C., Speagle, J. S., & Finkbeiner, D. 2019, *ApJ*, 887, 93

Grevesse, N. & Sauval, A. J. 1998, *Space Sci. Rev.*, 85, 161

Hardorp, J. 1978, *A&A*, 63, 383

Hinkel, N. R., Timmes, F. X., Young, P. A., Pagano, M. D., & Turnbull, M. C. 2014, *AJ*, 148, 54

Holmberg, J., Flynn, C., & Portinari, L. 2006, *MNRAS*, 367, 449

Houdek, G. & Gough, D. O. 2011, *MNRAS*, 418, 1217

Huber, D., Zinn, J., Bojsen-Hansen, M., et al. 2017, *ApJ*, 844, 102

Israelian, G., Delgado Mena, E., Santos, N. C., et al. 2009, *Nature*, 462, 189

Israelian, G., Santos, N. C., Mayor, M., & Rebolo, R. 2004, *A&A*, 414, 601

Jofré, P., Heiter, U., Worley, C. C., et al. 2017, *A&A*, 601, A38

Johnson, J. W., Weinberg, D. H., Vincenzo, F., et al. 2021, *MNRAS*, 508, 4484

Jørgensen, B. R. & Lindegreen, L. 2005, *A&A*, 436, 127

Katz, D., Sartoretti, P., Guerrier, A., et al. 2023, *A&A*, 674, A5

King, J. R., Boesgaard, A. M., & Schuler, S. C. 2005, *AJ*, 130, 2318

Kordopatis, G., Schultheis, M., McMillan, P. J., et al. 2023, *A&A*, 669, A104

Kroupa, P. 2001, *MNRAS*, 322, 231

Laws, C., Gonzalez, G., Walker, K. M., et al. 2003, *AJ*, 125, 2664

Lehmann, C., Murphy, M. T., Liu, F., & Flynn, C. 2025, *MNRAS*, 536, 498

Lehmann, C., Murphy, M. T., Liu, F., Flynn, C., & Berke, D. A. 2022, *MNRAS*, 512, 11

Lehmann, C., Murphy, M. T., Liu, F., et al. 2023, *MNRAS*, 521, 148

Leike, R. H., Glatzle, M., & Enßlin, T. A. 2020, *A&A*, 639, A138

Liu, F., Asplund, M., Yong, D., et al. 2019, *A&A*, 627, A117

Liu, F., Yong, D., Asplund, M., et al. 2020, *MNRAS*, 495, 3961

López-Valdivia, R., Bertone, E., & Chávez, M. 2017, *MNRAS*, 467, 2412

López-Valdivia, R., Bertone, E., Chávez, M., et al. 2014, *MNRAS*, 444, 2251

Lorenzo-Oliveira, D., Freitas, F. C., Meléndez, J., et al. 2018, *A&A*, 619, A73

Luck, R. E. 2018, *AJ*, 156, 171

Magrini, L., Viscasillas Vázquez, C., Spina, L., et al. 2023, *A&A*, 669, A119

Mahdi, D., Soubiran, C., Blanco-Cuaresma, S., & Chemin, L. 2016, *A&A*, 587, A131

Majewski, S. R., Schiavon, R. P., Frinchaboy, P. M., et al. 2017, *AJ*, 154, 94

Martos, G., Meléndez, J., Rathsam, A., & Carvalho Silva, G. 2023, *MNRAS*, 522, 3217

Martos, G., Meléndez, J., Spina, L., & Lucatello, S. 2025, *A&A*, 699, A46

Mayor, M., Pepe, F., Queloz, D., et al. 2003, *The Messenger*, 114, 20

Meléndez, J., Asplund, M., Gustafsson, B., & Yong, D. 2009, *ApJ*, 704, L66

Meléndez, J., Dodds-Eden, K., & Robles, J. A. 2006, *ApJ*, 641, L133

Meléndez, J. & Ramírez, I. 2007, *ApJ*, 669, L89

Minchev, I., Chiappini, C., & Martig, M. 2013, *A&A*, 558, A9

Mor, R., Robin, A. C., Figueiras, F., Roca-Fàbregas, S., & Luri, X. 2019, *A&A*, 624, L1

Ness, M., Hogg, D. W., Rix, H. W., Ho, A. Y. Q., & Zasowski, G. 2015, *ApJ*, 808, 16

Ness, M. K., Johnston, K. V., Blancato, K., et al. 2019, *ApJ*, 883, 177

Ness, M. K., Wheeler, A. J., McKinnon, K., et al. 2022, *ApJ*, 926, 144

Neves, V., Santos, N. C., Sousa, S. G., Correia, A. C. M., & Israelian, G. 2009, *A&A*, 497, 563

Nibauer, J., Baxter, E. J., Jain, B., et al. 2021, *ApJ*, 907, 116

Nissen, P. E. 2015, *A&A*, 579, A52

Nissen, P. E. 2016, *A&A*, 593, A65

Nissen, P. E., Christensen-Dalsgaard, J., Mosumgaard, J. R., et al. 2020, *A&A*, 640, A81

Nissen, P. E. & Gustafsson, B. 2018, *A&A Rev.*, 26, 6

Palicio, P. A., Recio-Blanco, A., Poggio, E., et al. 2023, *A&A*, 670, L7

Palla, M., Magrini, L., Spitoni, E., et al. 2024, *A&A*, 690, A334

Pasquini, L., Biazzo, K., Bonifacio, P., Randich, S., & Bedin, L. R. 2008, *A&A*, 489, 677

Patterson, C. 1956, *Geochim. Cosmochim. Acta*, 10, 230

Perdigon, J., de Laverny, P., Recio-Blanco, A., et al. 2021, *A&A*, 647, A162

Plotnikova, A., Spina, L., Ratcliffe, B., Casali, G., & Carraro, G. 2024, *A&A*, 691, A298

Porto de Mello, G. F. & da Silva, L. 1997, *ApJ*, 482, L89

Porto de Mello, G. F., da Silva, R., da Silva, L., & de Nader, R. V. 2014, *A&A*, 563, A52

Prša, A., Harmanec, P., Torres, G., et al. 2016, *AJ*, 152, 41

Ramírez, I., Meléndez, J., & Asplund, M. 2009, *A&A*, 508, L17

Ramírez, I., Meléndez, J., Bean, J., et al. 2014, *A&A*, 572, A48

Rampalli, R., Ness, M. K., Edwards, G. H., Newton, E. R., & Bedell, M. 2024, *ApJ*, 965, 176

Rathsam, A., Meléndez, J., & Carvalho Silva, G. 2023, *MNRAS*, 525, 4642

Recio-Blanco, A., de Laverny, P., Allende Prieto, C., et al. 2016, *A&A*, 585, A93

Recio-Blanco, A., de Laverny, P., Palicio, P. A., et al. 2024, *A&A*, 692, A235

Recio-Blanco, A., de Laverny, P., Palicio, P. A., et al. 2023, *A&A*, 674, A29

Reddy, A. B. S. & Lambert, D. L. 2017, *ApJ*, 845, 151

Riello, M., De Angelis, F., Evans, D. W., et al. 2021, *A&A*, 649, A3

Ruiz-Lara, T., Gallart, C., Bernard, E. J., & Cassisi, S. 2020, *Nature Astronomy*, 4, 965

Rybicki, J., Green, G. M., Rix, H.-W., et al. 2022, *MNRAS*, 510, 2597

Sahlholdt, C. 2020, *csahlholdt/SAMD*: First SAMD release

Salaris, M., Chieffi, A., & Straniero, O. 1993, *ApJ*, 414, 580

Schirbel, L., Meléndez, J., Karakas, A. I., et al. 2015, *A&A*, 584, A116

Schönrich, R., Binney, J., & Dehnen, W. 2010, *MNRAS*, 403, 1829

Sharma, S., Hayden, M. R., Bland-Hawthorn, J., et al. 2022, *MNRAS*, 510, 734

Sharma, S., Stello, D., Budar, S., et al. 2018, *MNRAS*, 473, 2004

Sheejelamimal, J., Meléndez, J., Rathsam, A., & Martos, G. 2024, *A&A*, 690, A107

Skrutskie, M. F., Cutri, R. M., Stiening, R., et al. 2006, *AJ*, 131, 1163

Soubiran, C. & TrPrsa2016d, A. 2004, *A&A*, 418, 1089

Sousa, S. G., Santos, N. C., Israelian, G., Mayor, M., & Udry, S. 2011, *A&A*, 533, A141

Sousa, S. G., Santos, N. C., Mayor, M., et al. 2008, *A&A*, 487, 373

Souto, D., Allende Prieto, C., Cunha, K., et al. 2019, *ApJ*, 874, 97

Spina, L., Meléndez, J., Karakas, A. I., et al. 2018, *MNRAS*, 474, 2580

Spina, L., Meléndez, J., Karakas, A. I., et al. 2016a, *A&A*, 593, A125

Spina, L., Meléndez, J., & Ramírez, I. 2016b, *A&A*, 585, A152

Spina, L., Sharma, P., Meléndez, J., et al. 2021, *Nature Astronomy*, 5, 1163

Spitoni, E., Recio-Blanco, A., de Laverny, P., et al. 2023, *A&A*, 670, A109

Sun, Q., Ji, C., Wang, S. X., et al. 2025a, *A&A*, 701, A107

Sun, Q., Wang, S. X., Gan, T., et al. 2025b, *ApJ*, 980, 179

Sun, T., Bi, S., Chen, X., et al. 2025c, *Nature Communications*, 16, 1581

Takeda, Y., Kawanomoto, S., Honda, S., Ando, H., & Sakurai, T. 2007, *A&A*, 468, 663

Takeda, Y. & Tajitsu, A. 2009, *PASJ*, 61, 471

Tal-Or, L., Trifonov, T., Zucker, S., Mazeh, T., & Zechmeister, M. 2019, *MNRAS*, 484, L8

Taniguchi, D., Matsunaga, N., Kobayashi, N., et al. 2025, *A&A*, 693, A163

Taniguchi, D., Tsujimoto, T., de Laverny, P., Recio-Blanco, A., & Palicio, P. A. 2026, *A&A*, XXX, AXXX

Tsantaki, M., Sousa, S. G., Adibekyan, V. Z., et al. 2013, *A&A*, 555, A150

Tsujimoto, T. 2021, *ApJ*, 920, L32

Tsujimoto, T., Nomoto, K., Yoshii, Y., et al. 1995, *MNRAS*, 277, 945

Tsujimoto, T., Taniguchi, D., Recio-Blanco, A., Palicio, P. A., & de Laverny, P. 2026, *A&A*, XXX, AXXX

Tucci Maia, M., Ramírez, I., Meléndez, J., et al. 2016, *A&A*, 590, A32

Turcotte, S. & Wimmer-Scheingruber, R. F. 2002, *Journal of Geophysical Research (Space Physics)*, 107, 1442

Walsen, K., Jofré, P., Budar, S., et al. 2024, *MNRAS*, 529, 2946

Willmer, C. N. A. 2018, *ApJS*, 236, 47

Yana Galarza, J., López-Valdivia, R., Lorenzo-Oliveira, D., et al. 2021, *MNRAS*, 504, 1873

Yana Galarza, J., Meléndez, J., Lorenzo-Oliveira, D., et al. 2019, *MNRAS*, 490, L86

Yong, D., Grundahl, F., & Norris, J. E. 2015, *MNRAS*, 446, 3319

Zwitter, T., Kos, J., Chiavassa, A., et al. 2018, *MNRAS*, 481, 645

Zwitter, T., Matijević, G., Breddels, M. A., et al. 2010, *A&A*, 522, A54

Appendix A: Zero-point corrections of GSP-Spec stellar parameters

The accuracy of the GSP-Spec stellar parameters is generally sufficient for many types of analyses. Even though, for Solar-twin studies, which require very high zero-point accuracy relative to the Solar values, the GSP-Spec zero-point accuracy is insufficient. In fact, comparisons with differentially derived Solar-twin stellar parameters have revealed systematic zero-point biases (Fouesneau et al. 2023; Gaia Collaboration et al. 2023a). To quantify such biases in our dataset, we compared our GSP-Spec stellar parameters with those determined by Tucci Maia et al. (2016), Nissen et al. (2020), and Shejelammal et al. (2024). These three studies are extensions and reanalyses of former studies by Ramírez et al. (2014), Nissen (2015, 2016), and Spina et al. (2018); Martos et al. (2023); Rathsam et al. (2023), respectively. We arbitrarily selected these particular studies, among several that also meet the criteria below, for three reasons. First, they employed line-by-line differential analyses relative to the Solar spectrum, ensuring reliable zero points. Second, they derived atmospheric parameters with high precision using high-quality spectra, i.e., S/N of $\gtrsim 500$ using the MIKE (Bernstein et al. 2003) or HARPS (Mayor et al. 2003) high-resolution spectrographs. Third, their samples contain a sufficiently large overlap of several tens of stars with ours.

Figure A.1 compares our GSP-Spec stellar parameters with those from these three studies. Only stars meeting all of the following conditions are included:

- their literature parameters (not GSP-Spec values) satisfy our Solar-twin criteria, i.e., T_{eff} , $\log g$, and $[\text{M}/\text{H}]$ within ± 200 K, ± 0.2 , and ± 0.1 dex of the Solar values;
- they satisfy the quality assessments described in Sect. 2.1;
- they have $\text{S/N}(\text{rv_expected_sig_to_noise}) > 80$ and reduced χ^2 (logchisq_gspspec) < -3.7 , ensuring best precision in GSP-Spec.

We note that, the literature targets lie near the bright end of our GSP-Spec sample, and thus the third criterion on the precision of the GSP-Spec parameters excludes only one star.

The three comparisons show excellent agreement in T_{eff} , given the scatter. Similar levels of agreement are found in comparisons with other studies not shown in the figure. In contrast, clear residual biases remain in GSP-Spec $\log g$ and $[\text{M}/\text{H}]$, despite our prior calibration of these parameters using the relations presented by Recio-Blanco et al. (2024), which were designed to match the $\log g$ and $[\text{M}/\text{H}]$ scales to APOGEE DR17 (Abdurro'uf et al. 2022) and GALAH DR3 (Buder et al. 2021) catalogs.

In order to ensure that the GSP-Spec stellar parameters are strictly differential with respect to the Solar values, we further calibrated GSP-Spec stellar parameters. For T_{eff} and $[\text{M}/\text{H}]$, we calculated the mean of the difference between GSP-Spec and literature parameters, and added these offsets, 1 K in T_{eff} and 0.062 dex in $[\text{M}/\text{H}]$, to the GSP-Spec parameters.

For $\log g$, we found that GSP-Spec $\log g$ values for stars with literature $\log g \sim 4.5$ exhibit a broad distribution extending up to ~ 4.8 . The cause of this discrepancy is unclear, but it is possibly related to model-grid issues in GSP-Spec and/or in the literature. Given that the three literature sources employed high-resolution and high-S/N spectra and that the trends between GSP-Spec and literature $\log g$ are similar among the three studies, we decided to fit the GSP-Spec and literature $\log g$ data with a smoothly connected broken line. The choice of relying on the literature values is supported by the fact that there is a good linear relation

between $\log g$ in the three literature sources and bolometric luminosity (and hence evolutionary $\log g$). The obtained relation is

$$y_1 = (x - 4.44) + b_1 \quad (\text{A.1})$$

$$y_2 = a_2(x - 4.44) + b_2 \quad (\text{A.2})$$

$$y - 4.44 = -\frac{1}{\alpha} \ln(e^{-\alpha y_1} + e^{-\alpha y_2}), \quad (\text{A.3})$$

where x and y represent the GSP-Spec parameters with the calibration described by Recio-Blanco et al. (2024) and the literature parameters, respectively. Equations A.1 and A.2 correspond to the lines for smaller and larger $\log g$, respectively, and Equation A.3 represents a LogSumExp-type smooth minimum function with the parameter α arbitrary chosen as 20. Fitting to the data points shown in Fig. A.1 yields $a_2 = 0.133$, $b_1 = 0.121$, and $b_2 = 0.032$. The fitted line is shown in the figure as the red thick line. Using Equation A.3, we calibrated our GSP-Spec $\log g$ values and their errors.

Another possible approach, which we have not adopted here, would be to rely on the relative $\log g$ values of GSP-Spec, and simply add a 0.104 offset to the GSP-Spec $\log g$ values, ignoring the broken relation seen in Fig. A.1. This alternative might be supported by the seemingly linear relations with unit slope between GSP-Spec $\log g$ and those determined by Gonzalez et al. (2010), Gonzalez (2014), Porto de Mello et al. (2014), and Spina et al. (2021) up to $\log g \sim 4.5$ –4.6.

Appendix B: Further interpolation of the isochrone library

To accurately recover the age (and M_{ini}) of a Solar twin, the HR diagram and the Kiel diagram need to be densely covered with isochrone grid points, with a spacing comparable to or smaller than the observational uncertainties. The uncertainties of $[\text{M}/\text{H}]$, T_{eff} , $\log g$, M_G , and M_{K_s} in our final Solar-twin catalog are 0.01–0.06 dex, ~ 20 –100 K, 0.01–0.1, 0.003–0.05, and 0.02–0.03, respectively, for most stars (5% and 95% percentiles). The steps in the isochrone library should ideally be comparable to, or finer than, the minimum values of these precision ranges (e.g., finer than 20 K). The condition for $[\text{M}/\text{H}]$ is satisfied, given that we retrieved the isochrone library with 0.005 dex increments in $[\text{M}/\text{H}]_{\text{ini}}$. Hence, we here check the increments of the other four parameters.

Our selection of Solar twins covers both main-sequence stars and old main-sequence turn-off stars. For turn-off stars, our grid with 0.1 Gyr increments retrieved from the CMD 3.8 web interface provides sufficiently high density on the T_{eff} vs $\log g$ Kiel diagram. Indeed, for the 10 Gyr isochrone, the age difference of 0.1 Gyr at the turn-off corresponds to a T_{eff} difference of 5 K, which is a few times finer than the best T_{eff} precision. Also, the $\log g$ spacing around the turn-off is small, $\lesssim 0.05$, owing to the fine M_{ini} increment of $\lesssim 0.01 M_{\odot}$ around there, which is comparable to the upper 5% percentile of the $\log g$ precision of 0.045. Still, the M_G and M_{K_s} spacing around the turn-off of ~ 0.1 mag is an order worse than the typical precision of our photometric data.

In contrast, the M_{ini} increments in the retrieved grid for main-sequence stars are not fine enough for T_{eff} , M_G , and M_{K_s} . The M_{ini} increments for main-sequence stars range from < 0.01 to $0.05 M_{\odot}$. The resulting $\log g$ step at $1 M_{\odot}$ is up to ~ 0.03 , which is sufficient for recovering ages. However, given $|\partial T_{\text{eff}}/\partial M_{\text{ini}}| \sim 3500 \text{ K}/M_{\odot}$ along main-sequence isochrones, the T_{eff} step becomes > 150 K in the worst cases, which is several times coarser

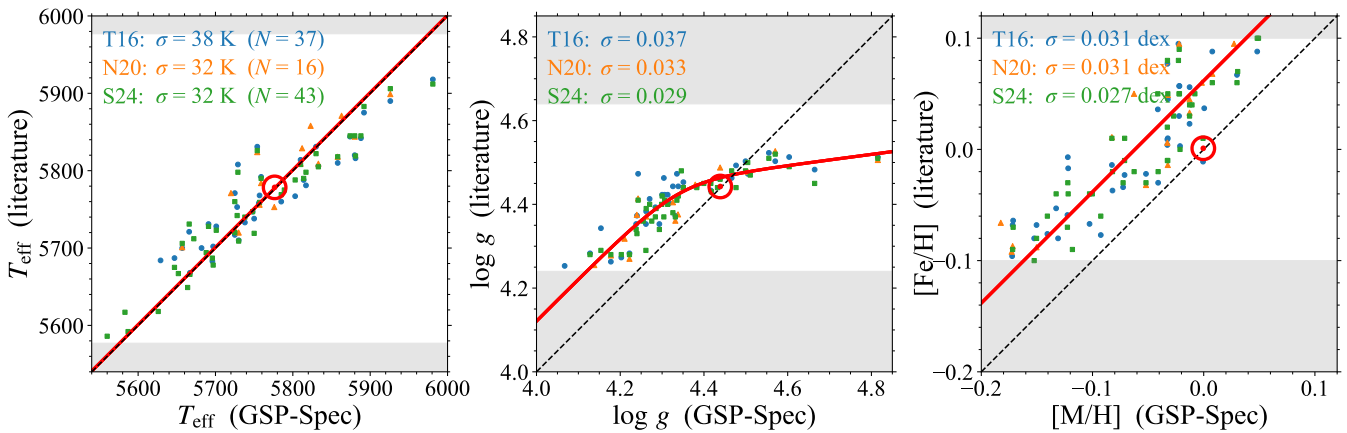


Fig. A.1: Our *Gaia* DR3 GSP-Spec and literature stellar parameters of Solar twins. GSP-Spec parameters were already calibrated following [Recio-Blanco et al. \(2024\)](#). Blue circles, orange triangles, and green squares represent comparisons with [Tucci Maia et al. \(2016\)](#), T16; 37 stars), [Nissen et al. \(2020\)](#), N20; 16 stars), and [Sheejelammal et al. \(2024\)](#), S24; 43 stars), respectively. Typical quoted errors are $\sim 5\text{--}10\text{ K}$ in T_{eff} , 0.02 in $\log g$, and 0.005–0.01 dex in $[\text{M}/\text{H}]$, for both GSP-Spec and literature parameters. Only stars with literature parameters satisfying our Solar-twin criteria are shown (i.e., stars in gray-shaded areas are excluded). The red open marker indicates the parameters of the Sun. Red thick lines show our adopted relations to convert GSP-Spec parameters to the literature scales. The scatters around the adopted relations are annotated in each panel.

than the typical observational T_{eff} precision. Similarly, gradients of M_G and M_{K_s} of 5–8 and 3–7 mag/ M_{\odot} , respectively, correspond to steps of ~ 0.4 mag in the worst cases. These coarse T_{eff} , M_G and M_{K_s} steps are particularly evident in young isochrones with ages $\lesssim 1.5$ Gyr, where M_{ini} increments are typically $0.05 M_{\odot}$. Thus, if we were to determine ages and M_{ini} using the retrieved isochrone grid as it is, the likelihood would tend to place most of the weight on the nearest M_{ini} grid points, even when the true value lies between them, thereby pulling the inferred M_{ini} toward those grid points and introducing systematic biases. Once M_{ini} is biased in this way, the simultaneously inferred age is biased as well, despite the fine age grid.

In order to overcome the issue of the coarse grid, we added isochrone points with $0.001 M_{\odot}$ increments, by linearly interpolating existing isochrone grid points. The resulting maximum steps of T_{eff} , $\log g$, M_G , and M_{K_s} along the isochrones are ~ 4 K, 0.003, 0.01 mag, and 0.01 mag, respectively.

Appendix C: Mimicking the errors in stellar parameters

In Sect. 4.3.1, we constructed a mock catalog of Solar twins, by mimicking the observed stellar parameters, for which errors had to be assigned. To guide this assignment, we first investigated how S/N depends on magnitude and stellar parameters. We then examined how the errors in six parameters (T_{eff} , $\log g$, $[\text{M}/\text{H}]$, $[\alpha/\text{Fe}]$, M_G and M_{K_s}) in our Solar-twin catalog depend on the stellar parameters (T_{eff} , $\log g$, and $[\text{M}/\text{H}]$) and on S/N. We note that here we use the “original” values (i.e., those before the calibration in Appendix A) for the $\log g$ error, while we use the “calibrated” values for the other parameters including $\log g$ itself. We also note that for $[\text{M}/\text{H}]$ and its error, we use the values before correcting for the effect of $[\alpha/\text{Fe}]$.

For the sample in this section, we considered 27,782 *Gaia* DR3 stars that (1) have the first 13 GSP-Spec Quality Flags, except for the seventh one, equal to zero, (2) have parameters that pass our Solar-twin selections in Sects. 2.1 and 2.4, and (3) satisfy $G < 12$. These conditions are intended to avoid imposing

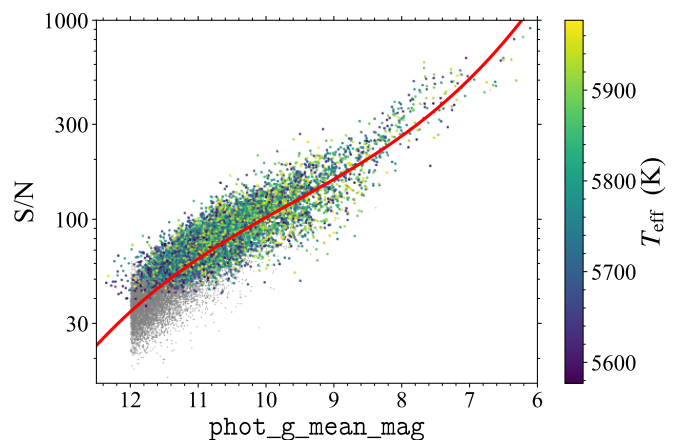
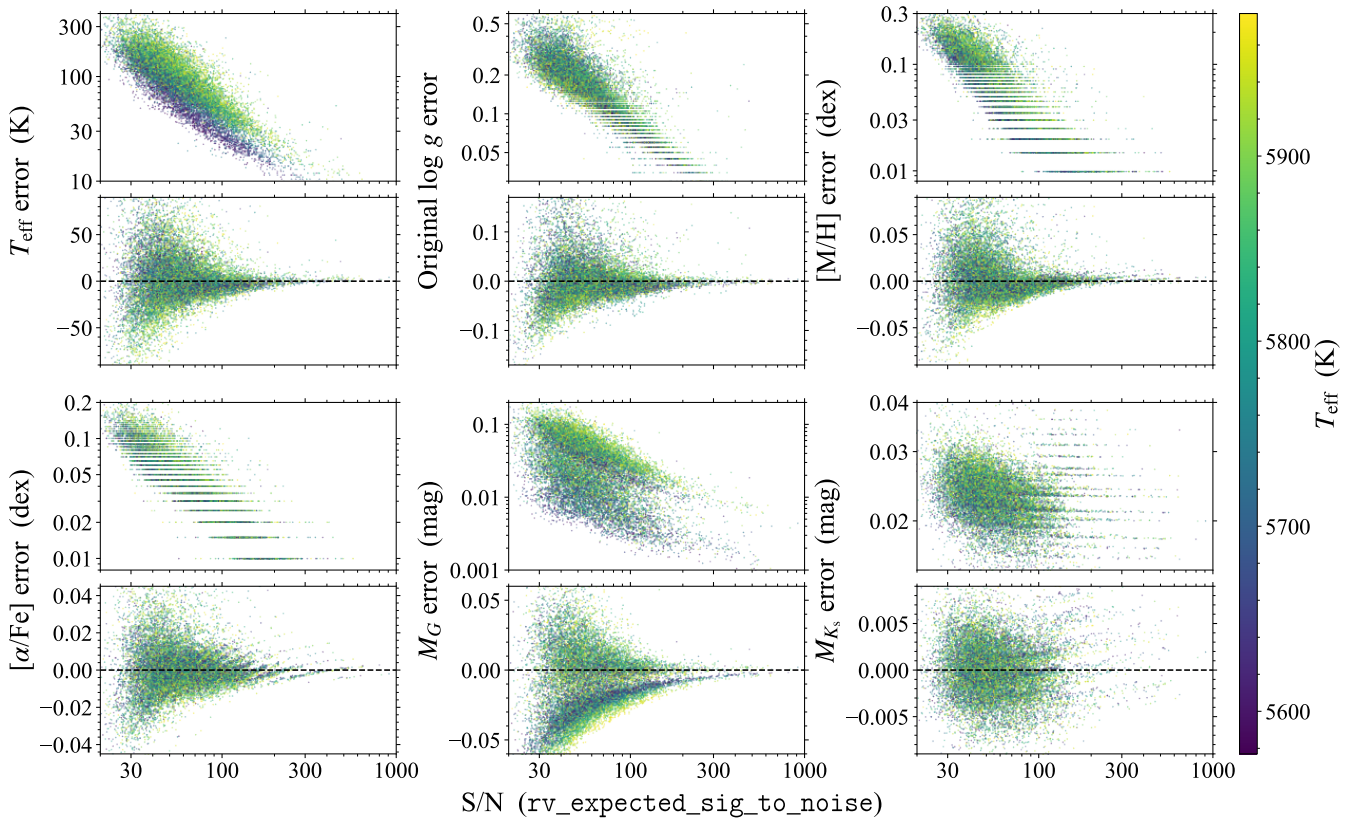
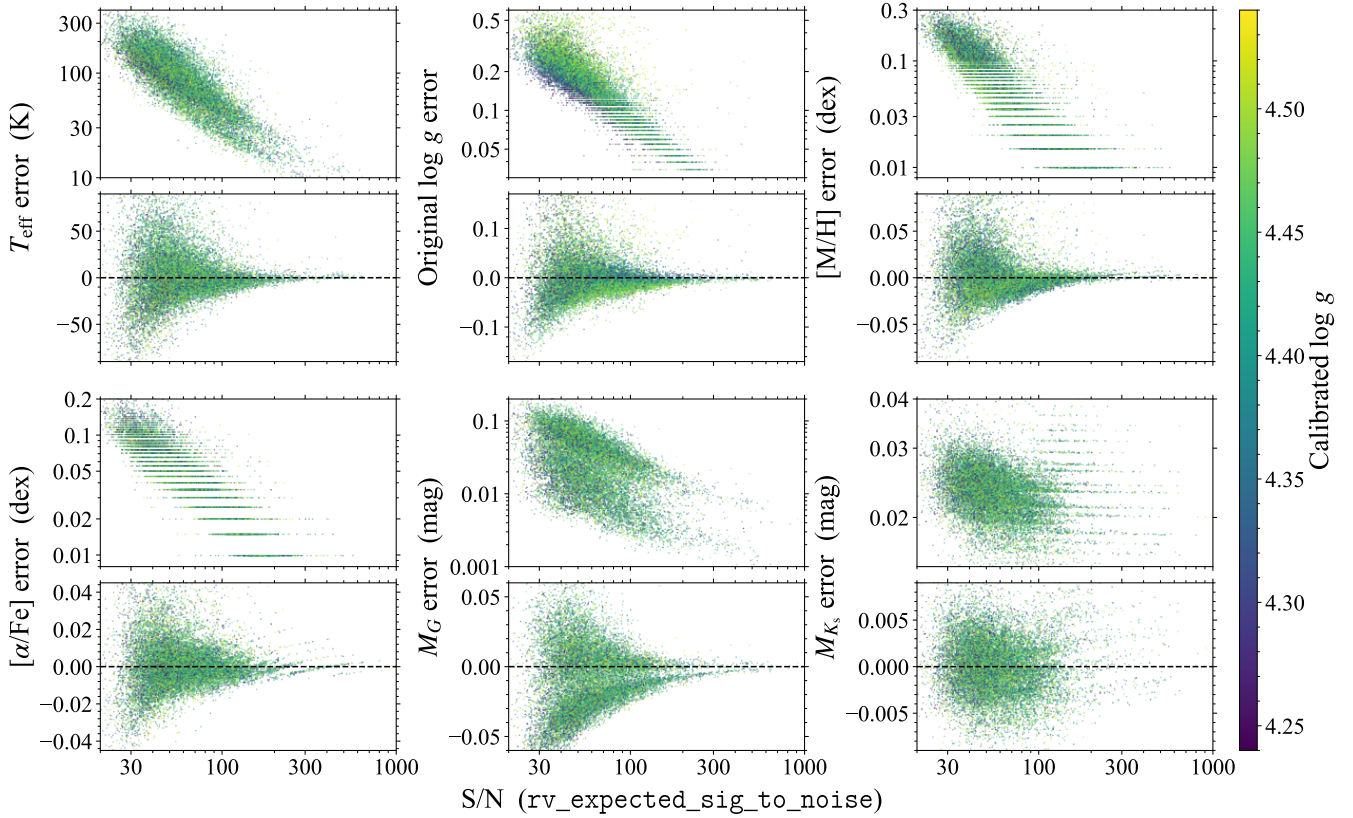


Fig. C.1: Dependence of S/N on the G -band magnitude. Dots color-coded by T_{eff} show our final 6,594 Solar twins, while gray dots represent 27,782 stars without imposing the condition on the seventh digit of the GSP-Spec Quality Flags on parameterization uncertainties. Red thick curve shows the cubic polynomial relation between the G -band magnitude and the common logarithm of S/N, obtained by fitting the gray data points.

any threshold on parameterization uncertainties, thereby allowing stars with large uncertainties to be included.

Figure C.1 shows the relation between the G -band magnitude and the common logarithm of S/N. We see no dependence of this relation on T_{eff} , as shown by the colored dots (i.e., our final 6,594 Solar twins) in the figure. We also see no dependence on $\log g$ or $[\text{M}/\text{H}]$, though these are not shown in the figure. In contrast, we see a clear lower boundary of S/N around 50 in the final sample, which is the result of the seventh digit of GSP-Spec Quality Flag (i.e., upper thresholds on the parameterization uncertainties of T_{eff} , $\log g$, $[\text{M}/\text{H}]$, and $[\alpha/\text{Fe}]$). To properly account for this selection criterion, we fitted the gray dots in Fig. C.1 (i.e., the sample without imposing the thresholds on parameterization uncertainties, namely the sample defined in this section) and ob-

Fig. C.2: Dependence of the errors in stellar parameters on S/N and T_{eff} .Fig. C.3: Same as Fig. C.2, but color-coded by calibrated $\log g$.

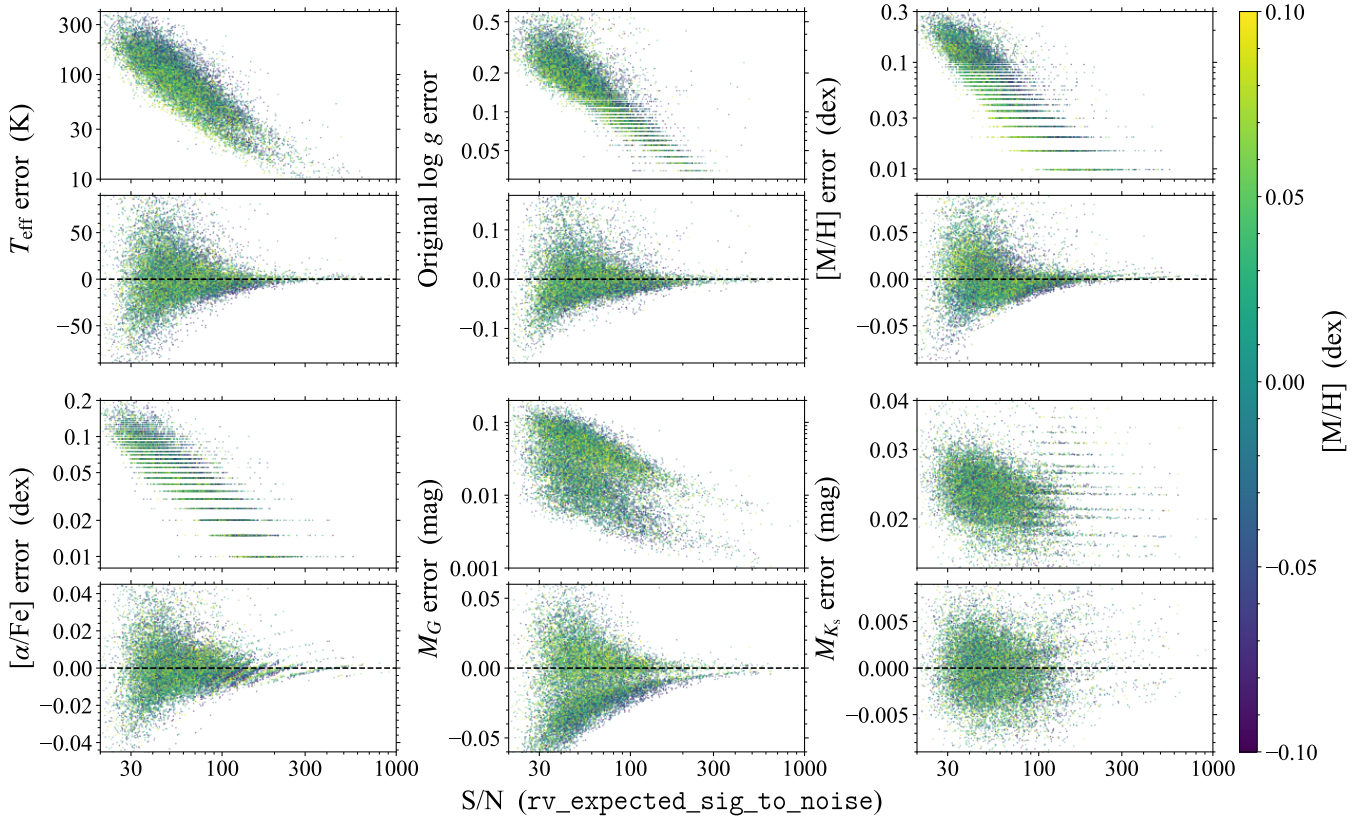


Fig. C.4: Same as Fig. C.2, but color-coded by [M/H].

Table C.1: Linear coefficients in Equation C.2 to estimate the errors in Solar-twin parameters as a function of S/N and some stellar parameters.

Parameter	a_0	$a_{S/N}$	$a_{T_{\text{eff}}}$	$a_{T_{\text{eff}}^2}$	$a_{\log g}$	$a_{[\text{M}/\text{H}]}$	RMS
T_{eff} (K)	+4.0288	-1.1752	+0.0747	-0.0194	+0.0116	-0.0753	0.1142
Original $\log g$	+1.0109	-1.0101	+0.0113	-0.0109	+0.0547	-0.0378	0.1108
$[\text{M}/\text{H}]$ (dex)	+1.3692	-1.4653	+0.0379		-0.0142	-0.0928	0.1477
$[\alpha/\text{Fe}]$ (dex)	+0.7201	-1.1574	+0.0176		-0.0102	-0.0449	0.1109
M_G (mag)	+0.4061	-1.0211	+0.0623		+0.0103	-0.0350	0.1722
M_{K_s} (mag)	-1.4829	-0.0870	+0.0074				0.0660

tained the relation,

$$\log_{10}(\text{S/N}) = -0.0071388G^3 + 0.205971G^2 - 2.17006G + 10.2518, \quad (\text{C.1})$$

for which the RMS scatter around the relation is 0.0960.

With the G -S/N relation obtained, to mimic the relations between S/N and parameterization uncertainties, we show vertically arranged pairs of panels plotting the errors in the six parameters for our sample in Fig. C.2. The upper panel of each pair shows the relation between S/N (rv_expected_sig_to_noise from the *Gaia* DR3 catalog) and the error. As can be seen, there are good linear relations between the logarithms of the horizontal and vertical axes for most panels, indicating power-law relations between the S/N and error values. There are two exceptions: the errors in M_G and M_{K_s} . For M_G , the error is in many cases dominated by the error in the extinction A_G , which is determined using *Gaia* photometry and GSP-Spec stellar parameters. Hence, the error in M_G mainly depends on A_G and the errors in GSP-Spec stellar parameters. The latter correlates well with S/N, as illustrated in the other panels, but the former depends only weakly

on S/N through the distance. As a result, the trend between S/N and the M_G error has a large scatter. For M_{K_s} , the error is mostly dominated by the error in the 2MASS photometry, and hence depends only weakly on S/N.

The dependence of the errors on other parameters (T_{eff} , $\log g$, and $[\text{M}/\text{H}]$) is illustrated by the colors of the dots in Figs. C.2, C.3, and C.4, respectively. There is clear dependence of the errors of most parameters on T_{eff} , and some of them also (in most cases weakly) depend on $\log g$ and $[\text{M}/\text{H}]$ on top of the dependence on T_{eff} . Again, the error of M_{K_s} is an exception, which depends only weakly on T_{eff} but does not on $\log g$ nor $[\text{M}/\text{H}]$.

To model the dependence of the errors on S/N and stellar parameters, we fitted the common logarithms of the errors as linear functions of the form,

$$\log_{10}(\text{Error}) = a_0 + a_{S/N} \log_{10}(\text{S/N}) + a_{T_{\text{eff}}} \frac{T_{\text{eff}} - T_{\text{eff},\odot}}{100 \text{ K}} + a_{T_{\text{eff}}^2} \left(\frac{T_{\text{eff}} - T_{\text{eff},\odot}}{100 \text{ K}} \right)^2 + a_{\log g} \frac{\log g - \log g_{\odot}}{0.1} + a_{[\text{M}/\text{H}]} \frac{[\text{M}/\text{H}]}{0.1 \text{ dex}}, \quad (\text{C.2})$$

using least-squares minimization. We fixed some coefficients to zero when visual inspection showed no clear dependence of an error on a parameter, and when allowing the coefficients to vary produced negligible improvements in the root-mean-squares (RMS) of the fitting residuals. The resulting coefficients and RMS values of the fits are summarized in Table C.1. We used Equations C.2 and C.1, together with their scatter, to assign errors to mock Solar twins.

Appendix D: Review of previous large Solar-twin catalogs

In recent years, a few large catalogs of Solar twins have been published using spectra from large surveys. [Rampalli et al. \(2024\)](#) analyzed *Gaia* RVS spectra of Solar twins published in DR3 ([Cropper et al. 2018](#); [Gaia Collaboration et al. 2023c](#)) with a data-driven approach using The Cannon algorithm ([Ness et al. 2015](#)) to infer the stellar parameters and chemical abundances of 15 elements for 5,347 Solar twins (in our definition). They used high-resolution stellar parameters and chemical abundances of 34 Solar twins from [Hinkel et al. \(2014\)](#), [Brewer et al. \(2016\)](#), [Brewer & Fischer \(2018\)](#), and [Bedell et al. \(2018\)](#) as the reference during the training, among which most of the training stars are from [Brewer et al. \(2016\)](#) and [Brewer & Fischer \(2018\)](#). Among the four studies, only [Bedell et al. \(2018\)](#) focused exclusively on Solar twins, but given that [Brewer et al. \(2016\)](#) and [Brewer & Fischer \(2018\)](#) analyzed their high-resolution spectra with a differential analysis method, their parameters might be as reliable as those in studies focusing specifically on Solar twins. They achieved high internal precisions of 0.03–0.07 dex for many elements, supporting the effectiveness of the data-driven The Cannon method. Then, [Rampalli et al. \(2024\)](#) estimated isochrone ages using the `isoclassify` code ([Huber et al. 2017](#); [Berger et al. 2020](#)), with T_{eff} , $\log g$, and $[\text{Fe}/\text{H}]$ as input parameters, though they mentioned that they do not report their ages “as robust results for individual stars”. By plotting condensation temperature T_c –abundance trends, they independently confirmed that the Sun is depleted in refractory elements compared to their sample of Solar twins, regardless of whether those stars host terrestrial, close-in giant, or giant planets, or no planets at all.

There are also two large catalogs of Solar twins based on GALAH DR3 ([Buder et al. 2021](#)) data. As one of these two studies, [Walsen et al. \(2024\)](#) applied the data-driven The Cannon algorithm ([Ness et al. 2015](#)) to GALAH DR3 spectra to derive high-precision stellar parameters and 14 elemental abundances for a sample of 13,132 Solar twins (again, in our definition). They used stellar parameters and abundances from GALAH DR3 of 150 high-S/N stars, for which a sky-flat Solar spectrum was used to determine the zero-point in the chemical abundances, as the reference, though it is not clearly stated which parameters have been corrected for these zero-points. They also used GALAH DR3 abundances together with their derived The Cannon abundances, to see whether there are any differences between the results obtained with the two abundance catalogs. They adopted ages tabulated in GALAH DR3 ([Sharma et al. 2018](#); [Buder et al. 2021](#)), though [Buder et al. \(2021\)](#) and [Walsen et al. \(2024\)](#) noted a few limitations in the GALAH DR3 ages, for example, the overestimation of the Solar age by 1.26 Gyr. With these datasets, they compared the age–[X/Fe] relations for their sample to those from [Bedell et al. \(2018\)](#). They claimed that some elements (Mg, Al, Si, Ca, Sc, Ti, and Zn) show consistent trends between the two samples,

Table E.1: Final solar-twin catalog (available at CDS).

whereas some others (Na, Mn, Ni, Cu, Y, and Ba) show inconsistent trends, and argued that the discrepancies could be due, for example, to differences in precision and accuracy, distance range, or selection effects. At the same time, we suggest that the discrepancies that they found could be at least partly attributed to differences in the age range (\sim 0–8 Gyr in [Bedell et al. \(2018\)](#) vs \sim 3–12 Gyr in [Walsen et al. \(2024\)](#)) and in the metallicity range (± 0.1 dex around the Solar value by [Bedell et al. \(2018\)](#) vs ± 0.3 dex by [Walsen et al. \(2024\)](#)). They then constructed phylogenetic trees from [X/Fe] ratios to investigate the evolution of Galactic-disk stars. From the phylogenetic tree constructed from the combination of low- and high-eccentricity Solar twins, they found that there are two distinct clans that differ in eccentricities, metallicities, and chemical-clock relations (i.e., the age–[Y/Mg] relation).

In the other study using GALAH DR3, [Lehmann et al. \(2025\)](#) applied the equivalent-width-based data-driven EPIC algorithm ([Lehmann et al. 2022](#)) to derive precise T_{eff} , $\log g$, and $[\text{Fe}/\text{H}]$ for a large sample of Solar twins (14,571 stars in our definition). They employed the stacked GALAH DR2 spectra ([Zwitter et al. 2018](#)), whose stellar parameters had been determined using The Cannon by [Buder et al. \(2018\)](#)¹⁹, as the reference training sample. They achieved a factor of 2–4 higher precision (i.e., smaller errors) in the parameterization compared to the original GALAH pipeline. They then estimated isochrone ages with the `SAMD` code ([Sahlholdt 2020](#)) and used these ages together with orbital parameters to investigate the chemodynamic evolution of nearby moving groups defined as Solar twins having a common angular momentum L_z . In particular, they examined the age–metallicity relation for each moving group, without imposing the usual restriction of nearly Solar metallicity, to study radial migration within a moving group.

Appendix E: Additional tables and figures

¹⁹ We note that, unlike GALAH DR2, where The Cannon was used, [Buder et al. \(2021\)](#) chose not to use The Cannon (or any other data-driven approaches) for GALAH DR3 because such methods can suffer from signal aliasing and learn unphysical correlations between input data and output labels.

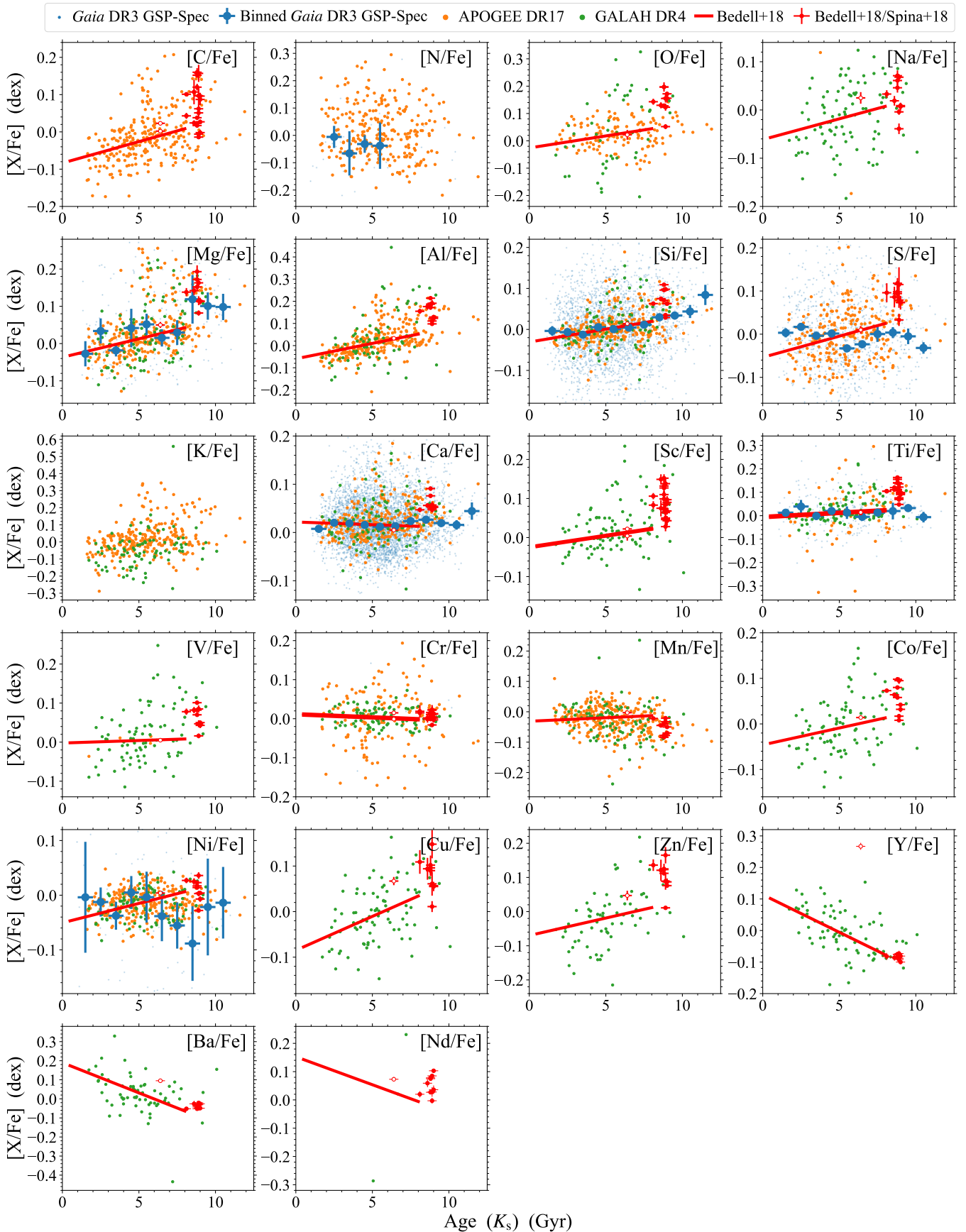


Fig. E.1: Age–abundance relations for all the elements. Symbols are the same as in Fig. 8.

Table E.2: Column description of the published Solar-twin catalog.

Column	Unit	Description
GDR3_source_id	—	<i>Gaia</i> DR3 source_id
2MASS	—	2MASS designation
RAdeg	deg	Right ascension in <i>Gaia</i> DR3
DEdeg	deg	Declination in <i>Gaia</i> DR3
Teff	K	Calibrated GSP-Spec effective temperature, T_{eff}
logg	(cgs)	Calibrated GSP-Spec surface gravity, $\log g$
[M/H]	dex	Calibrated GSP-Spec current surface metallicity, $[\text{M}/\text{H}]_{\text{curr}}$
[alpha/M]	dex	GSP-Spec α abundance, $[\alpha/\text{Fe}]$
A0	mag	Monochromatic extinction, A_0
BJ21_rgeo	pc	Geometric distance from Bailer-Jones et al. (2021) ^a
GMag	mag	Absolute magnitude in the <i>G</i> band of <i>Gaia</i> DR3
BPMag	mag	Absolute magnitude in the <i>BP</i> band of <i>Gaia</i> DR3
RPMag	mag	Absolute magnitude in the <i>RP</i> band of <i>Gaia</i> DR3
JMag	mag	Absolute magnitude in the <i>J</i> band of 2MASS
HMag	mag	Absolute magnitude in the <i>H</i> band of 2MASS
KsMag	mag	Absolute magnitude in the <i>Ks</i> band of 2MASS
Age(logg)	Gyr	Age determined with logg
Mini(logg)	M_{\odot}	Initial mass M_{ini} determined with logg
[M/H]ini(logg)	dex	Initial metallicity $[\text{M}/\text{H}]_{\text{ini}}$ determined with logg
Age(GMag)	Gyr	Age determined with GMag
Mini(GMag)	M_{\odot}	Initial mass M_{ini} determined with GMag
[M/H]ini(GMag)	dex	Initial metallicity $[\text{M}/\text{H}]_{\text{ini}}$ determined with GMag
Age(KsMag)	Gyr	Age determined with KsMag
Mini(KsMag)	M_{\odot}	Initial mass M_{ini} determined with KsMag
[M/H]ini(KsMag)	dex	Initial metallicity $[\text{M}/\text{H}]_{\text{ini}}$ determined with KsMag
ecc		Eccentricity
Lz	Sun	Vertical angular momentum
Rg	kpc	Guiding radius
Rapo	kpc	Apocenter distance
Rperi	kpc	Pericenter distance
Zmax	kpc	Maximum vertical distance
[X/Fe]	dex	Calibrated X abundance in <i>Gaia</i> DR3 GSP-Spec ^a
APOGEEDR17_FE_H	dex	Iron abundance in APOGEE DR17 (Majewski et al. 2017 ; Abdurro'uf et al. 2022)
APOGEEDR17_X_FE	dex	X abundance in APOGEE DR17 ^a
GALAHDR4_fe_h	dex	Iron abundance in GALAH DR4 (De Silva et al. 2015 ; Buder et al. 2025) ^a
GALAHDR4_x_fe	dex	X abundance in GALAH DR4 ^a
exoplanet	—	Known exoplanet in NASA Exoplanet Archive (Christiansen et al. 2025) ^a

Notes. We recommend using age, M_{ini} , and $[\text{M}/\text{H}]_{\text{ini}}$ determined from M_{K_s} . ^(a) These literature values are provided for quick analyses using this data set. Interested users must check the up-to-date data and cite original papers.

Table E.3: Added offsets to [X/Fe] abundances.

Element	GSP-Spec	APOGEE	GALAH
[C/Fe]		+0.011	
[N/Fe]	— ^a	— ^a	
[O/Fe]		-0.059	-0.120
[Na/Fe]		+0.103	-0.018
[Mg/Fe]	+0.031	-0.015	-0.044
[Al/Fe]		-0.125	-0.027
[Si/Fe]	-0.023	-0.075	-0.030
[S/Fe]	+0.025	+0.026	
[K/Fe]		— ^a	— ^a
[Ca/Fe]	+0.012	+0.034	+0.025
[Sc/Fe]			-0.027
[Ti/Fe]	+0.026	+0.143	+0.013
[V/Fe]		+0.014	-0.017
[Cr/Fe]	+0.006	+0.145	+0.004
[Mn/Fe]		-0.036	+0.006
[Co/Fe]			-0.035
[Ni/Fe]	+0.028	-0.041	-0.038
[Cu/Fe]			-0.021
[Zn/Fe]			-0.027
[Y/Fe]			+0.065
[Ba/Fe]			+0.082
[Nd/Fe]			-0.035

Notes. ^(a) The age-[X/Fe] relation is not available for these elements in [Bedell et al. \(2018\)](#).

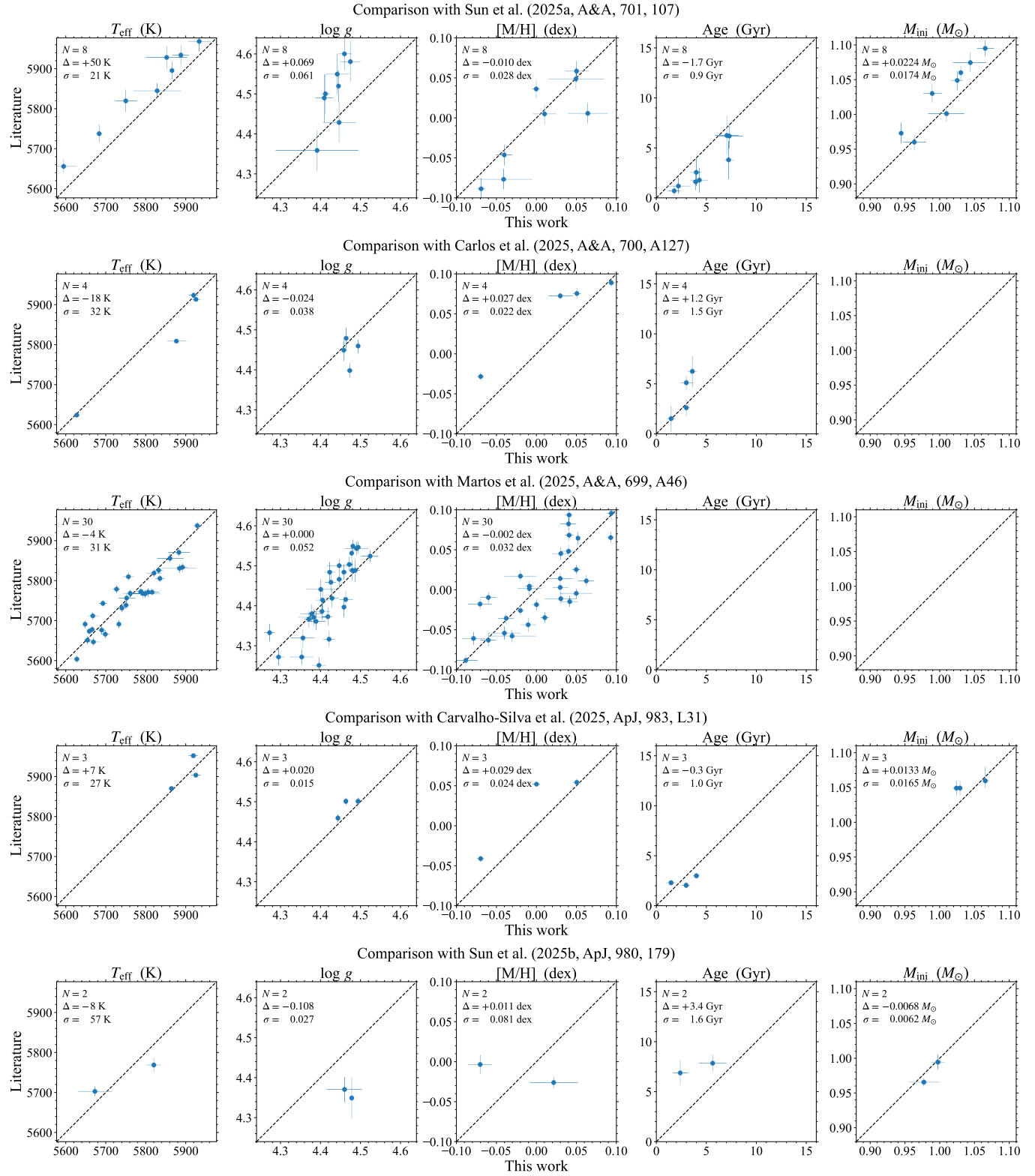


Fig. E.2: Comparison of stellar parameters with literature. Also available at Zenodo (<https://doi.org/10.5281/zenodo.XXXXXXXXX>).

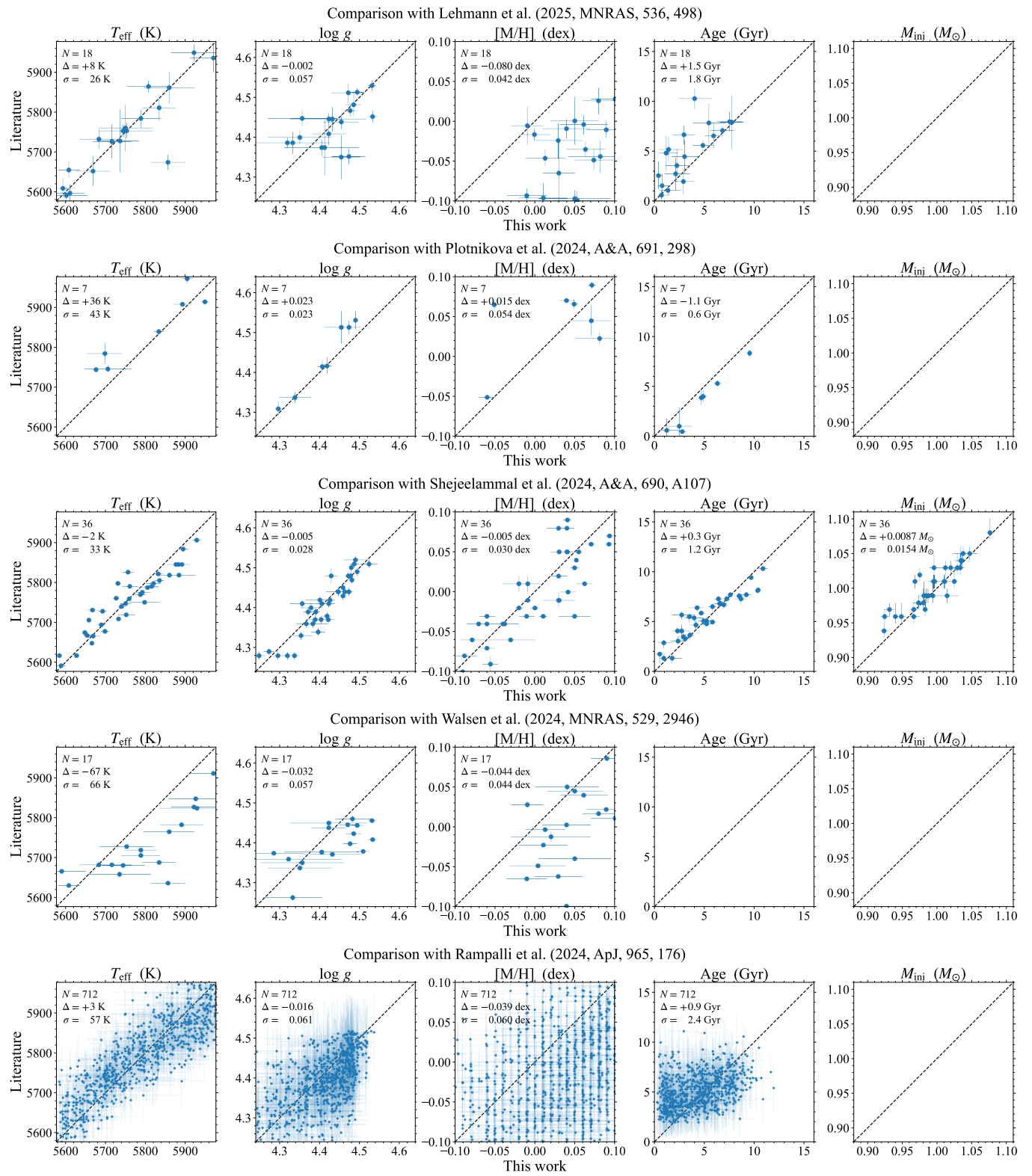


Fig. E.2: Continued.

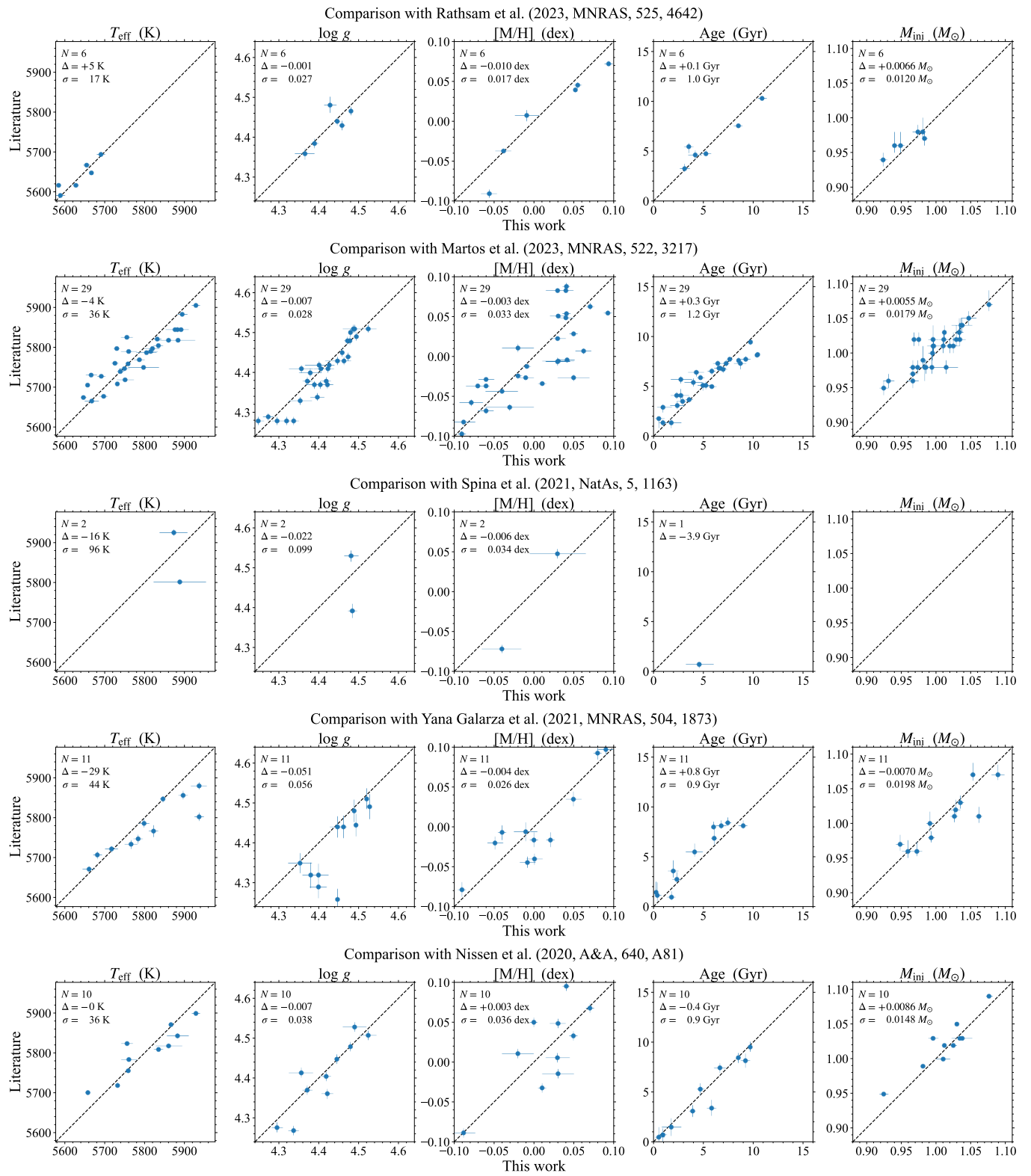


Fig. E.2: Continued.

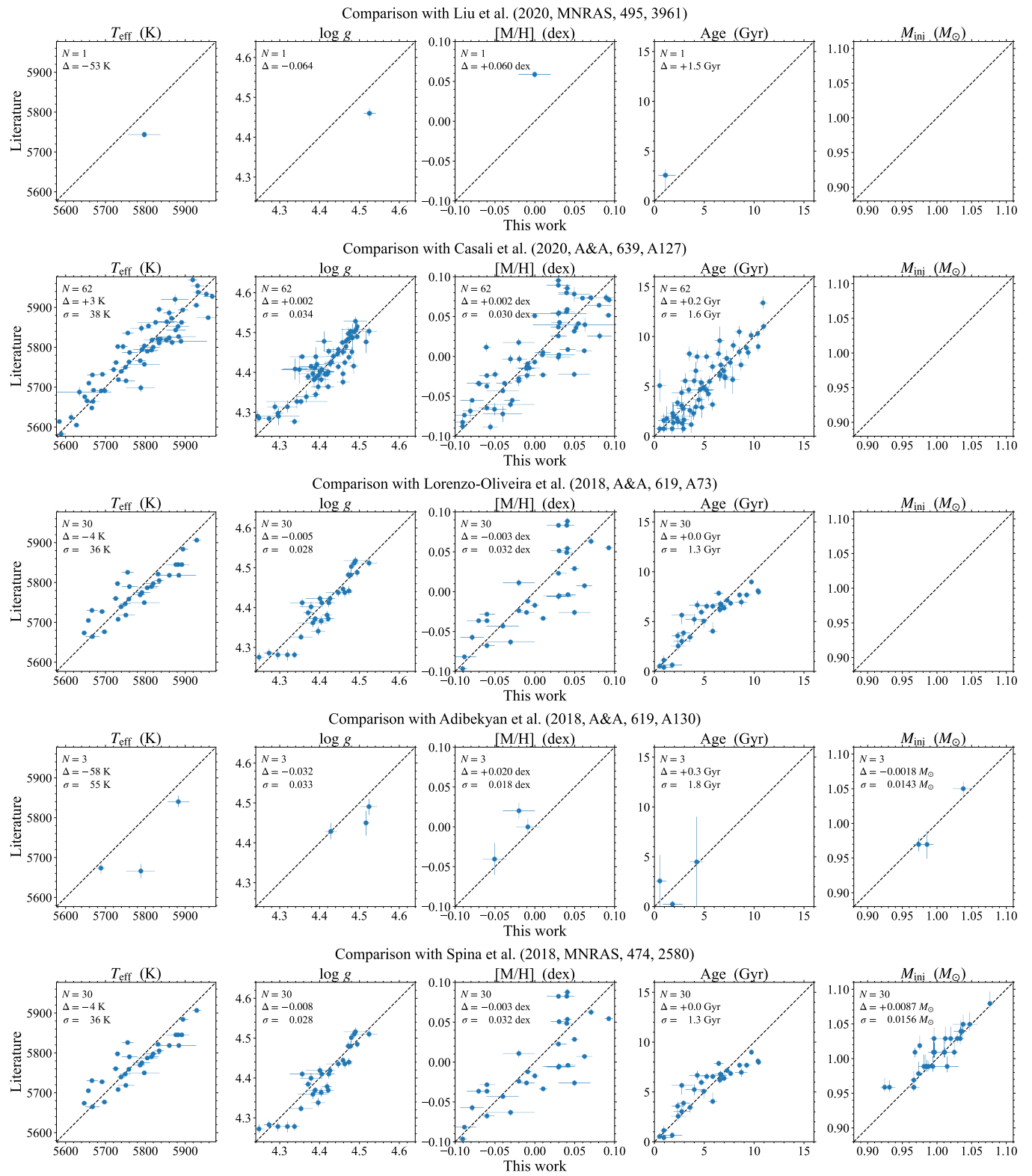


Fig. E.2: Continued.

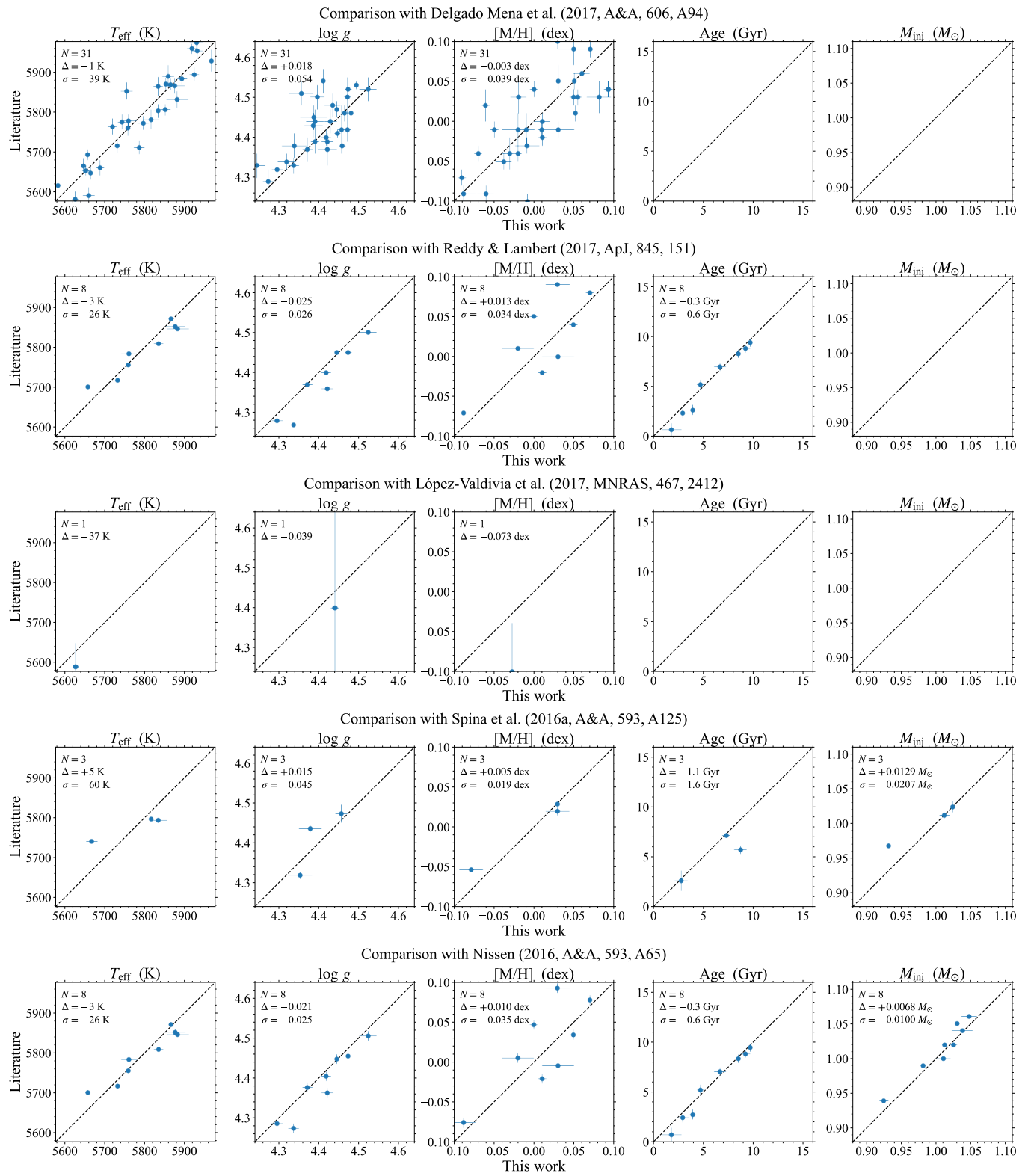


Fig. E.2: Continued.

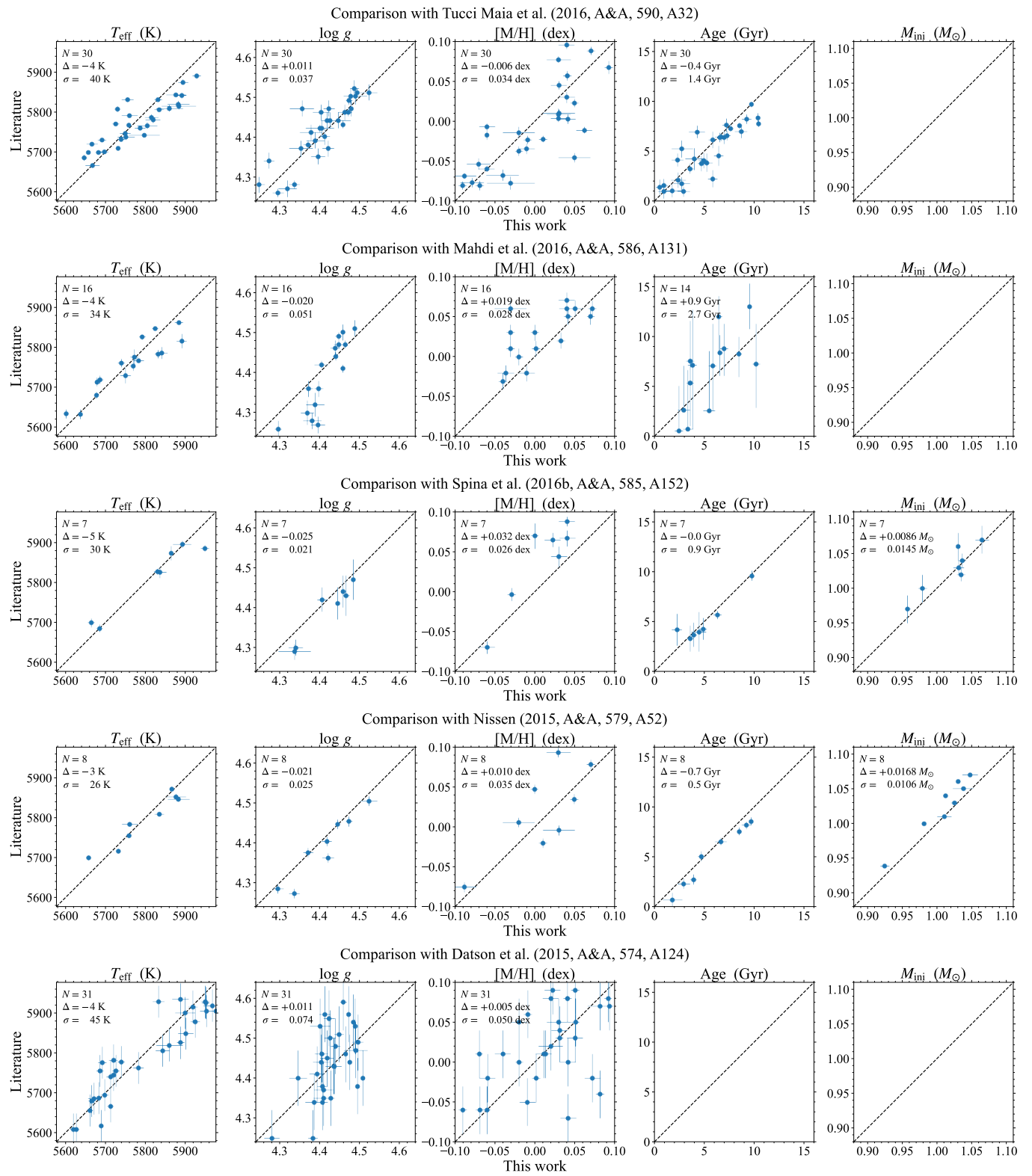


Fig. E.2: Continued.

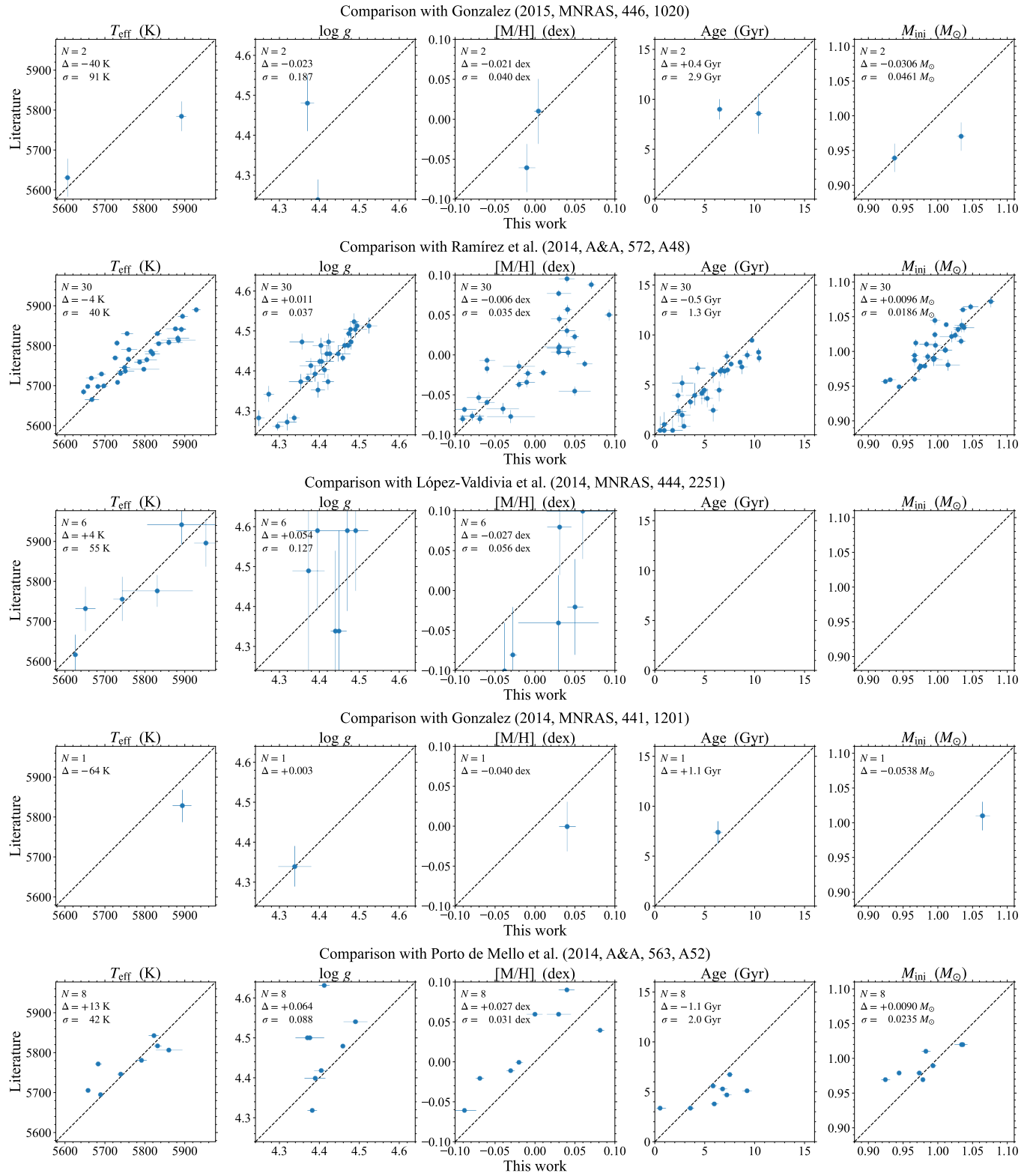


Fig. E.2: Continued.

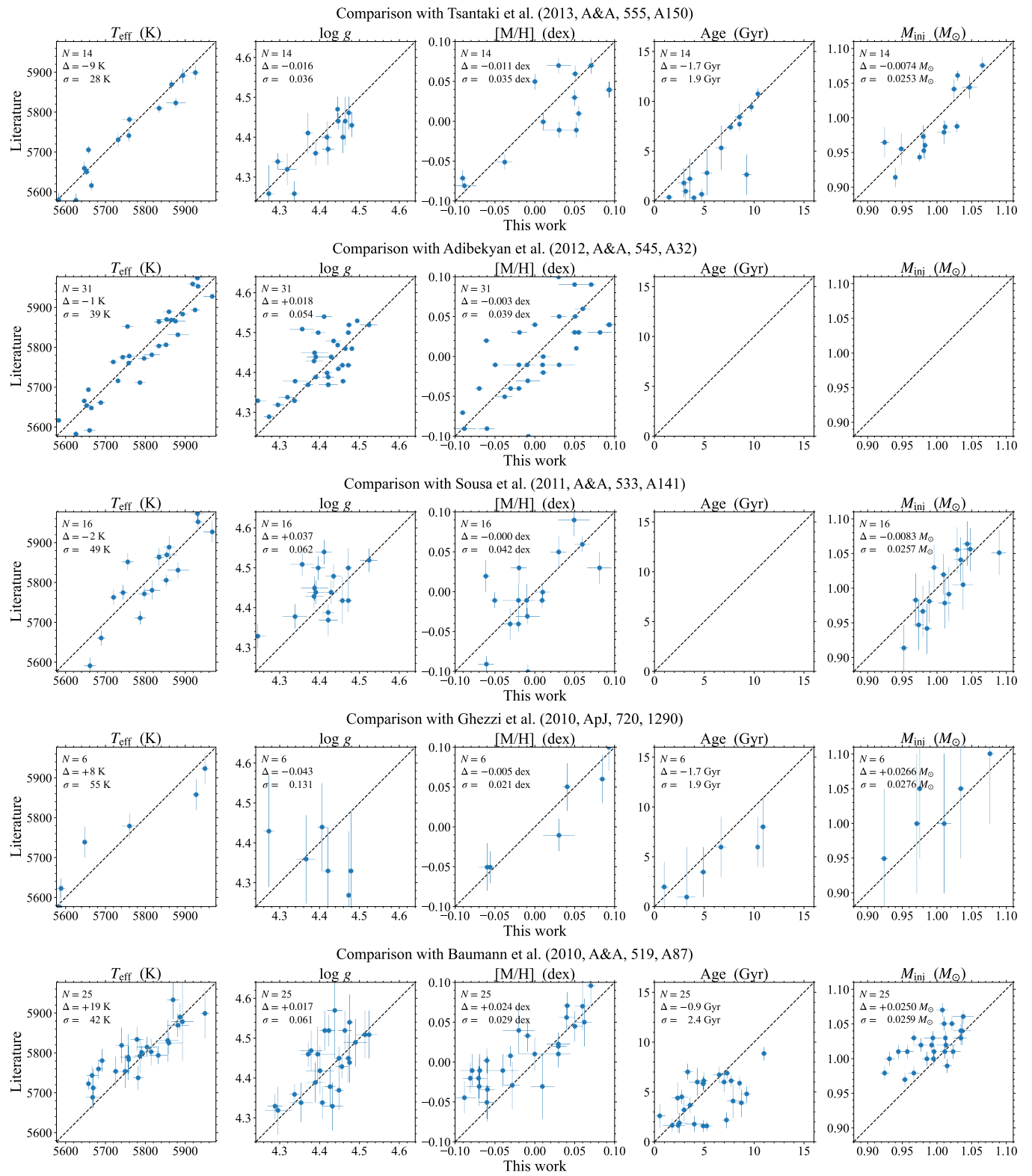


Fig. E.2: Continued.

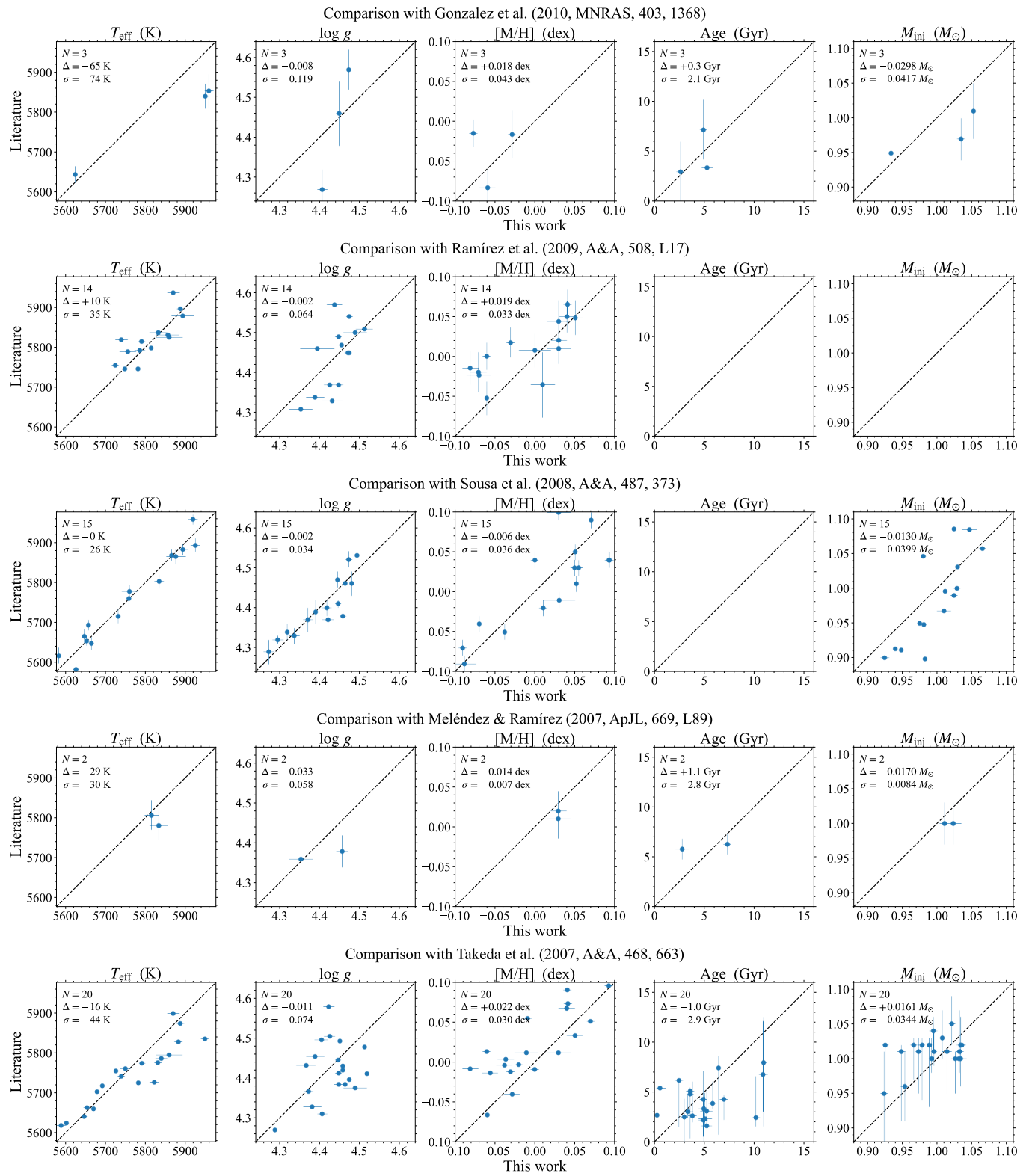


Fig. E.2: Continued.

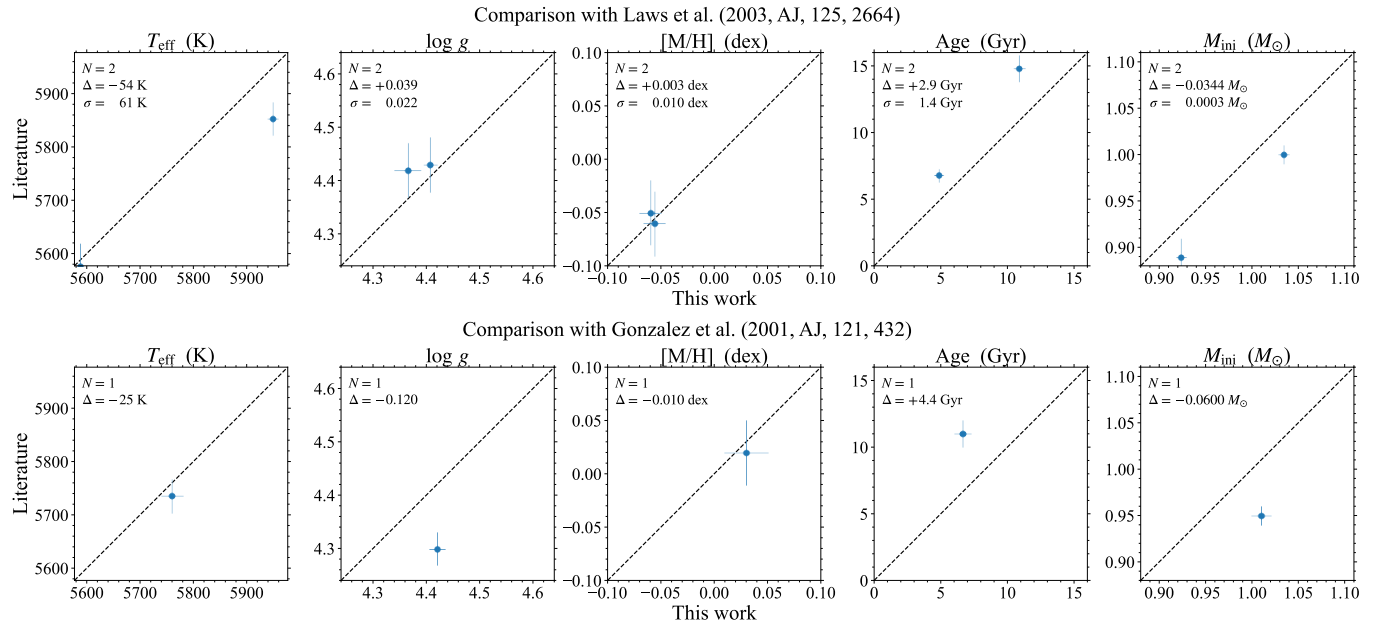


Fig. E.2: Continued.